

# On the multiresolution structure of Internet traffic traces\*

Konstantinos Drakakis<sup>†</sup>  
Princeton University

Dragan Radulović<sup>‡</sup>  
Yale University

October 15, 2018

## Abstract

Internet traffic on a network link can be modeled as a stochastic process. After detecting and quantifying the properties of this process, using statistical tools, a series of mathematical models is developed, culminating in one that is able to generate “traffic” that exhibits –as a key feature– the same difference in behavior for different time scales, as observed in real traffic, and is moreover indistinguishable from real traffic by other statistical tests as well. Tools inspired from the models are then used to determine and calibrate the type of activity taking place in each of the time scales. Surprisingly, the above procedure does *not* require any detailed information originating from either the network dynamics, or the decomposition of the total traffic into its constituent user connections, but rather only the compliance of these connections to very weak conditions.

## 1 Introduction

### 1.1 The problem

The object of this paper is the study of the behavior of Internet traffic, as observed on a network link (typically shared by a large number of network users), aiming to the identification, quantification, and justification of its salient features. Traffic observation here assumes the form of *data traces*, i.e. sequences of the form  $\{(t_i, d_i)\}_{i=1}^N$ , where  $d_i$  is a data quantity (possibly measured in bits, bytes etc.), and  $t_i$  is its *time stamp*, the time when  $d_i$  was observed. Throughout the paper, though, it will be more convenient to use *binned* data traces  $X_i^\Delta, i = 1, \dots, M = \lfloor \frac{t_N}{\Delta} \rfloor$ , with bin size  $\Delta$ , defined as:  $X_i^\Delta = \sum_{\{j|i\Delta < t_j < (i+1)\Delta\}} d_j$ . Our ignorance of the exact procedures taking place in the network, due either to their complexity, or to lack of information, as well as of the behavior of its users, forces us to view  $X^\Delta$  as a stochastic process [5].

This process has been the object of study of numerous researchers. It has unusual and initially unexpected properties, such as long range dependence [2, 7], nonstationarity [6, 9], and different behavior on different time scales [15, 18, 20, 16]. Moreover, even for the coarser time scales, its marginal distributions may be neither Gaussian, nor p-Stable. This is all the more surprising, since the Central Limit Theorems would lead one to expect the opposite, because a) the observed traffic is the aggregate result of many users, possibly acting independently [24, 10, 3] b) each  $X_i^\Delta$  is actually the sum of a large number of  $d_i$ 's, and c) for small time bins, traffic is uncorrelated.

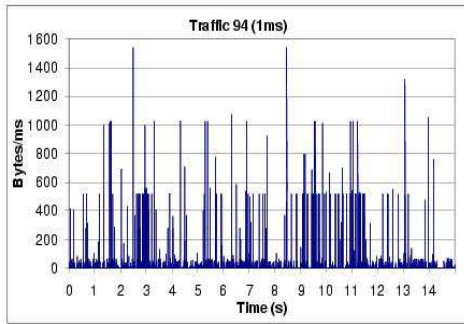
Indeed, despite the fact that “bursts” and “spikes” seem to persist for at least 4 orders of bin magnitude (Fig. 1 and 2), which argues against a Gaussian limit, it can be easily seen, using classical fitting techniques, that the marginal distributions do not possess the characteristic heavy tails of p-Stable variables either; instead, their tails appear to be exponential or Weibull (Fig. 3). Thus, the process seems “unwilling” to converge to any limit, in contrast to most of the processes observed in nature or industry, which do not exhibit this type of “wild” behavior, but rather get “attracted” to the (Gaussian or p-Stable) central limit much sooner (this behavior will be quantified more precisely in section 5 below).

The unusual properties of the traffic are generally attributed to the diversity of user applications, the network protocols, and the complexity of the network topology. Indeed, Internet traffic today is a result of numerous

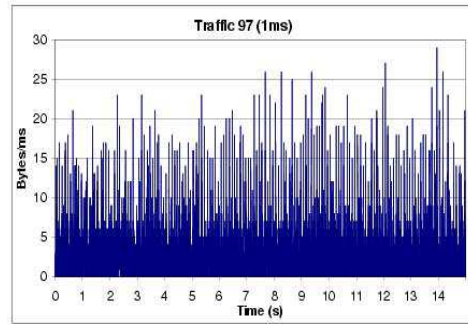
\*A preliminary version of this paper appeared in Proceedings of SPIE Vol. 4868 (2002) under the title: “Some results on the multiresolution structure of Internet traffic traces”.

<sup>†</sup>The author is a scholar of the Lilian Boudouris Foundation.

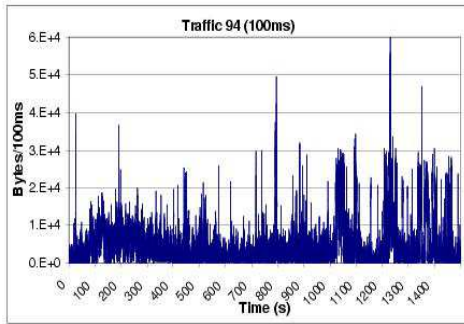
<sup>‡</sup>The largest portion of the research for this paper was conducted while the author was affiliated to Princeton University, and was partially supported by AT&T Research Center.



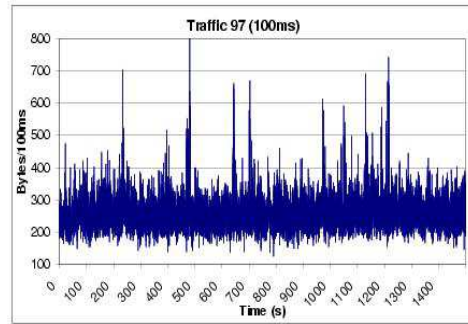
(a)



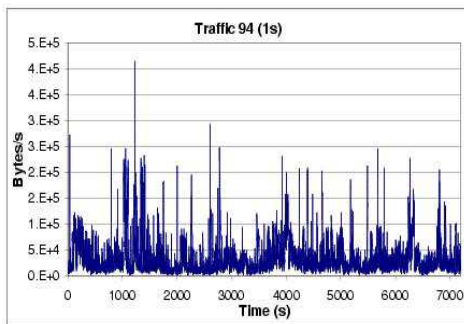
(b)



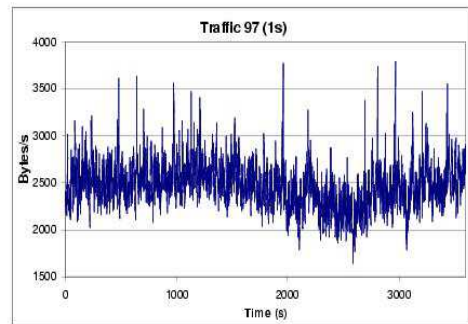
(c)



(d)

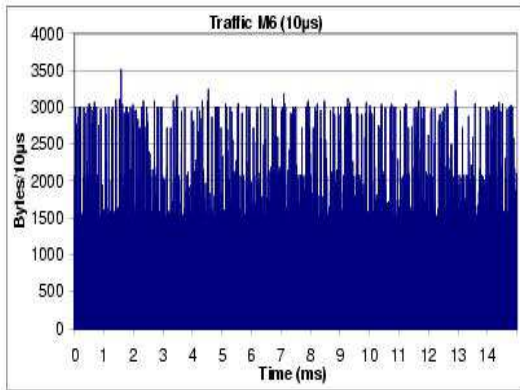


(e)

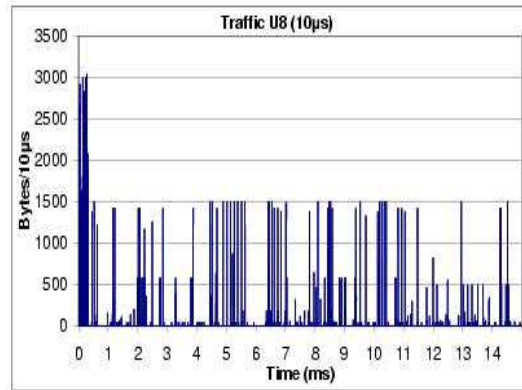


(f)

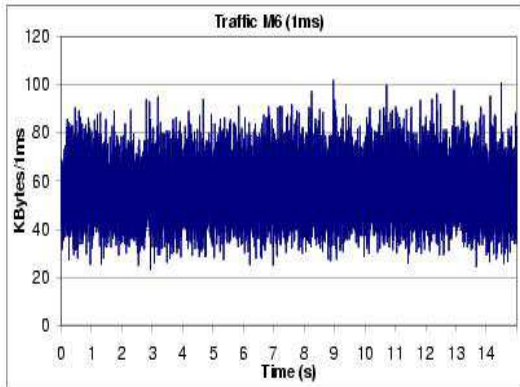
Figure 1: Traces 94 -(a),(c),(e)- and 97 -(b),(d),(f)- binned with 3 different time bins: 1ms,100ms,1s. The data sets 94 and 97 are two of the eight data sets used in this paper; for more details, see section 1.2 below.



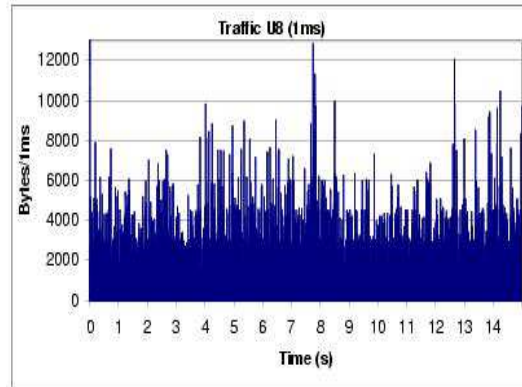
(a)



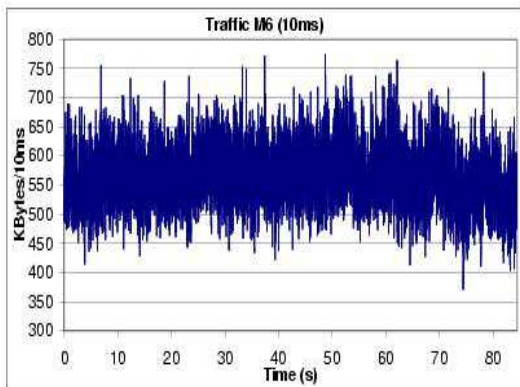
(b)



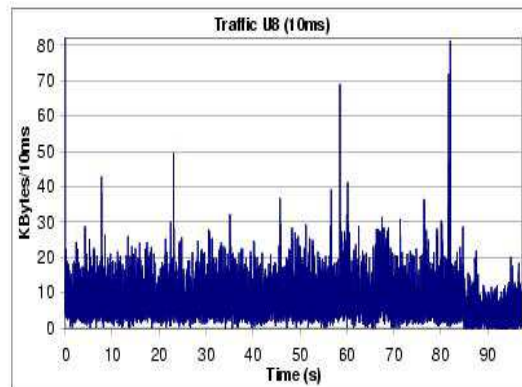
(c)



(d)



(e)



(f)

Figure 2: Traces M6 -(a),(c),(e)- and U8 -(b),(d),(f)- binned with 3 different time bins:  $10\mu\text{s}$ ,  $1\text{ms}$ ,  $10\text{ms}$ . The data sets 94 and 97 are two of the eight data sets used in this paper; for more details, see section 1.2 below.

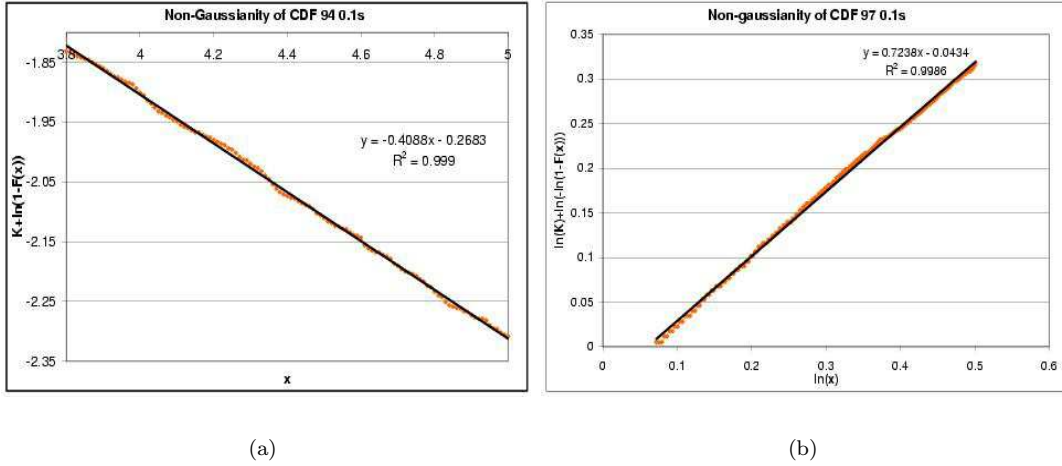


Figure 3: Demonstration of the non-Gaussianity of the marginal CDFs of sets 94 -(a)-, and 97 -(b)-, through least squares fitting: the very high value of R in both cases shows that the curve is essentially linear, and thus that the tail in (a) is exponential and in (b) Weibull. Both sets have been binned using a time bin of 0.1s.

applications: e-mail, WWW, FTP, music and video streams, etc. The duration and the size of the sessions of these applications often vary within several orders of magnitude. Furthermore, the details of the data transfer over the network are regulated by protocols, which control, among other things, the transfer rate at each time instant, and the fragmentation of the data to be transferred into packets. Finally, the transfer rate heavily depends on the state of the network at a particular moment (link availability, congestion, ISP contracts, routing tables,...), which in turn influences (and is influenced by) network topology.

The traffic, though, is typically the result of the activity of a large number of network users. It is expected that many of the features present in each user's own subtraffic will just average out, leaving no trace in the aggregate traffic, whereas others may persist; it is not obvious, however, whether a particular feature will belong to the former, or the latter category.

To sum up, it appears there is a consensus about the factors that shape the traffic, as well as about the inadequacy of the Gaussian distribution for the description of the shape of the traffic. This paper explores how different factors affect the traffic. This necessitates the development of tools that will calibrate the traffic behavior, along with appropriate simulations, on which these tools will be tested.

## 1.2 Description of the data sets and the simulations

This section will provide a short description of both real and simulated traces used. Some of the relevant definitions will be given later.

In what follows, eight data sets (traces), coded 89, 94, 97, L4, L5, M6, M7 and U8 will be used systematically. Data sets 89, 94, L4, and L5 are available on the Web, at <http://ita.ee.lbl.gov/html/traces.html>, and data sets M6, M7, and U8 are also available on the Web, at <http://pma.nlanr.net>. These Web pages also contain extensive information about the data sets. More precisely:

- 89 is the trace BCP-Aug89, and it contains “one million packet arrivals seen on an Ethernet at the Bellcore Morristown Research and Engineering facility”. It was collected on AUG 29, 1989, starting at 11.25, and lasts approximately 3,143 seconds. It is by far the oldest trace used here. The volume exchanged is approximately 434 MB.
- 94 is the trace LBL-TCP-3, collected on JAN 20, 1994, between 14.10 and 16.10. The volume exchanged is approximately 244 MB.
- L4 is the trace LBL-PKT-4, collected on Jan 28, 1994, between 14.00 and 15.00. The volume exchanged is approximately 131 MB.

- L5 is the trace LBL-PKT-5, collected on Jan 28, 1994, between 15.00 and 16.00. The volume exchanged is approximately 94 MB.
- 97 contains 1 hour of the total traffic of users subscribing to WorldNet via modems, measured at the WorldNet gateway, on JUL 22, 1997, starting at 22.00, and using a time bin of 1ms. The volume exchanged is approximately 9 MB.
- M6 is the trace MRA-1015686621-1, collected on MAR 09, 2002. Approximately, it lasts for 81 seconds, and the volume exchanged is 4.8 GB.
- M7 is the trace MRA-1015764522-1, collected on MAR 10, 2002. Approximately, it lasts for 82 seconds, and the volume exchanged is 3.7 GB.
- U8 is the trace ODU-1015816310, collected on MAR 11, 2002. Approximately, it lasts for 89 seconds, and the volume exchanged is 76 MB.

For data sets 89 and 97, information on their individual connections is not available.

The sizes and dates of the traces described span quite a broad range: some of them contain only a few MB of information, whereas others contain 1000 times as much; some are extremely recent, whereas others are more than a decade old. This variety will allow for the examination of the properties of the traffic, and for their validation, in general or specific network conditions.

A set of simulated traces will also be used: 0-1 is a self-similar process with continuous ON/OFF intervals (as in [24]) and will be the outcome of model A below; ARR (standing for ARRival process) takes into account the fragmentation of the information to be transmitted into packets (model B below); RH (standing for Random Heights) is the reward model, and RH HT (standing for Random Heights + Heavy Tails) is the  $\alpha - \beta$  traffic model described in [23]; ARRRH (standing for ARRival process with Random Heights) is a combination of RH and ARR; EXP IID is a sequence of i.i.d. exponential variables, and, similarly, HT IID is a sequence of heavy-tailed i.i.d. variables. Finally, a model that combines ARR with the new idea of “levels”, introduced in section 6, will also be used; its simulations will be labeled by the time scales of the levels, and an S will be added if the levels are “sharp”, e.g. 8, 12S, 7S/12/17 etc (see section 6).

### 1.3 The State of the Art

As a result of the intensive research on Internet traffic, many models have been proposed. A requirement imposed was that they be *parsimonious* [2]: they should use a very limited set of parameters, as opposed to the millions of details present in a real network. In what follows, some of the most common ones will be presented and discussed.

**The Self-Similar Model (SSM):** This is perhaps the simplest model conceptually. Its main assumption is that each of the  $n$  users generates a data stream or connection  $W_i(t)$ ,  $i = 1, \dots, n$ , the traffic being their sum:  $X(t) = \sum_{i=1}^n W_i(t)$ ,  $t \in \mathbf{R}^+$ . The users are supposed to act independently, and the data streams are composed of intervals of value 0 (where the user is silent), alternating with intervals of value 1 (where the user sends data), whose lengths are random, independent, and cross-independent. The degrees of freedom of this model then are just two: the distributions of the lengths of the aforementioned intervals. If chosen appropriately, e.g. *heavy-tailed*<sup>1</sup> distributions are allowed, they can lead to *self-similar* simulated traffic [24] For a more precise statement, see Theorem A (Section 3).

The self-similarity of the traffic, and the heavy-tailed distributions of the intervals of silence and/or activity for each user, have been verified in real traces. The violation of the traditional Poisson model [1, 8], and the long range dependence, i.e. slowly decaying autocorrelation (illustrated in Fig. 8 and 9 in section 3), which are both consequences of the heavy tail distributions, are perhaps the most striking results. However, this model is not entirely successful: the traffic it produces is not as “spiky” as real traffic (Fig. 4). Moreover, the *Energy function*, which gives, for each time scale, the contribution of the behavior at that scale to the total energy (more details in Section 2, or [15, 16]), can clearly distinguish between the simulation and the real traffic. For the simulation, the Energy function gives a straight line, whereas the Energy function of the real traffic curves (see Fig. 6 below, summarizing the Energy for data as well as simulations according to several models).

<sup>1</sup>A distribution will be henceforth called *heavy-tailed* iff its variance is infinite, otherwise it will be called *light-tailed*. This definition differs slightly from the one implied in [8].

The “curving of the Energy function” for Internet traffic traces has played an important role as a motivation for certain models of Internet data traffic, ever since its first observation in [15]. It will be used as one of the cornerstones of this work as well. As Section 2 will explain, though, a slightly different definition for the Energy function than the one in 2 will be used; the Energy function herein used is the average of the translation non-invariant concept in 2 over all possible choices of the “origin” ( $t = 0$  plays a special role in 2). This is similar to averaging procedures in many other applications of wavelet expansions. The result is that the Energy function, as defined in this paper, remains reliable even for very large scales (whereas the standard Energy function produces large oscillations and becomes unreliable for scales above 15 in Fig. 6), making it possible to observe and quantify the “curving” or “bumpiness” of the Energy function even at these large scales. The issue will be further analyzed in Section 6.

In this paper, simulations according to this model (our model A) will bear the label “0-1”.

**Reward Model (RM):** In an attempt to make the SSM “spikier”, it was proposed [10, 11] to change the values of ON-intervals from 1 to some positive random value, which would be kept constant throughout the interval, values of different intervals being independent. This would reflect the non-equivalence of the users, in terms of the amount of data they can send: some may have faster connections, may run applications generating higher volumes of data etc. Needless to say, the distribution of values for the ON-intervals can be itself heavy-tailed. A result proved for this model states that, in the limit of infinite users, the (properly normalized) total traffic can be either a self-similar or a  $p$ -Stable process [22].

This model resembles real traffic a bit better (compare Fig. 4 and 1), however the two types of traffic can still be discriminated visually. Moreover, the marginal distribution of a part of the traffic generated by this model will always be either  $p$ -Stable or Gaussian, whereas in the case of the real traffic different parts may have different marginals (see Fig. 12 in section 4). Also, heavy-tailed value distributions lead to very high spikes, while distributions of finite second mean average out in the limit, leading to the same results as SSM (Fig. 4 (b),(d), and (f)). Thus, the model does not allow for very fine control of the form of the spikes. In addition, its Energy function is once more a straight line, but an additional risk is that it can be *meaningless*, in the case of a heavy-tailed value distribution (see Section 2). Finally, as noted earlier, real traffic *does not have heavy-tailed spikes*.

In this paper, simulations according to this model (our model B) will bear the label “RH”.

**$\alpha$  and  $\beta$  Traffic model:** This model, proposed and studied in [23], adopts a different approach, decoupling the spikes and the main body of the traffic, and dealing with each of the two separately. It suggests that Internet traffic can be viewed as a superposition of two independent processes: the first ( $\beta$  traffic) is self-similar Gaussian, and has no spikes, the second ( $\alpha$  traffic) is a train of isolated spikes. The inter-spike intervals are independent and approximately exponential, i.e. spike arrivals are approximately Poisson.

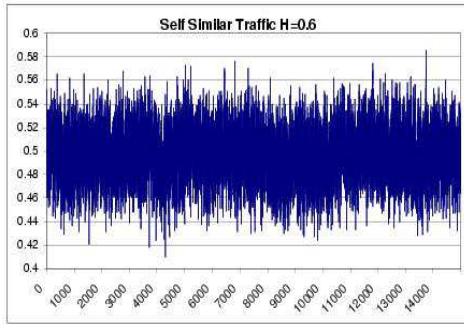
This model was derived from, and calibrated on real traffic traces, and all of the assumptions above were shown to hold. No distribution for the spike heights was proposed in [23]; motivated, however, by the observed exponential marginals of the traces considered here, we will be using an exponential one in the simulations. The result of the simulation and the real traffic are almost indistinguishable visually (compare Fig. 5, 1 and 2). An example with a  $p$ -Stable distribution is also provided.

To sum up,  $\beta$ -traffic accounts for the long range dependence, and  $\alpha$ -traffic for the spikes. Thus, the model matches, to some extent, the appearance, and the slowly decaying autocorrelation of the real traffic (Fig. 8 and 9). Even better, the marginal distributions of parts of the traffic oscillate between Gaussianity and  $p$ -Stability, a feature shared by real traffic [23]. Unfortunately, the Energy function of the simulation is again oversimplifying reality (Fig. 6).

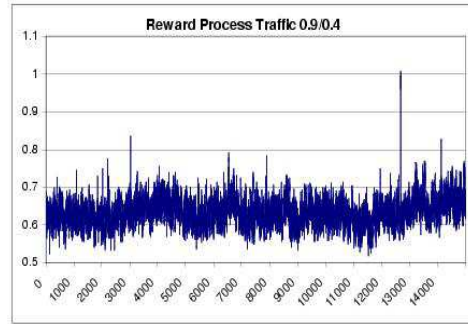
Simulations according to this model will bear the label “RH HT”.

**Infinite Source Poisson Model (ISPM):** This is a variant of the SSM. According to this model, the traffic is the sum of independent piecewise continuous connections, whose range is  $\{0, 1\}$ , and whose support is compact and connected. The beginning points of their supports are given by a Poisson process of rate  $\lambda$ , and their sizes by a heavy tailed distribution of infinite variance (see [29] and references therein for more details).

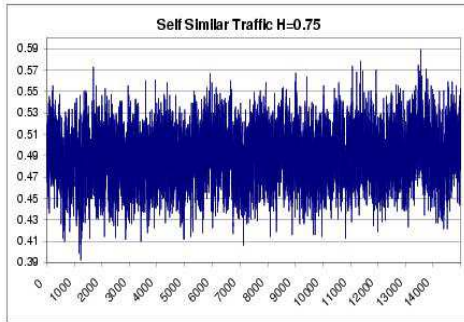
Obviously, the support of the total traffic consisting of a finite number of connections is also finite; thus, contrary to the SSM, this model evolves in time, as the number of connections  $n$  increases. In order to capture this evolution, the traffic can be normalized in time by a parameter  $T$ , which denotes time resolution, i.e. the time scale at which traffic is viewed. If the two limits  $n \rightarrow \infty$  and  $T \rightarrow \infty$  are taken simultaneously, the limit process can be either



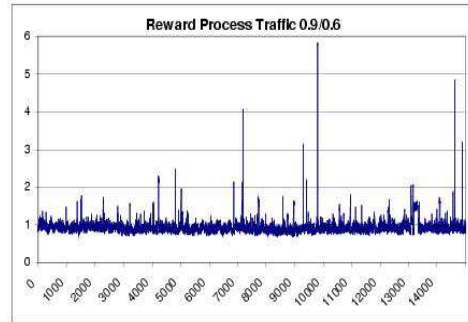
(a)



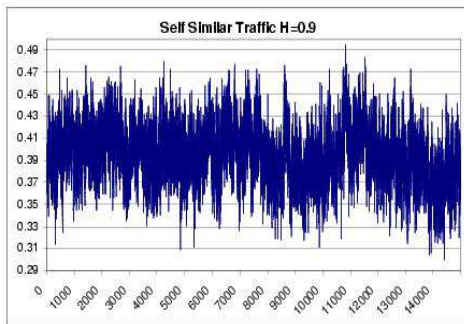
(b)



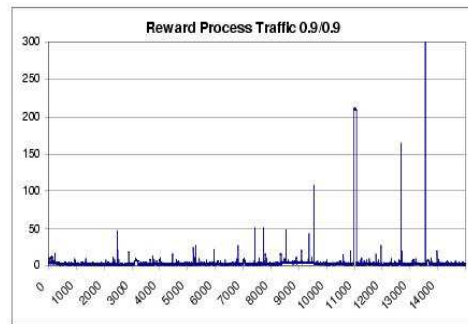
(c)



(d)



(e)



(f)

Figure 4: Three instances of a Self-similar and a Reward process: the durations of the ON intervals and, in the latter case, the height of the ON intervals, are distributed according to  $\frac{1}{x^H}$ ,  $x \sim U(0, 1)$ . (a),(c),(e) features  $H = .6, .75$ , and  $.9$ , respectively, whereas in (b),(d),(f)  $H = .9$  fixed for the ON-interval lengths, and  $H = .4, .6, .9$  for the heights, respectively. OFF-intervals are exponentially distributed with mean equal to their corresponding ON-intervals.

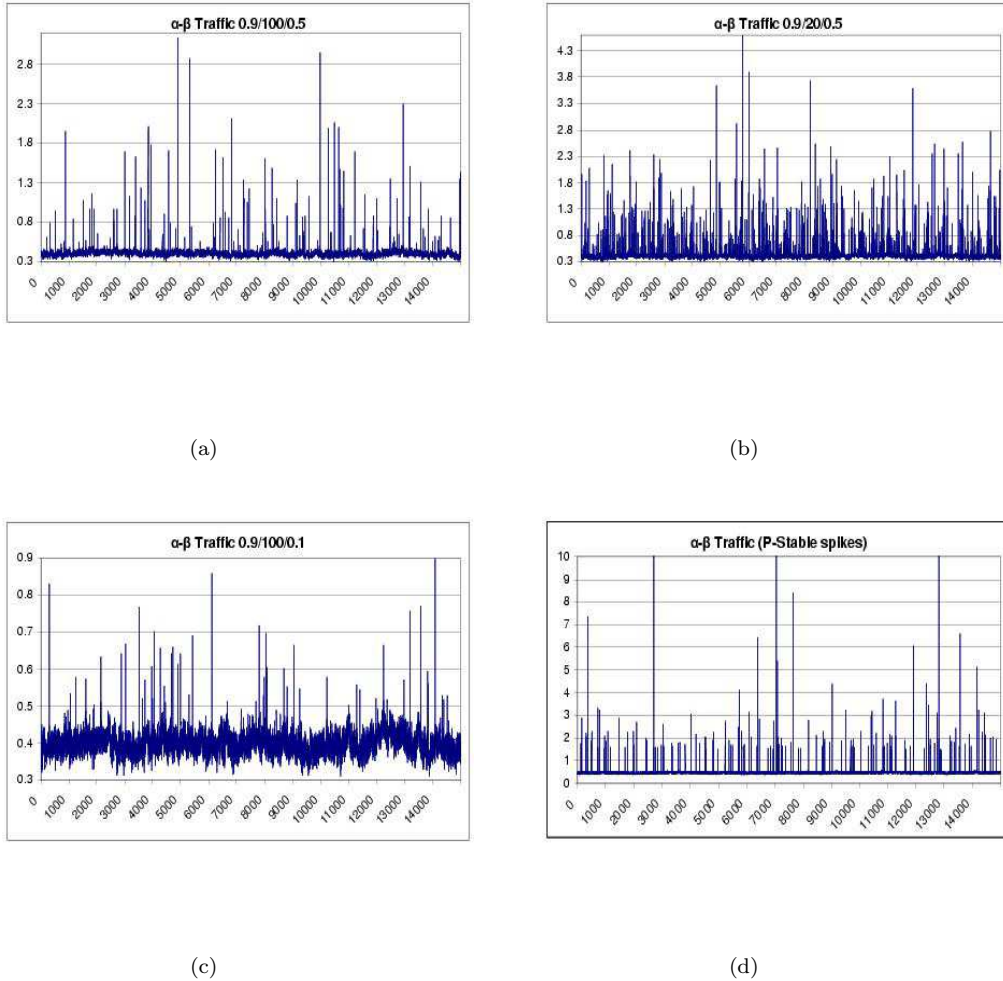


Figure 5: Traffic generated by the  $\alpha$  and  $\beta$  model: (a), (b), and (c) feature spikes with exponentially distributed heights (with mean 0.5, 0.5, and 0.1 respectively) and exponentially distributed interarrival times (with means 100, 20, and 100 respectively). (d) features p-Stable spikes having exponential interarrival times with mean 100. For the  $\beta$  traffic, the same model was used as in Fig. 4, with  $H = .9$ .

Gaussian or p-Stable, depending on their relative rates (see the discussion in [29]). This behavior will appear again in Section 5.

Unfortunately, it seems that this limit process cannot be linked back to real traffic in an obvious way.

It is very striking that the Energy function for these four models are very linear (as shown in Fig. 6, at least up to scale 15; at coarser scales, Fig. 6 is no longer accurate, but the modified definition of the Energy function given in Section 2, which remains accurate at large scales, the linearity is seen to persist until even the coarsest scales). Indeed, as many authors (including us) have found, “local” models (in which the traffic is generated as an average over simulated sessions “unrolling” in time) typically produce such nice, linear, but therefore unrealistic Energy functions.

Although each of the models is represented by a single simulation only in Fig. 6(b), we did in fact check many values for the parameters of these models; for other parameter values, one finds a change in the slope of the corresponding Energy function but not in its essentially linear character.

In simulations for the models listed above, the features of the model seem to control only the slope, or, at best, introduce only one slope change from one scale onwards (Fig. 6). Moreover, the Energy function appears to be

insensitive to the “spikiness” of the process (compare EXP IID with HT IID in Fig. 6(b)), although it seems to depend on the autocorrelation.

The failure of these models to produce curved Energy functions stimulated researchers to seek more “exotic” models, such as cascades, and multifractal processes in general [21, 22, 15, 3]. These models, however, are not linked in any way to a description of user or connection behavior.

**Multifractal models:** Multifractal models, unlike all of the preceding models, produce curving Energy functions [15]. They also produce nontrivial *multifractal spectra* [22]. The simplest representatives of this category are the *random cascades* [15, 22]. However, in our view, these models are “global” rather than “local”: the stochastic process that generates the simulated sessions is not inspired by network mechanisms or user characteristics, or the structure of these in time. To the contrary, these processes typically treat the whole observation time interval as an entity, and link probabilities of certain behavior in a subinterval to the probability of other behavior elsewhere, without any motivation, other than that it produces Energy functions similar to those observed in real traces. Since they do not take into account network mechanisms, at least in a straightforward manner, they offer little help towards understanding these mechanisms. For this reason they will be considered no further here.

**Network simulation models:** These models adopt a completely different point of view, trying to incorporate into the model every single detail of the routers, the links, the protocols etc. Examples are the Network Simulator and (NS)(see [14] and references therein), and the Scalable Simulation Framework (SSF) (see <http://www.ssfnet.org/homePage.html> for more information). As expected, they produce very good results, but the overwhelming number of parameters violates the parsimony principle, and makes it hard to estimate the impact of each of them on the traffic. For these reasons, this approach falls outside the scope of the present paper.

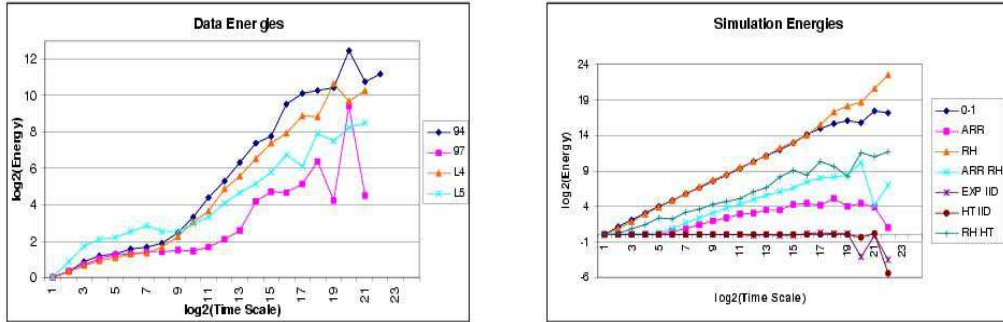
**Summary:** In the list of models above, some follow an empirical approach, which attempts to capture properties of the traffic, but ignores the underlying mechanisms ( $\alpha - \beta$  Traffic, Random Cascades); others present mathematical constructions that are motivated by network and user behavior, but produce traffic that only partially corresponds to reality (SSM, RH). As far as we know, there exists no model that produces traces a) that have the spikiness and long-range dependence of real traffic traces, b) whose marginals match the behavior of the observed marginals, which are sometimes close to and at other times deviate far from Gaussianity, and c) with a curving Energy function. Obtaining a curving Energy function via a “local” model seems particularly hard: extensive experimentation by the authors with simulations of the models described above and in Section 1.2 always produced linear, or at best essentially piecewise linear graphs (as in Fig. 6(b) and 26(a)), except for our model D described in Section 6.

Random Cascade models do produce curving Energy functions; they are however not satisfactory, not only because they offer no explanation of the underlying mechanism, relating to network protocols or user behavior, but also because the resulting traffic still contradicts real traces in various other aspects (auto-correlation, marginal distributions etc.).

## 1.4 Summary of our results

The purpose of this paper is to present a model that describes Internet traffic on a network link; the main guideline in the construction of this model will be the incorporation, into the SSM, of additional network mechanisms and aspects of user behavior that will be identified as responsible for shaping the traffic. It will turn out that enriching the SSM with only a few extra features leads to simulations exhibiting spikiness (i.e. marginals), long-range dependence, curving of the Energy function, and wide oscillations in the deviation of its marginals from Gaussianity that are qualitatively and quantitatively indistinguishable from the same features of real traces. The impact of these features on the traffic will be rigorously determined by means of theorems, and the predictions of these theorems will be subsequently validated against real traffic. The success of this validation will suggest that the factors that have been identified as important for shaping the traffic are indeed important, and may explain the behavior of the real traffic singled out by the four criteria above.

In order to increase clarity, the construction will proceed incrementally in 4 steps, labeled A, B, C, and D. At each step, a theorem will state and prove the properties of the model built so far. Step A will be the plain old SSM; step B will take into account that information transmission does not take place continuously, but rather in packets spaced apart by variable time intervals, which in turn are determined by the Round Trip Times; step C will then introduce the Slow Start feature of the TCP protocol into the model, arguing that the small volume of information



(a)

(b)

Figure 6: Energy functions, according to the standard definition (Definition 1 in Section 2, for (a) data and (b) simulations). They are normalized up to an additive constant, so that they all start at 0. Notice that the Energy functions in (b), corresponding to the simulations described in Section 1.2, are approximately linear. Notice also the large oscillations at coarse time scales, caused by a lack of accuracy at coarse scales; Definition 2 will take care of this. Finally, note that HT IID and 0-1 produce indistinguishable results, although they have completely different properties.

exchanged by the majority of the connections is such as to allow Slow Start to impact the traffic heavily; and, finally, step D will enrich the model with other, longer time scales, characteristic of network activity, originating from either user behavior (e.g. switch of application), or protocol actions (e.g. congestion control).

**Step A:** The basic model, which will serve as the founding ground for the rest, will be the SSM, introduced and studied in [24]. Theorem A states and proves its properties.

**Step B:** Here, a finer structure will be imposed upon the ON-intervals of the SSM: each value of 1 will be followed by a RTT, and RTTs will be modeled by means of random variables. In general, little is known about their distribution [12, 14], but in large capacity links of the Internet backbone, packet interarrival times tend to be exponentially distributed and independent [9]. Fortunately, this is not a serious issue, since Theorem B below asserts that the simulated traffic is insensitive to this distribution, as long as it has finite variance. Moreover, Theorem B states that the traffic is actually Gaussian, and fairly uncorrelated at small time scales (Brownian motion), but that the correlation grows stronger in larger time scales (causing the process to become self-similar); this prediction is borne out by real data (Fig. 8 and 9).

**Step C:** This step incorporates features of the TCP/IP combination of protocols, responsible for the bulk of data transfer over the Internet today, into the model. One of the characteristics of TCP, the *Slow Start*, roughly stipulates that the number of packets sent at each emission time increases *geometrically* by a factor of 2 (1,2,4,8,...), until either loss occurs, a preset maximum is reached, or all data is sent (for more details, see e.g. [25]). In detailed traces, which show individual connections, the Slow Start is easily discernible; this suggested its incorporation in the model, and the exploration of the consequences of its inclusion. Theorem C states that the traffic will tend to be either self-similar or p-stable, contingent upon the Slow Start maximum and the number of users. In practice, p-Stability cannot be distinguished from other very large deviations from Gaussianity, since observations can only last for a finite amount of time. Nevertheless, the fluctuation of the number of active users in time will allow for both self-similar regimes and regimes that deviate far from this self-similar behavior within the same trace, as is also observed in real traces. An increase of the number of users steers the process towards self-similarity.

**Step D:** User connections over the Internet seem to be governed by a hierarchy of time scales (*levels*); for example, a particular session of data 94 seems to live in six different time scales (Fig. 17), at approximately 2000, 500, 100,

40, 5, and 0.1s, and a session of trace M6 in three different time scales (Fig. 18), at approximately 2, 0.4, and 0.01s. To the best of our knowledge, there has been no effort yet towards the exact quantification and explanation of these levels at different scales, but it is commonly accepted that they exist [1, 3, 18]. A possible explanation could lie in the recursive structure within Internet applications (e.g. Web browsers opening multiple sessions, FTP applications establishing multiple connections, etc., TCP, which sends and waits for receipt acknowledgement, etc.), and the human work habits, according to which tasks are broken into subtasks recursively. Analysis of 50 typical (long enough) sessions of trace 94 reveals that levels are present in all of them, and are more or less similar. Moreover, their statistical properties (mean duration, variance, and range) are similar for other traces of the same time period.

So far, model A had just 1 level, and models B and C each had 2 levels. This step introduces more levels, at larger time scales. Theorem D then proves that such levels cause the Energy function to curve.

The paper is organized as follows: Section 2 describes the statistical tools used (including the modified definition of the Energy function), and sections 3, 4, 5, and 6 deal with models A,B,C and D respectively. Section 7 concludes the paper with a discussion and some applications; in particular, several simple tools are introduced that detect the presence and number of levels, and that quantify the behavior of the traffic.

## 2 Statistical Tools

Let  $\{X_k\}_{k=1}^n$  represent a time series. In what follows, extensive use of three standard statistical tools will be made:

1. Empirical marginal distributions:

$$F_n(t) = n^{-1} \sum_{i=1}^n 1_{X_i \leq t}$$

2. Autocorrelations:

$$Corr(k) = \frac{\sum_{i=1}^{n-k} (X_i - \bar{X}_n)(X_{i+k} - \bar{X}_n)}{\sum_{i=1}^n (X_i - \bar{X}_n)^2}$$

where  $\bar{X}_n = \frac{1}{n} \sum_{i=1}^n X_i$

3. The *Kolmogorov distance* between two Cumulative Density Functions (CDFs), which is defined as the maximum of the absolute value of their difference:

$$d_K(F_1, F_2) := \sup_{x \in \mathbb{R}} |F_1(x) - F_2(x)| \quad (1)$$

In addition, the Energy function will be used, as well as a more intuitively appealing (in our opinion) variant, the *p-Averaging function* (similar to the Normalized Variance appearing in [1]), introduced below.

The definition of the *p-Averaging function* will be completed in two steps: initially, a definition that ensures compatibility with the well established Energy function [15, 16] (in a sense to be made clear below) will be proposed. Then, a simple observation will lead to the redefinition of both Averaging and Energy functions.

**Definition 1.:** Given a stationary sequence  $\{X_i\}_{i=1}^M$ , for some  $M = 2^m$ , define

$$\begin{aligned} X_k^j &= 2^{-j} \sum_{i=(k-1)2^j+1}^{k2^j} X_i & j = 0, \dots, m & \quad k = 1, \dots, 2^{m-j} \\ m_k^j &= \left| X_{2k}^j - X_{2k-1}^j \right| & j = 0, \dots, m-1 & \quad k = 1, \dots, 2^{m-j-1} \\ \tilde{X}_k^j &= 2^{-j/2} \sum_{i=(k-1)2^j+1}^{k2^j} X_i & j = 0, \dots, m & \quad k = 1, \dots, 2^{m-j} \\ d_k^j &= \frac{1}{\sqrt{2}} \left| \tilde{X}_{2k}^j - \tilde{X}_{2k-1}^j \right| & j = 0, \dots, m-1 & \quad k = 1, \dots, 2^{m-j-1} \end{aligned}$$

For  $M_j = M/2^{j+1}$  and  $p > 0$ , define the **p-Averaging**

$$A_{j+1}^{[p]} = \left( \frac{1}{M_j} \sum_{k=1}^{M_j} (m_{j,k})^p \right)^{1/p}$$

and the **Energy**

$$E_{j+1} = \frac{1}{M_j} \sum_{k=1}^{M_j} (d_{j,k})^2, \quad j = 0, \dots, m-1$$

Notice the connection of this definition of the Energy function to the Haar wavelet coefficients as in [15, 16]. If  $p = 2$ , the relation between the two functions is elementary:

$$\log_2(E_j) = j - 2 + 2 \log_2 A_j^{[2]}, \quad j = 1, \dots, m$$

In the sequel,  $A_j^{[2]}$  will be used almost exclusively, because it is easier to analyze, and simply connected to the commonly adopted  $E_j$ ; it will be indicated just by  $A_j$  and referred to simply as *Averaging (function)*. When  $p \neq 2$  is considered, it will be stated explicitly.

This set of definitions has been motivated by the following heuristic:

**Heuristic:** Let  $X_i$  represent the value of the traffic for the  $i$ th time bin, taken to be the *initial* time bin, and assume the sequence is ergodic, (i.e.  $\frac{1}{n} \sum_{i=1}^n X_i \rightarrow EX_1$ ). What is the rate of this convergence? The way to determine

the rate is to find a function  $\psi(n)$  such that  $\psi(n) \sqrt{\mathbf{E} \left( \left| \frac{1}{n} \sum_{i=1}^n X_i - EX_1 \right|^2 \right)} \xrightarrow{n \rightarrow \infty} 1$ . Typically, the function  $\psi$  is increasing in  $n$ , at least for  $n$  sufficiently large, expressing the fact that the average  $\frac{1}{n} \sum_{i=1}^n X_i$  gets closer to  $\mathbf{E}(X_1)$  when  $n$  increases. In practice, because  $\mathbf{E}(X_1)$  is unknown, one can still get a handle on  $\psi$  by comparing two different averages:

$$\begin{aligned} \mathbf{E} \left( \psi^2(n) \left| \frac{1}{n} \sum_{i=1}^n X_i - \frac{1}{n} \sum_{i=1}^n X_{i+n} \right|^2 \right) &= \psi^2(n) \mathbf{E} \left( \left| \left( \frac{1}{n} \sum_{i=1}^n X_i - \mathbf{E}(X_1) \right) - \left( \frac{1}{n} \sum_{i=1}^n X_{i+n} - \mathbf{E}(X_1) \right) \right|^2 \right) = \\ &= \psi^2(n) \mathbf{E} \left( \left\{ \left| \frac{1}{n} \sum_{i=1}^n Y_i \right|^2 + \left| \frac{1}{n} \sum_{i=1}^n Y_{i+n} \right|^2 - 2 \left( \frac{1}{n} \sum_{i=1}^n Y_i \right) \left( \frac{1}{n} \sum_{i=1}^n Y_{i+n} \right) \right\} \right)^* = \\ &= \frac{\psi^2(n)}{n^2} \left\{ \sum_{i=1}^n \sum_{j=1}^n \mathbf{E}(Y_i Y_j) + \sum_{i=1}^n \sum_{j=1}^n \mathbf{E}(Y_{i+n} Y_{j+n}) - 2 \mathbf{E} \left( \left( \sum_{i=1}^n Y_i \right) \left( \sum_{i=1}^n Y_{i+n} \right) \right) \right\}^{**} = \\ &= 2 \frac{\psi^2(n)}{n^2} \left\{ \sum_{i=1}^n \sum_{j=1}^n \mathbf{E}(Y_i Y_j) - \sum_{i=1}^n \sum_{j=1}^n \mathbf{E}(Y_i Y_{j+n}) \right\} = 2 \frac{\psi^2(n)}{n^2} \left\{ \sum_{i=1}^n \sum_{j=1}^n [\mathbf{E}(Y_i Y_j) - \mathbf{E}(Y_i Y_{j+n})] \right\} \quad (2) \end{aligned}$$

where  $Y_i = X_i - \mathbf{E}(X_1)$  was set. In (\*\*) we used stationarity. Notice also that (\*) proves that  $0 \leq \lim(2) \leq 2$ .

We claim that, if the  $X_i$  are *asymptotically independent*, i.e.  $\forall i, \mathbf{E}(X_i X_{i+j}) - \mathbf{E}(X_1)^2 = \mathbf{E}(Y_i Y_{i+j}) \rightarrow 0$ , as  $j \rightarrow \infty$  (irrespectively of the rate), then (2) has a *strictly* positive limit, and, therefore, that it can be used to estimate  $\psi$  (within a multiplicative constant). Because asymptotical independence is satisfied by most processes arising in applications (it is extremely unlikely that two random variables arbitrarily long apart will exhibit strong dependence), this method can be applied to a wide range of processes, and is, for this reason, very powerful.

Indeed, as  $n \rightarrow \infty$ , for fixed  $i, j$ ,  $\mathbf{E}(Y_i Y_{n+j}) \rightarrow 0$ , and therefore it becomes infinitely smaller than  $\mathbf{E}(Y_i Y_j)$ . The RHS of (2) shows then that the limit has to be strictly positive.

Thus, if a random variable  $\epsilon_k^j$  is defined by:

$$\epsilon_k^j = \psi(2^j) \frac{1}{2^j} \left| \sum_{k2^{j+1}}^{(k+1)2^j} (X_i - \mathbf{E}(X_1)) \right| = \psi(2^j) |m_{j,k}|$$

then

$$A_{j+1} = \left( \frac{1}{M_j} \sum_{k=1}^{M_j} |m_{j,k}|^2 \right)^{1/2} = \frac{1}{\psi(2^j)} \left( \frac{1}{M_j} \sum_{k=1}^{M_j} |\epsilon_k^j|^2 \right)^{1/2} \approx \frac{C}{\psi(2^j)}$$

If  $M_j$  is large,  $A_{j+1}$  gives us a way to estimate  $\psi(2^j)$ . In particular, if  $\psi(n) = n^\alpha$ , then:

$$\log_2 A_{j+1}^{[p]} = K - \alpha j \text{ and } \log_2 E_{j+1} = 2K - 1 + j(1 - 2\alpha)$$

Therefore, the binary logarithms of the Averaging resp. Energy functions of the processes that “average” with a rate of  $n^{-\alpha}$  will be straight lines with a slope of  $-\alpha$  resp.  $1 - 2\alpha$ . Throughout the paper, the “curvature of the Energy or Averaging function” will refer to the curvature of their binary logarithms, plotted as functions of  $j$ .

**Remark 1.:** In the case of processes with a  $p$ -Stable component (heavy tailed marginals), the Energy function, as well as the  $A_j^{[p]}$ ,  $p \geq 2$ , are not well defined: their expected value is infinite, because the  $\epsilon_k^j$  do not have a second moment. This is the reason why the Energy function fails to distinguish spiky processes (with heavy tailed marginals) from ordinary white noise processes, as shown in Fig. 6(b), where the EXP IID simulation, which is very close to white noise, and the heavily spiky HT IID simulation are seen to have the same Energy function. The few experiments related to distributions with heavy-tailed marginals will be performed with  $p = 1$ .

**Remark 2.:**  $A_j$  has another interpretation that will prove essential later. Namely:

$$\begin{aligned} A_{j+1} &= \sqrt{\frac{1}{M_j} \sum_{k=1}^{M_j} (m_k^j)^2} \approx \sqrt{\mathbf{E} (m_1^j)^2} \\ &= \frac{1}{2^j} \sqrt{\mathbf{E} (X_2^j - \mathbf{E}X_2^j + \mathbf{E}X_1^j - X_1^j)^2} = \frac{\sqrt{2}}{2^j} \sqrt{\text{Var} (X_1^j) - \text{Cov} (X_1^j, X_2^j)} \end{aligned}$$

Applied to the process  $X_i := \frac{1}{\Delta} \int_{i\Delta}^{(i+1)\Delta} \frac{1}{\sqrt{n}} \sum_{l=1}^n W_l(t) dt$ , the above computation yields

$$A_{j+1} \approx K \sqrt{\frac{\text{Var} \left( \int_0^{2^j \Delta} W_1(t) dt \right) - \text{Cov} \left( \int_0^{2^j \Delta} W_1(t) dt, \int_{2^j \Delta}^{2^{j+1} \Delta} W_1(t) dt \right)}{2^j \Delta}}$$

for some positive constant  $K$ , which also absorbs  $n$ , as it is now fixed. This formula connects the Energy/ $p$ -Averaging function of the total traffic to the behavior of one user, who will be “typical” in the mathematical sense.

**Remark 3.:** Although the name “ $p$ -Averaging” may appear to be inappropriately chosen at first sight, it actually describes well the fundamental principle of the function, which may be buried under its complicated definition.

The  $p$ -Averaging function endeavors to measure the rate of convergence of averages of  $n$  consecutive points of the process to its true mean, as  $n$  increases, where “rate of convergence” denotes the deviation between the  $n$  point mean value estimator and the true mean. Unfortunately, the true mean is unknown. One way to circumvent this problem is to measure the rate by which two  $n$  point estimators converge to each other; the two aforementioned convergence rates should be essentially the same, their relative difference being at most 2 at all times (see the related discussion in the Heuristic above).

This basic idea will then subsequently be elaborated in Definition 2 below, which ensures that the rate gets measured accurately, by comparing a large number  $N$  of pairs of  $n$  point estimators,  $n$  increasing geometrically, and, in addition, that it gets measured equally accurately for all  $n$ , by making  $N$  independent of  $n$ . These details aside, though, it is clear that the  $p$ -Averaging function “averages” the traces in order to estimate their mean, or rather how difficult it is to estimate their mean, hence the name “Averaging function”.

It has been implicitly assumed, of course, that  $X_i$  is stationary. Although there are many arguments against Internet traffic being stationary, it can be assumed to be so over reasonably short time intervals. This could mean a couple of hours, according to [9]), so the older data sets (before 1997), with a duration of at most 2 hours, can be considered to be stationary. The more recent ones only last for less than 2 minutes, but they are also the products of a much faster network. Are they also stationary? We give two reasons why we believe they are: a) Non-stationarities, such as the diurnal day cycle, that are an artifact of human activity, do not become faster, as the network gets faster. b) In the older traces, consecutive packets in the link seem to be 0.1ms apart, whereas in the newer traces they seem to be  $1\mu\text{s}$  apart, in order of magnitude, i.e. the network has become faster by approximately 100 times. So, what needed an hour before needs now approximately a minute, and thus the duration of the old and new traces, normalized by the network speed, is the same.

Under the definitions above, the computation at the scale  $2^j$ , for either the Energy or the Averaging functions, involves a mean value over  $2^{m-j-1}$  numbers. Consequently, for  $j$  close to  $m$ , the sum will comprise insufficiently many terms to produce a reliable mean, assuming that such a mean is indeed the ultimate goal of the computation, and undesirable oscillations may be observed (see Fig 6). Instinctively, it is expected that averaging over more numbers will lead to smoother curves. Thus, a modification of the definition of the Energy and  $p$ -Averaging functions is in order; the definition that follows will allow for averaging over the maximum number of terms possible, i.e.  $2^{m-1}$ , by using a standard technique of statistics, known as *overlapping blocks*.

From the point of view of wavelets, the definition change amounts to averaging the Energy function computations over all possible choices of the “origin” for the Haar basis underlying the definition of the  $d_{j,k}$ ; this type of averaging is now commonly done in situations where the use of a wavelet basis introduces a translation non-invariance that was not present earlier.

**Definition 2:** The operator  $\frac{1}{M_j} \sum_{i=1}^{M_j}$  in the above definitions will be formally replaced by  $\mathbf{E}$ , the expectation operator. Moreover, for reasons of clarity, the domain of  $A$  will be shifted left by 1, i.e. it will start with 0. The same name and notation will be kept for the new functions emerging out of these definitions, which, explicitly, take the form:

$$A_j^{[p]} = (\mathbf{E}(m_{j,1})^p)^{\frac{1}{p}}$$

and

$$E_j = \mathbf{E}(d_{j,1})^2$$

Remember here the stationarity assumption, which implies  $m_{j,k} = m_{j,1}$ , and  $d_{j,k} = d_{j,1}$ , the equality holding in distribution.

How different is the new definition from the old? Stationarity can now be fully exploited, in the sense that there is no “beginning of time” for the sequences: namely, it can be assumed that they are ordered circularly (on a ring), not linearly (on an interval). Thus, for example, computing  $A(0)$ , in addition to considering the differences used before, i.e.  $X_{0,1} - X_{0,2}, X_{0,3} - X_{0,4}, \dots, X_{0,2^{m-1}} - X_{0,2^m}$ , one will also take into account  $X_{0,2} - X_{0,3}, X_{0,4} - X_{0,5}, \dots, X_{0,2^{m-2}} - X_{0,2^{m-1}}, X_{0,2^m} - X_{0,1}$ . The circular folding of the indices is justified by the stationarity assumption. In practice, this means that the computations will be done according to the formula:

$$\begin{aligned}
A_j^{[p]} &\approx \left( \frac{1}{2^{j+1}} \sum_{l=0}^{2^{j+1}-1} \left( \frac{1}{2^{m-j-1}} \sum_{k=1}^{2^{m-j-1}} |F_{kl}^1(j) - F_{kl}^2(j)|^p \right) \right)^{1/p} \\
F_{kl}^1(j) &= \frac{1}{2^j} \sum_{i=1}^{2^j} X_{1+((k-1)2^{j+1}+l+i-1) \bmod 2^m} \\
F_{kl}^2(j) &= \frac{1}{2^j} \sum_{i=1}^{2^j} X_{1+((k-1)2^{j+1}+2^j+l+i-1) \bmod 2^m}
\end{aligned}$$

which can be simplified into:

$$\begin{aligned}
A_j^{[p]} &\approx \left( \frac{1}{2^{m+jp}} \sum_{l=0}^{2^{j+1}-1} \sum_{k=1}^{2^{m-j-1}} \left| \sum_{i=1}^{2^j} (G_{ikl}^1(j) - G_{ikl}^2(j)) \right|^p \right)^{1/p} \\
G_{ikl}^1(j) &= X_{1+((k-1)2^{j+1}+l+i-1) \bmod 2^m} \\
G_{ikl}^2(j) &= X_{1+((k-1)2^{j+1}+2^j+l+i-1) \bmod 2^m}
\end{aligned}$$

and similarly for the Energy function. Observe that the inner mean value (on  $k$ ) is the previous definition. The outer (on  $l$ ) is the improvement: now, for every  $j$ , the calculation involves a mean value taken on  $2^m$  points.

In the case  $p = 2$ , an alternative representation exists:

$$A_j^{[2]} = \frac{\text{Var}(X)}{2^{j-1}} \left\{ 1 - R(2^j) + 2 \sum_{i=1}^{2^j-1} \left[ \left( 1 - \frac{i}{2^j} \right) [2R(i) - R(2^j+i) - R(2^j-i)] \right] \right\} \quad (3)$$

where  $R$  is the autocorrelation of the traffic. This representation proves that  $A_j$  is really a linear transformation of the autocorrelation, so one should expect it to be insensitive to the ‘‘spikiness’’ of the traffic. This is indeed the case (Fig. 7). Note that the  $A_j^{[p]}$  can be computed via a fast algorithm of complexity  $\Theta(m2^m)$ ; for  $A_j$  this can be seen directly from (3), since  $R$  as well as the convolution in the last term of (3) can be computed via the FFT. For general  $p$ , one can use the multiresolution character of what is essentially a computation with Haar wavelet coefficients to obtain a  $\Theta(m2^m)$  algorithm (this also works for  $p = 2$ ).

Under the new definition, data and simulation Energy functions assume a slightly different form (Fig. 7, compare to Fig. 6).

### 3 Model A

This model assumes that the traffic on a link consists of the data that  $n$  users are sending, i.e. it is the sum of their data streams  $W_i(t)$ ,  $i = 1, \dots, n$ . These are modeled as bi-valuate stochastic processes (at a given  $t$ ,  $W(t) = 0$  or 1), whose paths are piecewise constant. The intervals of value 1 and 0 will be strictly alternating, and their durations will be assumed to be i.i.d. for each of the two interval types and for each user, cross-independent between interval type and cross-independent between users.

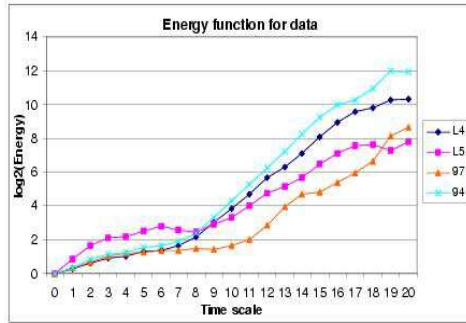
**Defining process A.** Let  $\{O_n^a(i)\}_{i=1}^\infty$  and  $\{O_f^a(i)\}_{i=1}^\infty$  be i.i.d. sequences of positive random variables with the following properties:

$$t^p \mathbf{P}(O_n^a(1) > t) \xrightarrow{t \rightarrow \infty} C \text{ for } p \in (1, 2) \text{ and } 0 < C < \infty \quad (4)$$

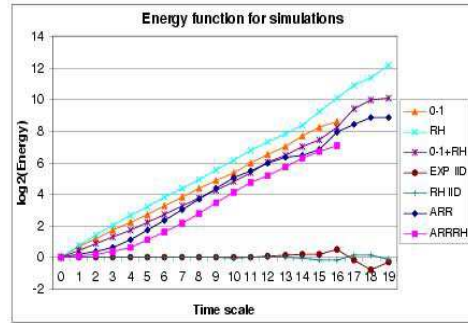
and

$$EO_f^a(i)^2 < \infty$$

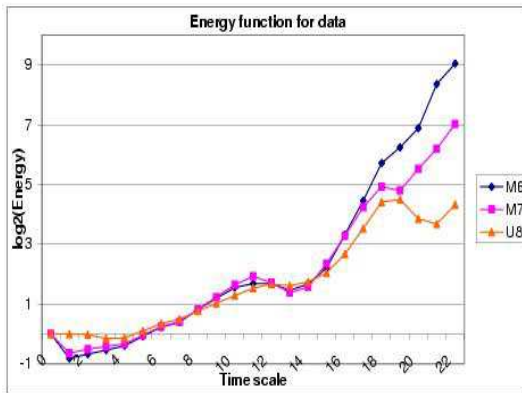
Define a process  $\widetilde{W}^a(t)$  as follows:



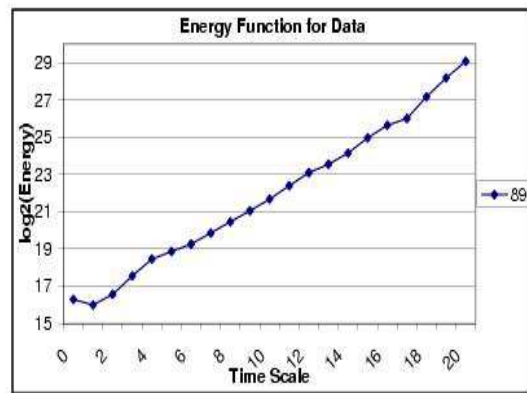
(a)



(b)



(c)



(d)

Figure 7: Energy functions, according to Definition 2, for data -(a), (c), and (d)- and simulations -(b). Compare to Fig. 6.

$$\widetilde{W}^a(t) = \begin{cases} 1 & \text{if } \sum_{i=1}^{k-1} (O_f^a(i) + O_n^a(i)) + O_f(k) \leq t \leq \sum_{i=1}^k (O_f^a(i) + O_n^a(i)) \\ 0 & \text{Otherwise} \end{cases}$$

and consider  $W^a(t)$  to be a “stationary” version of  $\widetilde{W}^a(t)$ , i.e. let  $u$  be uniformly distributed on the interval  $[0, O_f^a(1) + O_n^a(1)]$  and define  $W^a(t) = \widetilde{W}^a(u+t)$ <sup>2</sup>. Finally, let  $\{W_i^a(t)\}$  be i.i.d. such that  $W_i^a(t) \stackrel{\mathcal{L}}{=} W^a(t)$ , where  $\stackrel{\mathcal{L}}{=}$  denotes equality in the sense of all finite dimensional distributions of any order, i.e.

$$\forall n \in \mathbf{N}, \forall (t_1, \dots, t_n), \mathbf{p}(W(t_1), \dots, W(t_n)) = \mathbf{p}(W_i(t_1), \dots, W_i(t_n))$$

We will also use the notions of *weak convergence* in the sense of the finite dimensional distributions, i.e. *finite dimensional convergence*, denoted by  $W_m(t) \xrightarrow{W} W(t)$ :

$$\forall n \in \mathbf{N}, \forall (t_1, \dots, t_n), \lim_{m \rightarrow \infty} \mathbf{p}(W_m(t_1), \dots, W_m(t_n)) = \mathbf{p}(W(t_1), \dots, W(t_n))$$

and *stochastic equicontinuity*:

$$\lim_{\delta \rightarrow 0} \limsup_{n \rightarrow \infty} \mathbf{P} \left( \sup_{|t-s| \leq \delta} |W_n(t) - W_n(s)| > \varepsilon \right) = 0$$

Finally, a stochastic process  $W(t)$  will be called *self-similar* iff  $\exists H > 0: \forall t > 0, W(t) \stackrel{\mathcal{L}}{=} t^H W(1)$ . This is certainly not the only possible definition (see [5] for some alternatives), but it is the most usual.

This setting yielded a seminal mathematical result about the properties of Internet traffic, explaining its self-similarity in a LAN [24]. Theorem A is closely connected to this. The partial proof offered spells out in more detail some steps skipped in [24]:

**Theorem A.** Let  $T_n^a(t) = \int_0^t \frac{1}{\sqrt{n}} \sum_{i=1}^n W_i^a(s) ds$ . Then:

$$Z_n^a(t) = T_n^a(t) - \mathbf{E}T_n^a(t) \xrightarrow{W} G^a(t), \quad t \in [0, T]$$

where  $G(t)$  is a centered Gaussian self-similar process with covariance structure:

$$\mathbf{Cov}(G^a(s), G^a(t)) = \mathbf{E} \left( \int_0^s W_1^a(x) dx \int_0^t W_1^a(x) dx \right) - \mathbf{E} \left( \int_0^s W_1^a(x) dx \right) \mathbf{E} \left( \int_0^t W_1^a(x) dx \right)$$

*Proof.* First of all, it is straightforward that:

$$\begin{aligned} \mathbf{Cov}(Z_n^a(s), Z_n^a(t)) &= \frac{1}{n} \sum_{i=1}^n \sum_{j=1}^n \mathbf{E}((X_i^s - \mathbf{E}X_i^s)(X_j^t - \mathbf{E}X_j^t)) \\ &= \mathbf{E} \left( \int_0^s W_1^a(x) dx \int_0^t W_1^a(x) dx \right) - \mathbf{E} \left( \int_0^s W_1^a(x) dx \right) \mathbf{E} \left( \int_0^t W_1^a(x) dx \right) \end{aligned}$$

Now, fix  $t \in [0, T]$  and define  $X_i^t = \int_0^t W_i^a(x) dx$ . With this notation  $Z_n^a(t) = \frac{1}{\sqrt{n}} \sum_{i=1}^n (X_i^t - \mathbf{E}X_i^t)$ .

To show finite dimensional convergence, it is sufficient to prove that:  $\forall k \in \mathbf{N}, \forall t_1, \dots, t_k \in [0, T], \forall \alpha_1, \dots, \alpha_k \in \mathbb{R}$   $\sum_{j=1}^k \alpha_j Z_n^a(t_j) \rightarrow N(0, \sigma^2)$ , where  $\sigma^2$  depends on  $\alpha$ 's and  $t$ 's. Easily

$$\sum_{j=1}^k \alpha_j Z_n^a(t_j) = \frac{1}{\sqrt{n}} \sum_{i=1}^n \sum_{j=1}^k (\alpha_j X_i^{t_j} - \mathbf{E}(\alpha_j X_i^{t_j})) = \frac{1}{\sqrt{n}} \sum_{i=1}^n (Y_i^a - \mathbf{E}Y_i^a)$$

<sup>2</sup>This technique was also used in [29]

where  $Y_i^a = \sum_{j=1}^k \alpha_j \int_0^{t_j} W_i^a(x) dx$ . Clearly  $Y_i^a$ 's are i.i.d. and bounded so classical CLT can be invoked.

The next step is to establish tightness. For this it is sufficient (and necessary) to show *stochastic equicontinuity*. That is,  $\forall \varepsilon > 0$

$$\lim_{\delta \rightarrow 0} \limsup_{n \rightarrow \infty} \mathbf{P} \left( \sup_{|t-s| \leq \delta} |Z_n^a(t) - Z_n^a(s)| > \varepsilon \right) = 0 \quad (5)$$

The following estimate will be needed:

$$\begin{aligned} \mathbf{E}(Z_n^a(t) - Z_n^a(s))^2 &= \text{Var}(Z_n^a(t) - Z_n^a(s)) \\ &= \text{Var}(X_i^t - X_i^s) \leq \mathbf{E}(X_i^t - X_i^s)^2 = \mathbf{E} \left( \int_s^t W_i^a(x) dx \right)^2 \leq (t-s)^2 \end{aligned}$$

A classical ‘‘chaining’’ result (see [28] Thm. 11.1) yields the following:

**Lemma A.** *Let  $\xi_t$  be a real-valued stochastic process  $\xi_t$  such that  $\forall s, t \in \mathbb{R} : (\mathbf{E}(\xi_t - \xi_s)^p)^{1/p} \leq d(s, t)$ . Then  $\forall A \subset \mathbb{R} : \text{Card}(A) < \infty$*

$$\mathbf{E} \left( \sup_{d(s,t) \leq \delta, s, t \in A} |\xi_t - \xi_s| \right) \leq 8 \int_0^\delta \sqrt[4]{N(A, d, x)} dx$$

where  $d(\cdot, \cdot)$  is any pseudo distance on  $\mathbb{R}$  and  $N(A, d, x)$  is minimum number of ‘‘balls’’ of radius  $x$  (under distance  $d$ ) needed to cover  $A$ .

In order to use this lemma we first observe that in our case  $p = 2$ ,  $d(s, t) = |t - s|$  and

$$N(A, d, x) \leq N([0, T], d, x) = Tx^{-1}$$

Since the right hand side does not depend on  $A$  or  $n$ , the restriction  $\text{Card}(A) < \infty$  can be removed (see Theorem 11.6 in [28]). Thus:

$$\mathbf{P} \left( \sup_{|t-s| \leq \delta} |Z_n(t) - Z_n(s)| > \varepsilon \right) \leq \varepsilon^{-1} \mathbf{E} \left( \sup_{|t-s| \leq \delta} |Z_n(t) - Z_n(s)| \right) \leq \frac{8}{\varepsilon} \int_0^\delta \sqrt{N([0, T], d, x)} dx = \frac{16}{\varepsilon} T^{1/2} \delta^{1/2}$$

This establishes stochastic equicontinuity.

The proof of the self-similarity of the process  $G^a$  has already appeared in [24], and therefore it will not be reproduced here. □

## 4 Model B

The first criticism to the usual bi-valuate SSM (model A) is the continuity of the ON-intervals. The data transfer between computers is quantized (in *packets*), and although a continuous approximation may be acceptable, if only time scales much larger than the typical RTT are of interest, for studies of traffic in the sub-second ranges a more detailed model has to be considered.

Thus, the first modification is the discretization of ON-intervals. Consider the usual SSM, with  $W_i^b(t)$  independent (for  $i = 1, \dots, n$ ). For a fixed connection (fixed  $i$ ), the OFF-intervals will have lengths  $O_f^b(j)$ ,  $j \in N$ , where the  $O_f$ 's are i.i.d. random variables of finite variance. At the end of an OFF-interval, a *heavy tail distributed random integer*  $L$  will be assigned, representing the ‘‘load’’ (number of packets) the user wishes to send in this particular session. More precisely,

$$\exists p \in (1, 2), \exists C > 0 : t^p \mathbf{P}(L > t) \xrightarrow{t \rightarrow \infty} C \quad (6)$$

At this point, an ON-interval begins, but, in this model, packet emissions assume the form of delta functions, expressing mathematically the fact that information is transmitted in individual packets and in particular time instants, and the  $j$ -th packet emission of the  $i$ -th ON-interval is followed by the idle time interval  $R_{i,j} > 0$ : these are random variables i.i.d. in  $i$  and  $j$  (with  $\mathbf{E}(R_{i,j}^2) < \infty$ ), independent of the OFF-interval lengths and the session loads  $L$ . After all of the  $L$  packets have been sent, an OFF-interval follows, and the cycle restarts. Notice that ON-intervals (representing sessions) are heavy-tailed, as consisting of a heavy-tailed number of light tailed time intervals.

The random inter-arrival times  $R_{i,j}$ 's are designed to address the uncertainty of the length of RTT's. Since exponential distribution has the highest entropy (for any positive random variable), it would be a reasonable choice.

The total traffic from time 0 until time  $t$  is defined by  $T_n^b(t) = \int_0^t \sum_{i=1}^n W_i^b(s) ds$ . Theorem B below asserts the convergence of properly normalized total traffic, under very general conditions on the distributions of the  $L$  and  $R_{i,j}$ , to a centered Gaussian process with continuous sample paths.

**Defining process B.** Let  $\{O_f^b(i)\}_{i=1}^\infty$  be the same as  $\{O_f^a(i)\}_{i=1}^\infty$  and let  $\{L^b(i)\}_{i=1}^\infty$  be the same as  $\{O_n^a(i)\}_{i=1}^\infty$ , but with the extra requirement that  $L^b(i)$  be integer valued. Let also  $\{R_{i,j}^b\}_{i,j=1}^\infty$  be an i.i.d. array of random variables so that:

$$R_{i,j}^b \geq 0 \text{ a.s.}, \quad \mathbf{E}(R_{i,j}^b)^2 < \infty, \quad R_{i,0}^b = 0 \text{ a.s.}$$

and

$$\lim_{\delta \rightarrow 0} \delta^{-1} \mathbf{P}(R_{i,j}^b < \delta) \leq M < \infty \quad (7)$$

Let also  $O_n^b(i) = \sum_{j=1}^{L(i)} R_{i,j}^b$ . Finally, define formally the “delta” function  $\widehat{\delta}_x(s)$  with the properties that  $\widehat{\delta}_x(s) = 0$  if  $x \neq s$  and  $\int_{x-h}^{x+h} \widehat{\delta}_x(s) ds = 1$  for all  $h > 0$ . Using these conventions, define further:

$$\widetilde{W}^b(t) = \begin{cases} \widehat{\delta}_t(t) & \text{if } t = \sum_{i=1}^{k-1} (O_f^b(i) + O_n^b(i)) + O_f^b(k) + \sum_{i=1}^l R_{k,i}^b, \quad l \leq L^b(k) \\ 0 & \text{Otherwise} \end{cases}$$

As was the case before, define  $W^b(t)$  to be a stationary version of  $\widetilde{W}^b(t)$ , and let  $\{W_i^b(t)\}$  be i.i.d. versions of  $W^b(t)$ . Finally, define a constant  $\mathbf{E}W^b$  such that  $E \int_s^t W^b(x) dx = \mathbf{E}W^b |t - s|$ .

For this process, a result analogous to Theorem A holds:

**Theorem B.** Let  $T_n^b(t) = \int_0^t \frac{1}{\sqrt{n}} \sum_{i=1}^n W_i^b(s) ds$ . Then:

$$Z_n^b(t) = T_n^b(t) - ET_n^b(t) \xrightarrow{W} G^b(t), \quad \text{for } t \in [0, T]$$

where  $G^b(t)$  is a centered Gaussian process with covariance structure:

$$\mathbf{Cov}(G^b(s), G^b(t)) = \mathbf{E} \left( \int_0^s W_1^b(x) dx \int_0^t W_1^b(x) dx \right) - \mathbf{E} \left( \int_0^s W_1^b(x) dx \right) \mathbf{E} \left( \int_0^t W_1^b(x) dx \right)$$

*Proof.* The assertion will be proved under a slightly stronger condition on the  $R_{i,j}^b$  than (7); more precisely, it will be assumed here (as well as throughout the paper) that  $\exists \beta > 0$ :

$$0 < \beta \leq R_{i,j}^b \text{ a.s.} \quad (8)$$

The proof under the less restrictive assumption (7) is more technical, and the differences will be commented upon in the course of the proof; these comments will be indicated by square brackets [ ].

The finite dimensional convergence follows exactly in the same line as in Theorem A. Namely,  $Z_n^b(t) = \frac{1}{\sqrt{n}} \sum_{i=1}^n (X_i^t - \mathbf{E}(X_i^t))$ , where  $X_i^t = \int_0^t W_i^b(x) dx$ . Under the assumption (8),  $X_i^t$  are bounded by  $\beta^{-1}T$  and classical CLT can be used. [A short computation reveals that, under the original assumption (7),  $X_i^t$  has exponential tails and one can still use the same argument.]

Stochastic equicontinuity (5) will be proved in two steps:

*Step 1.* It is sufficient to show that for every  $\varepsilon > 0$  and  $\gamma > 0$

$$\lim_{\delta \rightarrow 0} \limsup_{n \rightarrow \infty} \mathbf{P} \left( \sup_{\gamma n^{-1/2} \leq |t-s| \leq \delta} |Z_n^b(t) - Z_n^b(s)| > \varepsilon \right) = 0 \quad (9)$$

Proof:  $\forall \varepsilon > 0$  consider the partition  $\Lambda_n = \left\{ t_i = \frac{i}{K_\varepsilon \sqrt{n}} : i = 0, \dots, K_\varepsilon \sqrt{n} T \right\}$  where  $K_\varepsilon = \varepsilon^{-1} 8 \mathbf{E} W_1^b$ . For every  $t$ , define functions  $\phi_1^n$  and  $\phi_2^n: [0, T] \rightarrow \Lambda_n$ , such that  $\phi_1^n(t) = t_j \leq t \leq t_{j+1} = \phi_2^n(t)$  for some  $j \leq K_\varepsilon \sqrt{n} T$ .

In other words  $\phi_1^n$  and  $\phi_2^n$  are closest elements to  $t$  from the cover  $\Lambda_n$  that enclose  $t$ .

Clearly

$$T_n^b(\phi_1^n(t)) \leq T_n^b(t) \leq T_n^b(\phi_2^n(t))$$

which implies

$$\begin{aligned} Z_n^b(t) - Z_n^b(s) &= T_n^b(t) - \mathbf{E}(T_n^b(t)) - T_n^b(s) + \mathbf{E}(T_n^b(s)) \\ &\leq T_n^b(\phi_2^n(t)) - \mathbf{E}(T_n^b(\phi_1^n(t))) - T_n^b(\phi_1^n(s)) + \mathbf{E}(T_n^b(\phi_2^n(t))) = \\ &= T_n^b(\phi_2^n(t)) - \mathbf{E}(T_n^b(\phi_2^n(t))) + \mathbf{E}(T_n^b(\phi_2^n(t))) - \mathbf{E}(T_n^b(\phi_1^n(t))) \\ &\quad + \mathbf{E}(T_n^b(\phi_1^n(s))) - T_n^b(\phi_1^n(s)) + \mathbf{E}(T_n^b(\phi_2^n(t))) - \mathbf{E}(T_n^b(\phi_1^n(s))) \end{aligned} \quad (10)$$

Since  $\mathbf{E}(T_n^b(\phi_2^n(t))) - \mathbf{E}(T_n^b(\phi_1^n(t))) = \mathbf{E} \left( \frac{1}{\sqrt{n}} \sum_{i=1}^n \int_{\phi_1^n(t)}^{\phi_2^n(t)} W_1^b(x) dx \right) = \sqrt{n}(\phi_2^n(t) - \phi_1^n(t)) \mathbf{E} W_1^b = \mathbf{E} W_1^b / K_\varepsilon = \varepsilon/8$ ,

one gets:

$$Z_n^b(t) - Z_n^b(s) \leq Z_n^b(\phi_2^n(t)) - Z_n^b(\phi_1^n(s)) + \varepsilon/4$$

Similarly

$$Z_n^b(s) - Z_n^b(t) \leq Z_n^b(\phi_2^n(s)) - Z_n^b(\phi_1^n(t)) + \varepsilon/4$$

Combining the two inequalities:

$$|Z_n^b(t) - Z_n^b(s)| \leq |Z_n^b(\phi_2^n(t)) - Z_n^b(\phi_1^n(s))| + |Z_n^b(\phi_2^n(s)) - Z_n^b(\phi_1^n(t))| + \varepsilon/2$$

and since  $\sup_{|t-s| \leq \delta} |Z_n^b(\phi_2^n(t)) - Z_n^b(\phi_1^n(s))| = \sup_{|t-s| \leq \delta} |Z_n^b(\phi_2^n(s)) - Z_n^b(\phi_1^n(t))|$ :

$$\begin{aligned} \mathbf{P} \left( \sup_{|t-s| \leq \delta} |Z_n^b(t) - Z_n^b(s)| > \varepsilon \right) &\leq \mathbf{P} \left( \sup_{|t-s| \leq \delta} |Z_n^b(\phi_2^n(t)) - Z_n^b(\phi_1^n(s))| > \varepsilon/4 \right)^* \leq \\ &\mathbf{P} \left( \sup_{K_\varepsilon^{-1} n^{-1/2} \leq |t-s| \leq \delta} |Z_n^b(\phi_2^n(t)) - Z_n^b(\phi_1^n(s))| > \varepsilon/4 \right) \end{aligned}$$

where in (\*) we used that  $|t-s| \leq \delta \Rightarrow \phi_2^n(t) - \phi_1^n(s) \geq K_\varepsilon^{-1} n^{-1/2}$ .

This proves Step 1.

*Step 2.* The goal here is to show that (9) holds for all  $\varepsilon, \gamma > 0$

$$\lim_{\delta \rightarrow 0} \limsup_{n \rightarrow \infty} \mathbf{P} \left( \sup_{\gamma n^{-1/2} \leq |t-s| \leq \delta} |Z_n^b(t) - Z_n^b(s)| > \varepsilon \right) = 0$$

Using the notation  $X_i^t = \int_0^t W_i^b(x)dx$ ,  $Z_n^b(t) = \frac{1}{\sqrt{n}} \sum_{i=1}^n (X_i^t - \mathbf{E}(X_i^t))$ :

$$\begin{aligned} \mathbf{E} (Z_n^b(t) - Z_n^b(s))^4 &= \mathbf{E} \left( \frac{1}{\sqrt{n}} \sum_{i=1}^n [(X_i^t - X_i^s) - \mathbf{E}(X_i^t - X_i^s)] \right)^4 \\ &\leq \frac{1}{n} \mathbf{E} ((X_1^t - X_1^s) - \mathbf{E}(X_1^t - X_1^s))^4 + 6 \left( \mathbf{E} ((X_1^t - X_1^s) - \mathbf{E}(X_1^t - X_1^s))^2 \right)^2 \\ &\leq \frac{1}{n} \left( \mathbf{E}(X_1^t - X_1^s)^4 + 6\mathbf{E}(X_1^t - X_1^s)^2 (\mathbf{E}(X_1^t - X_1^s))^2 \right) + 6 (\mathbf{E}(X_1^t - X_1^s)^2)^2 \quad (11) \end{aligned}$$

Let us examine the distribution of  $Q_{s,t} = X_1^t - X_1^s = \int_s^t W_1^b(x)dx$ . The assumption (8) coupled with the definition of  $W_i^b(x)$  implies that for  $\delta$  small enough, there exists a constant  $C$  such that

$$Q_{s,t} = 1 \text{ with probability } C|t - s|$$

$$Q_{s,t} = 0 \text{ with probability } 1 - C|t - s| \quad (12)$$

Thus, for  $\delta$  small enough, the above expression (11) is bounded by  $C(|t - s|^2 + |t - s|/n)$  for some (possibly different) constant  $C$ . Therefore, for  $1 > \delta \geq |t - s| > 1/\sqrt{n}$ ,  $\exists C_1 > 0$  such that:

$$\|Z_n^b(t) - Z_n^b(s)\|_{L_4} \leq C_1|t - s|^{1/2} \quad (13)$$

[It is not hard to show that, under the original assumption (7), there exist constants  $\nu_1, \nu_2 > 0$  such that, for  $\delta$  small enough,

$$P(Q_{s,t} = k) \leq \nu_1|t - s|^k, \quad P(Q_{s,t} = 0) \geq 1 - \nu_2|t - s|. \quad (14)$$

With this estimate one can easily recover (13) under the original assumption (7).

Lemma A can be invoked now. Letting  $d(s, t) = |t - s|^{1/2}$  we have (up to a constant  $C_1$ )

$$\mathbf{E} \left( \sup_{\gamma n^{-1/2} \leq |t-s| \leq \delta} |Z_n^b(t) - Z_n^b(s)| \right) \leq 8 \int_0^\delta \sqrt[4]{N([0, T], d, x)} dx \leq 8 \int_0^\delta T^{1/2} x^{-1/2} dx = 16T^{1/2} \delta^{1/2}$$

□

Probably more interesting is Corollary B, which derives some properties of the limit process:

**Corollary B.** *The Gaussian process  $G^b(t)$  has the following properties. There exist constants  $0 < C_i < \infty$ ,  $i = 1, 2$ , such that:*

$$i) \frac{\mathbf{Var}(G^b(\Delta))}{\Delta^{2/p}} \xrightarrow{\Delta \rightarrow \infty} C_1$$

$$ii) \frac{\mathbf{Var}(G^b(\Delta))}{\Delta^{1/2}} \xrightarrow{\Delta \rightarrow 0} C_2$$

$$iii) \forall k \in \mathbb{N}, \mathbf{Cov}(G^b(\Delta), G^b((k+1)\Delta) - G^b(k\Delta)) \xrightarrow{\Delta \rightarrow \infty} k^{\frac{2-2p}{p}} \text{ (} p \text{ was defined in (6))}$$

$$iv) \forall k \in \mathbb{N}, \mathbf{Corr}(G^b(\Delta), G^b((k+1)\Delta) - G^b(k\Delta)) \xrightarrow{\Delta \rightarrow 0} 0$$

*Proof.* Arguments for *i)* and *iii)* are essentially the same as in [24]. Namely, it is easy to show that for “large”  $\Delta$  the processes  $G^a$  and  $G^b$  behave in a similar way. In particular, it can be shown that there exists  $0 < K_p < \infty$ , such that:

$$\frac{\mathbf{E}(G^b(\Delta))^p}{\mathbf{E}(G^a(\Delta))^p} \xrightarrow{\Delta \rightarrow \infty} K_p, \quad \forall p > 0$$

For *ii*) and *iv*) the same approach as in the proof for Theorem B will be used. Namely, details will be presented only under assumption (8), and comments will be given on the extension of the results under the original assumption (7).

For *ii*), one can show easily (using (12)) that for  $\Delta < \beta$

$$\mathbf{Var} (G^b(\Delta)) = \mathbf{Var} \left( \int_0^\Delta W_1^b(t) dt \right) = \mathbf{Var} (Q_{0,\Delta}) = C_2 \Delta$$

[Under the original assumption (7), estimate (14) holds which also implies *ii*.]

For *iv*), one gets:

$$\begin{aligned} \mathbf{Corr} (G^b(\Delta), G^b((k+1)\Delta) - G^b(k\Delta)) &= \\ &= \frac{\mathbf{E} \left( \int_0^\Delta W_1^b(t) dt \int_{k\Delta}^{(k+1)\Delta} W_1^b(t) dt \right) - \mathbf{E} \left( \int_0^\Delta W_1^b(t) dt \right) \mathbf{E} \left( \int_{k\Delta}^{(k+1)\Delta} W_1^b(t) dt \right)}{\mathbf{Var} \left( \int_0^\Delta W_1^b(t) dt \right)} \end{aligned}$$

Invoking the distribution of  $Q_{s,t} = \int_s^t W_1^b(t) dt$  for small  $\Delta$ , it follows that  $\mathbf{Var}(Q_{0,\Delta}) \approx \Delta$  and  $\mathbf{E}Q_{0,\Delta} \approx \Delta$ , as well as:

$$Q_{0,\Delta} Q_{k\Delta, (k+1)\Delta} = 0 \text{ a.s.}$$

The combination of these three estimates yields:

$$\mathbf{Corr} (G^b(\Delta), G^b((k+1)\Delta) - G^b(k\Delta)) \approx \Delta$$

[Again, under the original assumption (7), the proof turns out to be more involved. However, it is not hard to show (using the estimate (12)) that in this case  $\mathbf{E} (Q_{0,\Delta} Q_{k\Delta, (k+1)\Delta}) = C\Delta^2 + o(\Delta^2)$  which implies *iv*) as well.]  $\square$

The result suggests that the behavior of the process varies according to time scale: for coarse ones, it behaves like the SSM, but for fine ones it behaves more like a Brownian motion. This change of behavior is also reflected in the autocorrelation.

The autocorrelations of the data traces follow the same pattern (fast decay at fine time scales, long-range dependence at coarser scales; see Fig. 8 and 9), consistent with the predictions of Corrolary B. This argues against “pure” self-similarity of the true traffic, for it behaves differently on different time scales. Moreover, Theorem B reveals a mechanism that is responsible for this: the quantized form of data transfer (packets and RTTs). Note that the result is independent of the exact distribution of the RTTs, which makes it robust; it can be expected to persist even for the haphazard nature of RTT distribution behavior in the network.

It should be mentioned that similar behavior has been observed before. For instance, in large capacity links of the Internet backbone, packet interarrival times tend to be exponentially distributed and independent [9].

Model B was successful in capturing the autocorrelation of real traffic, but what about spikiness? Actually, Theorem B states that model B traffic is only as spiky as the SSM. Model C will introduce a new feature that will add spikiness to simulated traffic.

## 5 Model C

### 5.1 Introduction

Model B oversimplifies the data transfer between two computers: although it addresses the uncertainty in the network and the quantized nature of the transfer, it fails to take into account protocol specifications and connection speed variations. Indeed, the most widely adopted transport layer protocol, TCP, has the Slow Start feature, according to which the number of packets it sends each time increases geometrically by 2. This geometric increase

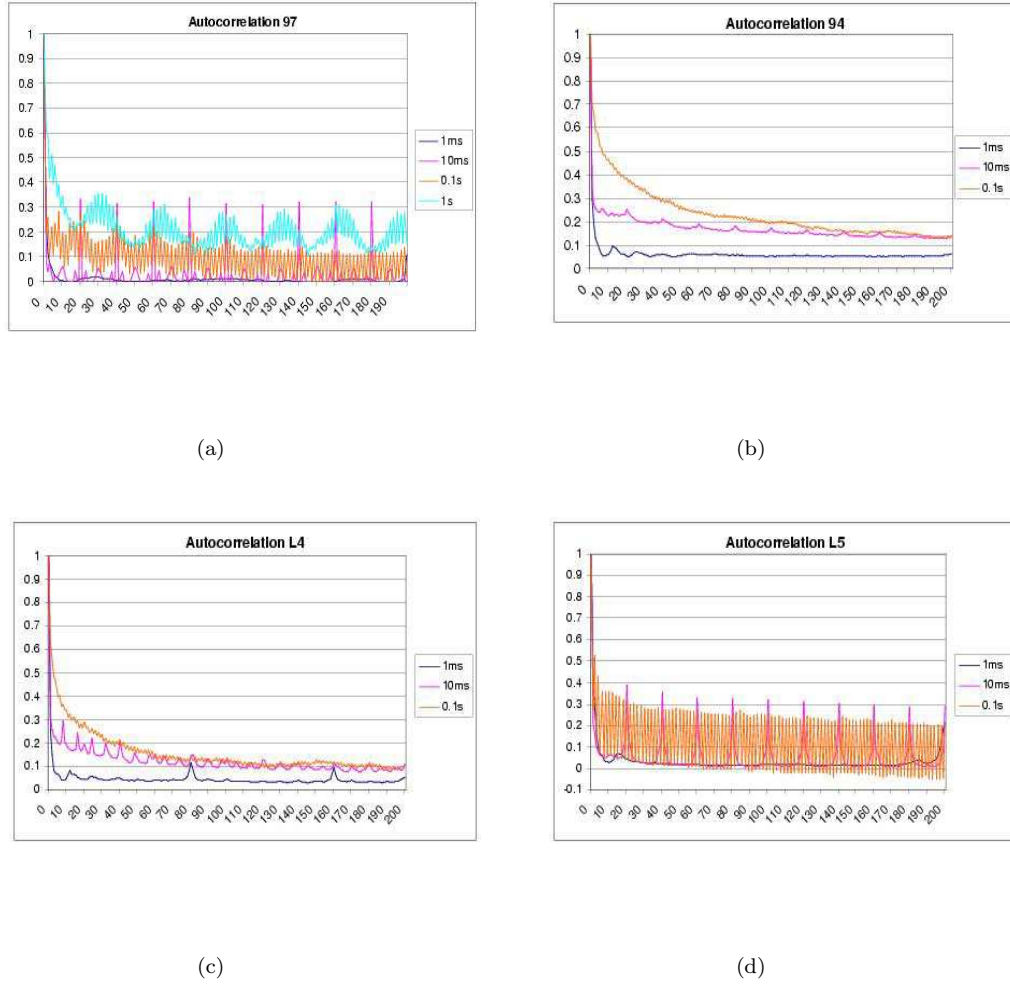


Figure 8: Trace autocorrelations at four different time bins (1ms, 10ms, 100ms, 1s): the long-range dependence in coarse time scales is obvious. 97 (a) and L5 (d) seem to have very strong periodic components, probably due to some monitoring protocol.

is readily observed in real traffic sessions (Fig. 10). Also, connection speeds can vary from 56K modems to extremely fast backbone links.

Therefore, within the framework of model B, a modification is made, so that the number of packets sent each time increases by 2, until either all of the  $L$  packets are sent, or a specified maximum  $Max$  is reached, after which it remains the same. Thus, the sequence of the number of packets sent, instead of  $1, 1, 1, \dots, 1$ , is now going to be  $1, 2, 4, 8, \dots, Max, Max, \dots$ , unless  $L$  is less than  $1 + 2 + 4 + \dots + Max$ . In other words, the delta functions will no longer have equal weights, but, instead, they will be multiplied by geometrically increasing coefficients. The different connection speeds can be modeled through different “packet sizes”, so that the sequence of packets sent from a particular user now becomes  $\lambda, 2\lambda, 4\lambda, \dots, \lambda Max, \dots$  [23]. Finally, packet losses can be incorporated in the model by allowing  $Max$  to be a random variable.

## 5.2 $p$ -Stable variables and processes

Theorem C will make use of  $p$ -Stable variables. The purpose of this paragraph is to familiarize the reader with this quite “exotic” type of random variables, and the random processes they generate. More information can be found in [22].

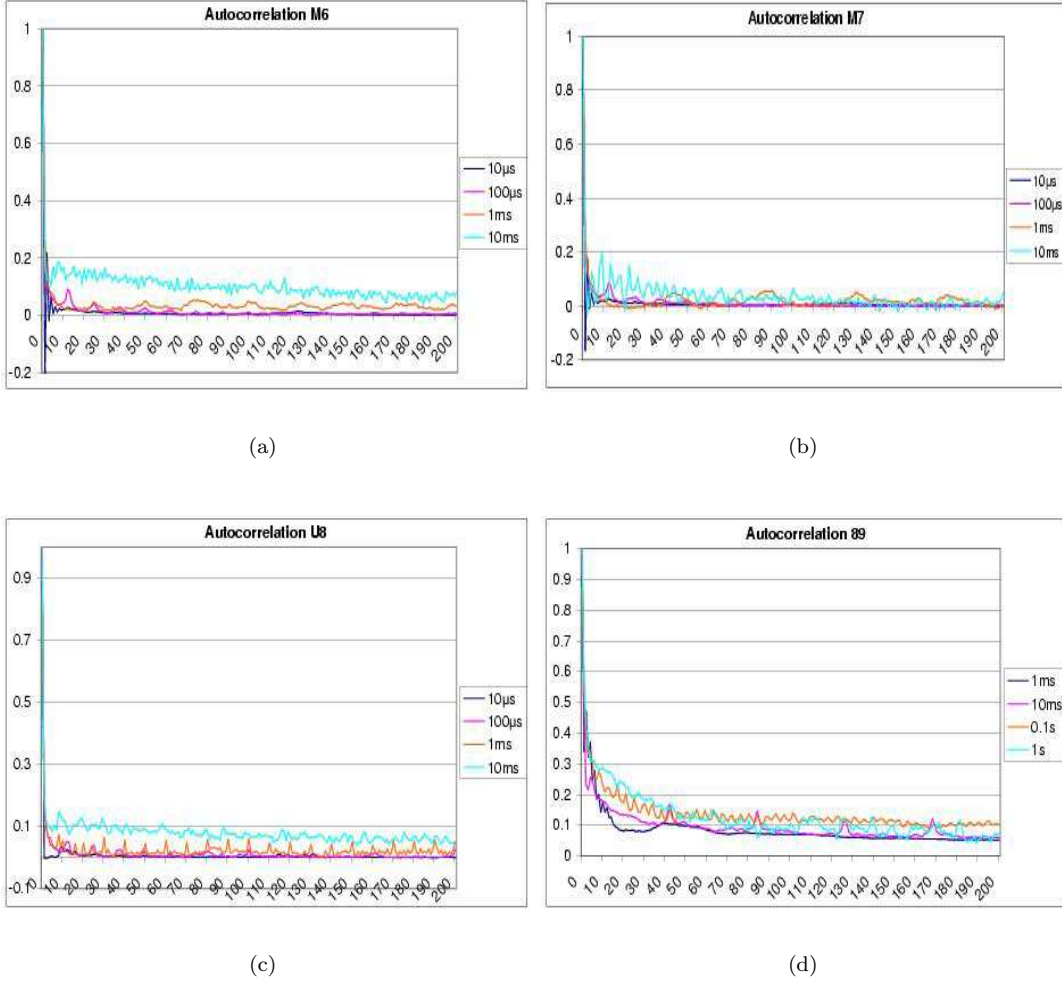


Figure 9: Trace autocorrelations at four different time bins:  $10\mu s$ ,  $100\mu s$ ,  $1ms$ ,  $10ms$  for M6, M7, and U8, and  $1ms$ ,  $10ms$ ,  $100ms$ ,  $1s$  for 89. Trace 89 shows a relatively strong correlation irrespective of the bin used. On the contrary, the newer traces seem to be uncorrelated, if binned with a bin other than  $10ms$ . If, however, the  $10ms$  bin is used, M7 remains uncorrelated, but M6 and U8 show a weak correlation.

A distribution is defined to be *stable* iff it remains invariant —within an affine transformation— under convolutions. More precisely, choose  $n$  and let  $X_1, \dots, X_n$  follow this distribution; it will be stable iff  $\exists a_n, b_n : X_1 + \dots + X_n \stackrel{\mathcal{L}}{=} a_n X + b_n$ . A  $p$ -Stable variable  $V$  is represented through its characteristic function, as no closed form for its distribution function is generally known:

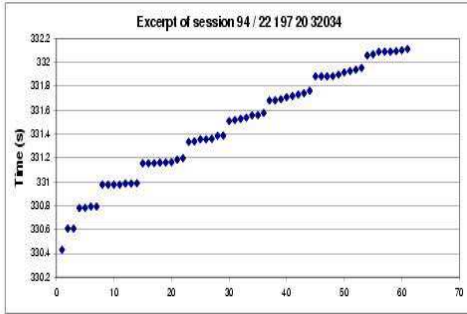
$$\mathbf{E}[\exp(i\theta V)] = \exp(-\sigma^p |\theta|^p + i\mu\theta), \quad 0 < p \leq 2$$

It is customary to write that  $V \sim SpS(\sigma)$ . Closed forms for the distribution are known in the cases where  $p = 1$  (Cauchy) and  $p = 2$  (Normal). The tails of the distributions, however, are known to follow power laws:

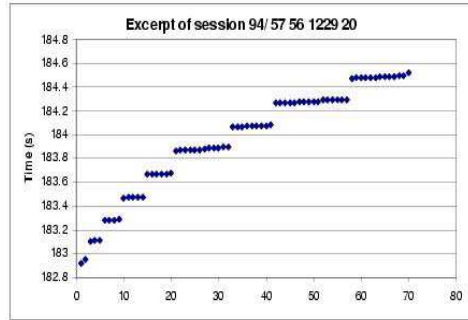
$$\lim_{\lambda \rightarrow \infty} \lambda^p \mathbf{P}(V > \lambda) = \lim_{\lambda \rightarrow \infty} \lambda^p \mathbf{P}(V < -\lambda) = C_p \sigma^p$$

A self-similar  $p$ -Stable random process with stationary increments and self-similarity factor  $H$  is usually denoted by  $L_{H,p}$  (see the definition of self-similarity in section 3). The stationary increments requirement, combined with self-similarity, imposes that:

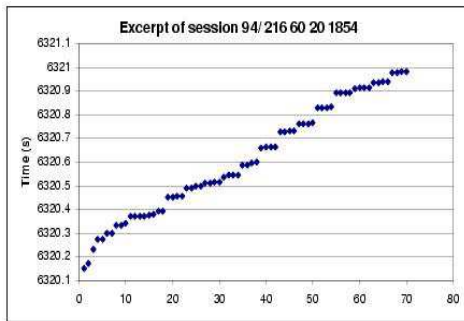
$$L_{H,p}(t) - L_{H,p}(s) \sim SpS(|t - s|^H \sigma_{V(1)})$$



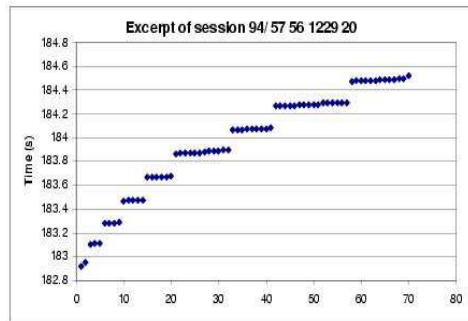
(a)



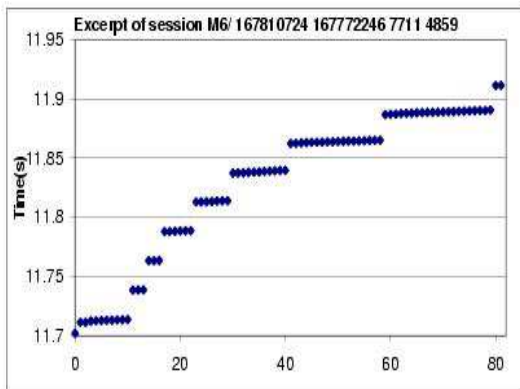
(b)



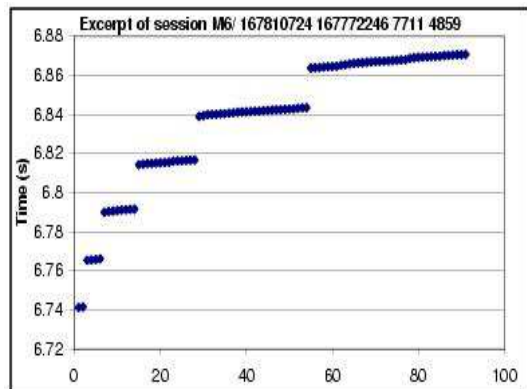
(c)



(d)



(e)



(f)

Figure 10: Multiple packet emission according to TCP’s Slow Start, as observed in 4 connections of trace 94 and 2 connections of trace M6 (remember here that a *connection* is the subset of the traffic corresponding to specific values of sender and receiver host and port numbers): in all cases except (c) Slow Start behaves *exactly* according to the TCP specifications! Slow Start may not always be as “pure” as in figures (a), (b), and (d), though; one also sees cases like (c), in which the increase of packet number is present but does not fit the protocol specifications as nicely. Nevertheless, our experimental observations correspond to our theoretical predictions.

The increments will also be independent iff  $H = 1/p$ , in which case the process is called a *Lévy Stable Motion*.

An important difference between  $p$ -Stable and Gaussian processes is that, in general, the paths of a  $p$ -Stable process with  $p < 2$  are discontinuous with probability 1. Notice also the larger number of parameters needed to specify a  $p$ -Stable variable completely, compared to a Gaussian variable (mean, variance, and  $p$  vs. mean and variance): it will become clear after the statement and proof of Theorem C, and the discussion afterwards, that estimating  $p$  from a given data set is by no means easy, but, fortunately, for this paper's purposes, its value will not be needed.

### 5.3 Statement and proof of Theorem C

Before the formal statement of Theorem C, a brief description of the notation is in order: the stream of data corresponding to the  $i$ -th user, with  $Max = M$ , will be  $W_{i,M}^c(s)$ .  $T_n^c(t)$  will denote the total aggregated traffic until time  $t$ . The function  $C(s, t)$  is the covariance structure of the Gaussian limit process, as given in (15). Finally,  $p$  is the exponent in (6).

**Defining process C.** Let  $\{O_f^c(i)\}_{i=1}^\infty, \{R_{i,j}^c\}_{i,j=0}^\infty$  and  $\{L^c(i)\}_{i=1}^\infty$  be the same as  $\{O_f^b(i)\}_{i=1}^\infty, \{R_{i,j}^b\}_{i,j=0}^\infty$  and  $\{L^b(i)\}_{i=1}^\infty$ .

Given  $M > 0$ , let  $\phi(l) = \left\lfloor \log_2(l \wedge M) + \frac{(l - 2M + 1)_+}{M} \right\rfloor + 1$ , where  $\lfloor X \rfloor$  stands for the largest integer which

is smaller than  $X$  and  $(X)_+$  stands for the positive part of  $X$ , as usual. Let  $O_{n,M}^c(i) = \sum_{j=1}^{\phi(L^c(i))} R_{i,j}^c$ . Recall also

the definition of the “delta” function  $b\widehat{\delta}_x(s)$  and its properties:  $b\widehat{\delta}_x(s) = 0$  if  $x \neq s$  and  $\int_{x-h}^{x+h} b\widehat{\delta}_x(s) ds = b$  for all  $h > 0$ . With this convention, define:

$$\widetilde{W}_M^c(t) = \begin{cases} (2^l \wedge M)\widehat{\delta}_t(t) & \text{if } t = \sum_{i=1}^{k-1} (O_f^c(i) + O_n^c(i)) + O_f^c(k) + \sum_{i=1}^l R_{k,i}^c, \quad l \leq \phi(L^c(k)) \\ 0 & \text{Otherwise} \end{cases}$$

As before, define further  $W_M^c(t)$  to be a stationary version of  $\widetilde{W}_M^c(t)$ . Finally, let  $\{W_{i,M}^c(t)\}$  be i.i.d. versions of  $W_M^c$ , define a constant  $\mathbf{E}W_M^c(x)$  such that

$$\mathbf{E} \left( \int_a^b W_M^c(x) dx \right) = \mathbf{E}W_M^c |b - a|,$$

and let

$$C(s, t) = \lim_{n \rightarrow \infty} \frac{1}{\sigma_n} \left( \mathbf{E} \left( \int_0^s W_{1,M_n}^c(x) dx \int_0^t W_{1,M_n}^c(x) dx \right) - \mathbf{E} \left( \int_0^s W_{1,M_n}^c(x) dx \right) \mathbf{E} \left( \int_0^t W_{1,M_n}^c(x) dx \right) \right) \quad (15)$$

where  $\sigma_n^2 = \mathbf{Var} \left( \int_0^T W_{i,M_n}^c(s) ds \right)$ . Recall also that  $\exists p \in (1, 2) : t^p \mathbf{P}(L^c(i) > t) = \Theta(1)$ , as  $t \rightarrow \infty$ , which is another way to say that the LHS of the expression is bounded above and below by a constant.

**Theorem C.** Let  $T_n^c(t) = \int_0^t \sum_{i=1}^n W_{i,M}^c(s) ds$ . Then

i) If  $M = M_n \nearrow \infty$  and  $M_n \leq n^q$  for  $q < 1/p$ , then, for fixed  $t$ :

$$Z_n^c(t) = \frac{1}{\sigma_n \sqrt{n}} (T_n^c(t) - \mathbf{E}T_n^c(t)) \xrightarrow{W} G^c(t), \quad t \in [0, T]$$

where  $\sigma_n^2 = \mathbf{Var} \left( \int_0^T W_{i,M_n}(s) ds \right)$  and  $G^c(t)$  is a centered Gaussian process with covariance structure  $C(s, t)$ .

ii) If  $M_n \geq n^q$  for  $q > 1/p$ , then, for fixed  $t$ :

$$Z_n^c(t) = \frac{1}{n^{1/p}} [T_n^c(t) - \mathbf{E}(T_n^c(t))] \xrightarrow{W} P^c(t), \quad t \in [0, T]$$

where  $P^c(t)$  is a  $p$ -Stable process.

Note: we will not pursue further the issues of what the exact value of  $p$  for  $P^c(t)$  is and how it can be estimated from a given data set (see the relevant remarks in section 5.2).

*Proof.* First of all, recall the equality

$$\mathbf{E}(|X|) = \int_0^\infty P(X > t) dt \quad (16)$$

which will prove repeatedly useful later.

For part *i*), finite dimensional convergence has to be established first. An easy computation yields

$$\frac{\sigma_{t,n}^2}{\sigma_n^2} = \frac{\mathbf{Var} \left( \int_0^t W_{i,n}^c(s) ds \right)}{\mathbf{Var} \left( \int_0^T W_{i,n}^c(s) ds \right)} \xrightarrow{n \rightarrow \infty} \gamma_t^2 \text{ for } 0 < \gamma_t^2 \leq 1.$$

Using the notation  $W_{1,n}^c = W_{i,M_n}^c$ ,  $X_{i,n}^t = \int_0^t W_{i,n}^c(x) dx$ , and  $\tilde{X}_{i,n} = \frac{1}{\sigma_{t,n}} (X_{i,n}^t - \mathbf{E}(X_{i,n}^t))$ , it is sufficient to show that

$$\frac{1}{\sqrt{n}} \sum_{i=1}^n \tilde{X}_{i,n} = \frac{1}{\sigma_{t,n} \sqrt{n}} \sum_{i=1}^n [X_{i,n}^t - \mathbf{E}(X_{i,n}^t)] \xrightarrow{W} N(0, 1)$$

Since the  $\tilde{X}_{i,n}$  are obviously i.i.d., centered and with  $\mathbf{Var}(\tilde{X}_{i,n}) = 1$ , the above follows easily (using a classical Lindeberg argument, see [27]), provided that

$$n^{-1/2} \mathbf{E} \left( |\tilde{X}_{i,n}|^3 \right) \rightarrow 0.$$

Clearly  $\mathbf{E}(X_{i,n}^t) \rightarrow C < \infty$ , hence the above is bounded (up to a constant) by

$$\frac{\mathbf{E}(|X_{i,n}^t|^3)}{\sqrt{n} \left( \mathbf{E}(|X_{i,n}^t|^2) \right)^{3/2}} \leq C \frac{M_n \mathbf{E}(|X_{i,n}^t|^2)}{\sqrt{n} \left( \mathbf{E}(|X_{i,n}^t|^2) \right)^{3/2}} = C \frac{M_n}{\sqrt{n \mathbf{E}(|X_{i,n}^t|^2)}} \stackrel{*}{\leq} C' \frac{M_n^{p/2}}{\sqrt{n}} \leq C' n^{\frac{pq-1}{2}} = C' n^{\frac{p}{2}(q-\frac{1}{p})} \xrightarrow{n \rightarrow \infty} 0$$

where in (\*) we used 16 and (6).

The stochastic equicontinuity follows after a computation very similar to the one presented in the proof of Theorem B.

Namely, one needs to estimate

$$\begin{aligned} \mathbf{E}(Z_n^c(t) - Z_n^c(s))^4 &= \mathbf{E} \left( \frac{1}{\sigma_n \sqrt{n}} \sum_{i=1}^n ((X_{i,n}^t - X_{i,n}^s) - \mathbf{E}(X_{i,n}^t - X_{i,n}^s)) \right)^4 \\ &\leq \frac{1}{n \sigma_n^4} \mathbf{E}((X_{1,n}^t - X_{1,n}^s) - \mathbf{E}(X_{1,n}^t - X_{1,n}^s))^4 + \frac{6}{\sigma_n^4} \left( \mathbf{E}((X_{1,n}^t - X_{1,n}^s) - \mathbf{E}(X_{1,n}^t - X_{1,n}^s))^2 \right)^2 \\ &\leq \frac{1}{n \sigma_n^4} \left( \mathbf{E}(X_{1,n}^t - X_{1,n}^s)^4 + 6 \mathbf{E}(X_{1,n}^t - X_{1,n}^s)^2 \left( \mathbf{E}(X_{1,n}^t - X_{1,n}^s) \right)^2 \right) + \frac{6}{\sigma_n^4} \left( \mathbf{E}(X_{1,n}^t - X_{1,n}^s)^2 \right)^2 \end{aligned}$$

It can be shown, using (16) that, for  $\delta$  small enough and  $\varepsilon = 1/p - q$ ,  $\exists C > 0$ :

$$\frac{\mathbf{E} (X_{1,n}^t - X_{1,n}^s)^2}{\sigma_n^2} \leq C|t - s|$$

and

$$\frac{\mathbf{E} (X_{1,n}^t - X_{1,n}^s)^4}{n\sigma_n^4} \leq Cn^{-\varepsilon}|t - s|$$

Therefore, for  $|t - s| > n^{-1/2}$ ,  $\exists C_1 > 0$ :

$$\|Z_n^c(t) - Z_n^c(s)\|_{L_4} \leq C_1|t - s|^{1/4+\varepsilon/2} \quad (17)$$

As in the proof for Theorem B, this allows for the replacement of the standard requirement for stochastic equicontinuity (5) with:

$$\lim_{\delta \rightarrow 0} \limsup_{n \rightarrow \infty} \mathbf{P} \left( \sup_{\gamma n^{-1/2} \leq |t-s| \leq \delta} |Z_n^c(t) - Z_n^c(s)| > \varepsilon \right) = 0$$

In order to prove the above, one can proceed as in the proof of Theorem B: construct the partition  $\Lambda_n = \{t_i = \frac{i}{K_\varepsilon \sqrt{n}} : i = 0, \dots, K_\varepsilon \sqrt{n} T\}$  where  $K_\varepsilon = \varepsilon^{-1} 8 \mathbf{E} W_{M_n}^c$ , and, for every  $t$ , define functions  $\phi_1^n$  and  $\phi_2^n: [0, T] \rightarrow \Lambda_n$  such that  $\phi_1^n(t) = t_j \leq t \leq t_{j+1} = \phi_2^n(t)$  for some  $j \leq K_\varepsilon \sqrt{n} T$ .

Clearly

$$T_n^c(\phi_1^n(t)) \leq T_n^c(t) \leq T_n^c(\phi_2^n(t))$$

which implies (by essentially the same computation as the one presented in (10))

$$Z_n^c(t) - Z_n^c(s) \leq Z_n^c(\phi_2^n(t)) - Z_n^c(\phi_1^n(s)) + \varepsilon/4$$

Observe now that  $\mathbf{E}(T_n^c(\phi_2^n(t))) - \mathbf{E}(T_n^c(\phi_1^n(s))) = \mathbf{E} \left( \frac{1}{\sigma_n \sqrt{n}} \sum_{i=1}^n \int_{\phi_1^n(t)}^{\phi_2^n(t)} W_{1,n}^c(x) dx \right) = \frac{\sqrt{n}}{\sigma_n} (\phi_2^n(t) - \phi_1^n(s)) \mathbf{E} W_{M_n}^c \leq \mathbf{E} W_{M_n}^c / K_\varepsilon = \varepsilon/8$ .

This proves part *i*) of Theorem C.

Proof for *ii*). Let us begin by giving a summary of some relevant convergence results found in [26], section 2.6 (see also section 5.2 above):

**Lemma D.** *Let  $\{X_i\}$  be a sequence of i.i.d. random variables, and suppose there exist two sequences  $\{a_n\}$  and  $\{b_n\}$  such that  $\frac{X_1 + \dots + X_n}{a_n} - b_n \xrightarrow{w} Z$  (in which case we say that  $X_i$  is in the domain of attraction of  $Z$ ). Then:*

- $Z$  can only be a  $p$ -Stable r.v., where  $0 < p \leq 2$ .
- $\exists C > 0 : a_n = Cn^{\frac{1}{p}}$ .
- $p = 2 \Leftrightarrow \mathbf{E}(X_1^2) < \infty$ , or, equivalently,  $p < 2 \Leftrightarrow \mathbf{E}(X_1^2) = \infty$ .
- If  $p = 2$ ,  $Z$  is Gaussian.

For fixed  $t$ , let  $Y_i^t = \int_0^t W_{i,\infty}^c(x) dx$ , where  $W_{i,\infty}^c$  stands for  $W_{i,M_n}^c$  with  $M_n = \infty$ . A straightforward calculation of  $\mathcal{L}(Y_i^t)$  shows that  $\mathbf{E}[(Y_i^t)^2] = \infty$ ; it follows then from Lemma D that  $Y_i^t$  is in the domain of attraction of a  $p$ -Stable random variable, i.e.

$$n^{-1/p} \sum_{i=1}^n (Y_i^t - \mathbf{E}(Y_i^t)) \rightarrow p\text{-Stable r.v.}$$

It is also a classical result (see [26]) that, if  $Y_i^t$  is replaced with its truncated version  $Y_{i,n}^t = Y_i^t \mathbf{1}_{|Y_i^t| < M_n}$ , the above convergence still holds. The result now follows since the tail behavior of  $Y_{i,n}^t$  is the same as for  $X_{i,n}^t =$

$$\int_0^t W_{i,M_n}^c(x) dx.$$

□

## 5.4 An interesting prediction: oscillation between Gaussianity and p-Stability

According to Theorem C, and contingent upon the relation between  $n$  and the maximum window size  $M_n$ , the limit process can be either Gaussian or p-Stable. Notice, however, that this condition does not depend on the length  $T$  of the time interval under consideration. Therefore, it can be conjectured that the result applies “locally”. This, in turn, suggests two possible mechanisms causing oscillations between Gaussianity and p-Stability.

On the one hand, although formally  $n$  users are active in  $[0, T]$ , their actual number may fluctuate, if examined on smaller time intervals (Fig. 14). Let then  $N_n(t)$  be the number of users, among the total  $n$  users of the simulation, who are in an ON-interval at time  $t$ . If  $(N_n(t))^q < M_n$ , the local behavior around  $t$  will tend to be p-Stable, if  $(N_n(t))^q > M_n$ , it will tend to be Gaussian. This oscillation is observed in practice (Fig. 12), and mere visual inspection reveals that the number of users and the Gaussianity of the process are well correlated (Table 1). The fluctuation of the number of active users in time can apparently be well modeled by model A. Finally, notice that the number of bins used to compute the marginals is *not* responsible for this oscillation, as it is kept fixed throughout the computation.

On the other hand,  $M_n$  itself can change, too. This happens actually in real networks built on TCP/IP, where, according to the protocol specifications, packet loss halves the window size. In other words, according to Theorem C, the more congested the network is, the more Gaussian the traffic should look like. This has indeed been confirmed [23, 9].

As a consequence, if incorporation of packet losses into this model is required,  $M_n$  can be allowed to be different for each user, and randomly selected, but constant.

## 5.5 Is oscillation between Gaussianity and p-Stability a reality?

Simulations of model C seem to be very successful in resembling the true traffic visually, and in capturing its long range dependence (see Fig. 13, 1, and 2). To test whether the other prediction of Theorem C, namely the oscillation between Gaussianity and p-Stability, is indeed seen in real traffic, the following experiment was designed. For simplicity, the description will be based on the 94 trace, when it comes to choosing values of parameters, but it can be easily translated into the context of newer traces, using the observation that transmission appears to be 100 times faster.

Start by binning the trace using a bin of  $0.1s$ . Since under a time bin of  $0.1ms$  it is mostly true that at most one packet falls into a particular time bin, the  $0.1ms$  bin size can be considered a “natural” time bin for the trace; taking a marginal distribution of the trace at this bin size would yield the marginal of the packet size itself. Consequently, the value of every bin is the sum of 1000 “natural” bins, i.e. the sum of 1000 identically distributed random variables, and actually distributed as the packet size, if 0 is allowed to be a legitimate packet size. One would hope that this number is sufficiently large to yield a reasonably accurate convergence to the Gaussian limit predicted by the CLT, if convergence to a Gaussian r.v. were to hold, or yield results that are observably at least non-Gaussian, if convergence to a p-Stable limit were to hold. Actual convergence to the p-Stable limit is too much to ask for, because a) a different normalization is required for that, compared to the Gaussian limit, and b) infinite variance is impossible to capture with a finite trace, so that a p-Stable variable cannot be distinguished from a large variance variable, in practice (see Fig. 11(e) and (f)).

In order to examine the trace behavior locally, we divide the trace using consecutive, equisized, non-overlapping windows and take the normalized marginal (corresponding to mean 0 and variance 1) within each window. We then compute the Kolmogorov distance (see (1)) between this marginal and a normal  $N(0,1)$  distribution, for each window; graphing this Kolmogorov distance as a function of the bin label illustrates changes in time of the local behavior. As in the case of the windowed Fourier transform, the window size is the result of a trade-off: small windows will yield well localized inaccurate results, whereas large windows will yield poorly localized accurate results. A size of 512 bins seemed a good choice, thus ending up with approximately 140 points in the graph (the trace consists of approximately 72000 bins). The resulting Kolmogorov distance graphs for the data sets are shown in Fig. 12(a), (c), and (d). In some cases, the Kolmogorov distance is small throughout (M6, M7, L4); in others it oscillates violently.

In order to calibrate these results, we performed the same computations on realizations of known distributions; the results are shown in Fig. 11(a), (b), and (c).

In Fig. 11(a) we compare a realization of the normal distribution with the theoretical curve; as expected, we find a very small Kolmogorov distance  $d_K$ . Based on this, we place the threshold of “not differing from Gaussianity” at  $d_K \approx 0.08$ .

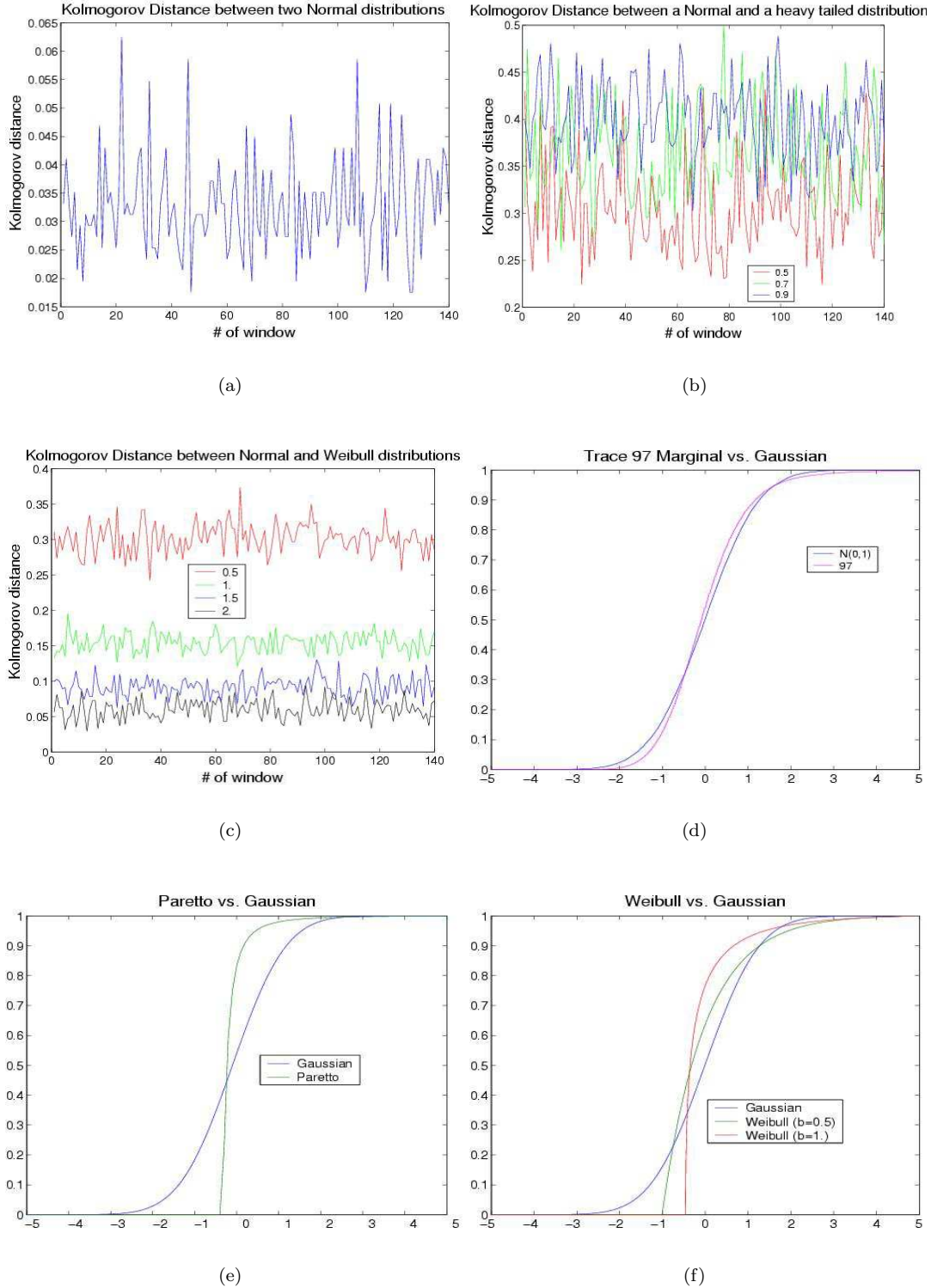


Figure 11: Kolmogorov Distances of normalized (a) Gaussian, (b) heavy-tailed, and (c) Weibull marginals from the  $N(0,1)$  distribution. Marginals have been computed using non-overlapping consecutive windows of  $2^9 = 512$  bins. The formula used for the Weibull is:  $F(x) = 1 - e^{-ax^b}$ . The heavy tailed distribution corresponds to the pure power law (Pareto)  $Y = \frac{a}{X^b}$ ,  $X \sim U(0, 1)$ . In both cases,  $a$  does not affect the results, due to the normalization, whereas the values for  $b$  used are shown in the legends. (d) shows that the trace 97 marginal is very close to a Gaussian, although its tails are Weibull, as seen in Section 1.1. Finally, (e) and (f) show the distance between a Gaussian and a Pareto (with  $b = 0.8$ ), and between a Gaussian and a Weibull (one with  $b = 1.$ , and one with  $b = 0.5$ ), respectively. Notice the similarity between the Weibull with  $b = 0.5$  and the Pareto.

Cross-correlation between Kolmogorov distances and traffic:

<i>Trace</i>	94	97	L4	L5	M6	M7	U8	89
<i>Correlation</i>	-0.300	0.392	-0.161	-0.244	0.031	-0.048	-0.787	-0.806

Table 1: Cross-correlation between Kolmogorov distances of windowed empirical marginals from  $N(0, 1)$  and the total traffic within the window, for the real traces.

In Fig. 11(b) one can see the results for the three heavy-tailed distributions of  $Y = ax^{-b}$ , where  $b = 0.5, 0.7, 0.9$  respectively; in these cases the oscillations of the local Kolmogorov distance to Normal have a larger amplitude (the difference between minimum and maximum is about 0.12 in all three cases, which is between 25 and 35% of the mean Kolmogorov distance), but they all are solidly above 0.2, and move further away from Normal as  $b$  increases, as is to be expected.

Fig. 11(c) shows the local Kolmogorov distance to Normal for four different Weibull distributions, with cumulative distributions  $F(x) = 1 - e^{-ax^b}$ . For  $b = 2$ , the graph is in the Gaussian range, as could be expected; as  $b$  decreases, one moves away from the Gaussian range, and the oscillations in the local behavior become more marked; nevertheless, their amplitude never exceeds 35% of the mean. For  $b \leq 1$  they remain well segregated from the Gaussian range at all times.

We can now evaluate the results for the data sets based on these calibrations. The data sets M6 and M7 look solidly Gaussian, as does the Slow Start simulation with  $Max = 8$ ; data 97 and simulations with  $Max = 16$  dart between Gaussianity and the region  $d_K \geq 0.1$ , with a total oscillation amplitude approaching 60% of their mean; data sets 94, L4 and L5, and simulations with  $Max = 32$  reach much larger  $d_K$ , but occasionally reach into Gaussianity, and their total oscillation amplitude exceeds their mean; finally, trace U8 is completely in the “far from Gaussianity” region  $d_K \geq 0.2$ , with again maximum oscillation exceeding its mean. However, what distinguishes these traces is that they reach local Kolmogorov distances typical of distributions with large variance, yet that, unlike e.g. the large variance Weibull distributions, they have very large amplitude that occasionally take them back to or close to Gaussianity. For  $Max$  in a “critical” range ( $Max = 16$  for our parameters), our simulations have the same character. This suggests that the data, as well as the simulation, exhibit an oscillation between Gaussian and far-from-Gaussian behavior, consistent with Theorem C.

## 5.6 Traffic amount is correlated with marginals locally

An experiment related to the previous one is the following: compute the Kolmogorov distances of the traces, as before, and also calculate the total traffic within each window. This procedure generates two new sequences. Table 1 gives their correlation for our different data sets, for 0.128s-binned traffic. Interestingly, it is non-negligible and negative for all the data sets that are clearly not uniformly Gaussian according to the discussion above (i.e. 94, L4, L5, U8, and 89).

This is again consistent with Theorem C, by the following argument: Theorem C states that the more numerous the active users are, the more Gaussian the traffic will be, and thus the smaller the Kolmogorov distance. On the other hand, the number of active users is highly and positively correlated with the traffic volume. The combination of the two statements implies that traffic volume and the Kolmogorov distances should be negatively correlated, unless, of course, the traffic is already (almost) Gaussian, in which case no prediction according to the theorems is possible (the data sets close to Gaussianity are traces 97, M6, and M7, whose correlations are indeed either negligible or positive). Note that Gaussian-type traffic is *not* extremely spiky. The negative correlations in Table 1 thus illustrate that when more users are active, and when traffic is heavier, it becomes less spiky. This seems counterintuitive; yet it is consistent with Theorem C, and borne out by the data.

Note here that the correlation can vary dramatically with the time bin used, due to the presence of “levels”, which will be discussed in Section 6. But, in general, for large time bins, the correlations are large, as Theorem C predicts.

## 5.7 A comment on Slow Start and heavy-tailed session sizes

Note that the importance of the impact of Slow Start on the traffic is intimately coupled to the fact that the distribution of  $L$  is heavy-tailed. If  $L$  is always very large, the window size will reach  $M$  and will stay there. Thus, with the exception of the first few times, the user will always be sending  $M$  packets at a time. This situation is little, if at all, different from model B. If, on the contrary,  $L$  is always very small, then the *effective*  $M$  will be very small, since Slow Start will be stopping at a very early stage, the session being over.

Consequently, Slow Start can be the star only when most of the sessions are small, but occasionally huge ones show up. It is precisely these latter ones that form spikes, taking advantage of a large value of  $M$ . Rephrasing in network terminology, “spikes are created by large sessions over fast links” [23]. Statistical analysis of the *flows* of e.g. trace 94 reveals that they are indeed very short, with occasional large ones.

The assumption made implicitly in the discussion above is that a spike is the result of one user, not the aggregate result of many of them. Although this has already been confirmed [23], an independent confirmation is offered here: divide the time axis into bins of constant size, and in each bin measure the number of active connections (i.e. connections that send in this interval more than one packet), and the average window size (i.e. the number of packets sent divided by the number of active connections). If, for a spiky traffic, it is the latter that is spiky, and not the former, then this indicates that some users must be sending a lot of packets. Fig. 14 shows that this is indeed the case for real traffic.

## 5.8 Earlier work on the Gaussianity and p-Stability of the traffic

The idea of a process that can be either self-similar or  $p$ -Stable, contingent upon the value of a parameter, already appears in the form of theorems in [29], and of observations in real world traces in [23]. More precisely:

- [23] analyzed empirically the oscillation of the traffic between Gaussianity and non-Gaussianity and offered a plausible networking explanation. No attempts were made, however, to explain it mathematically. Consequently, the authors were unable to justify the observed negative correlation between amount of traffic and spikiness.
- [29] provides an interesting variant of model A, the ISPM, and considers a process equivalent to  $Z_n^a(Tt)$ , according to the notation of section 3. It proves then that the limit process, as  $T \rightarrow \infty$  and  $n \rightarrow \infty$  simultaneously, can be either  $p$ -Stable or Gaussian, depending on the rates by which  $n$  and  $T$  tend to  $\infty$ . In our opinion, though, the limit process does not relate to Internet traffic in an obvious way, and its mathematical predictions, at least as stated in [29], cannot be directly translated in the language of networks, except yielding a result for the traffic at coarse scales on very busy links, which is exactly the situation the two limits above describe. Moreover, no attempt was made in [29] to corroborate the model’s assumptions by empirical evidence, or to compare the properties of the simulated traffic it produces with the corresponding properties of real traffic. Finally, the limit processes in [29] are strictly either self-similar or  $p$ -Stable; no allusion is made to the possibility of oscillation of the process between these two extremes.

# 6 Model D

## 6.1 Introduction

Models B and C were able to capture and explain crucial features of Internet traffic, such as its long range dependence, its different behavior in different time scales, and its spikiness (compare Fig. 13, 1, 2, and 8). Unfortunately, the Energy function of the simulation is still far from reality (compare Fig. 15 and 7). This suggests that pieces of the puzzle are still missing.

## 6.2 A closer look into Averaging functions

So far, the simulations failed to introduce a substantial curvature into the Averaging or Energy function (Fig. 7, 16), although the processes used spanned a variety of attributes (heavy/light-tailed marginals, independence/long-range dependence, etc.), and even combined them (as in the  $\alpha$ - $\beta$  traffic model). It was precisely this characteristic that stimulated research of “multifractality”, questioned the accuracy of traffic description through Poisson or

self-similar processes, and ended up demonstrating that the traffic is a fundamentally different process from these two [23, 16, 15].

The Averaging functions of the data traces (Fig. 16) are truly remarkable: recall that a slope  $\alpha$  at time scale  $\log_2(n)$  indicates a behavior of type  $n^{-\alpha}$  for the difference between two mean value estimators of  $n$  terms; if  $\alpha$  depends on  $n$ , the process is not self-similar. This is the case for all of the traces. Moreover, as explained in the heuristic argument in section 2, one expects, if the  $X_i$  are asymptotically independent, that the Averaging function will decrease monotonically as a function of  $n$ , at least for large  $n$ . This is not the case for our data. For instance, the Averaging function of trace 94 is constant in the region from  $n = 2^8 = 256$  till  $n = 2^{15} = 32768$ . In other traces the Averaging function even *increases* with  $n$ : trace 97 exhibits a little “bump” at time scale 13 (Fig. 16(a)), and trace M6 exhibits a bigger bump at time scale 18 (Fig. 16(c)); simulations carried out later in this section achieve an even more spectacular result (Fig. 25).

In our heuristic argument we assumed asymptotical independence of the  $X_i$ . We now know that the  $X_i$  in our traces cannot be considered asymptotically independent, at least relatively to the trace duration, and we interpret the “deviant behavior” of the Averaging function as a manifestation of this lack of independence. Why should it show up much more at some scales than in others? This is the question we address in this section.

### 6.3 Averaging functions and multiscale structure of the traffic — *levels*

There are essentially two important aspects of Internet traffic that have been overlooked throughout the discussion of the previous models:

On the one hand, the exact attributes of time intervals between packet emissions were hitherto supposed to be of little importance: in the theorems, they were assumed to follow any distribution of finite variance, and simulations were performed with an exponential one. The exact distribution has indeed been an object of study, and it turned out that the Poisson model for a single user fails [1], and that (bi)Pareto, Weibull, and empirical (Tcplib [1]) distributions come into play [8]. The former may violate the finite variance assumption.

On the other hand, traffic seems to comprise many phenomena that are hierarchically structured: for example, users organize texts in chapters, chapters in paragraphs, paragraphs in sentences etc., thus one expects a variety of durations of pauses and activity. This will have an effect on traffic, if one supposes the user types over the net. Also, during Web browsing, users read, process the information, and act accordingly. Finally, in the network there is protocol activity spanning many time scales: congestion control occurs every fraction of a second, but routing information is exchanged every half an hour, or so.

It appears then that many time scales are of importance, each for a different reason, but all because some kind of activity is taking place there. The exact values of these time scales, or other details about them, are still unclear, to the best of our knowledge, although they are generally accepted to exist [1, 3, 18], as the result of both user behavior and protocols. This activity in multiple time scales, however, can alter completely the autocorrelation of the traffic, introducing strong correlation in some time scales and weak in others. This, in turn, will impact the Averaging function as well, according to (3). Consequently, the curving of the Averaging function may have its roots in this multiscale activity, and this seems worth investigating.

### 6.4 Evidence for multiscale activity

A useful and simple tool for the detection of these time scales (*levels*) in the traffic is the *characteristic function* of a connection<sup>3</sup>. A *connection* is defined to consist of the entries of the trace corresponding to a particular value of sender host, receiver host, sender port, and receiver port, and is essentially what the  $W_i$  stand for in Theorems B and C. The characteristic function of a connection is a function of time, equal to 1 if that particular time is a time stamp belonging to the connection, and 0 otherwise.

Characteristic functions seem to have a fractal structure (see Fig. 17 and 18); moreover, analysis of the characteristic functions of the 50 largest connections of trace 94, and connections of trace M6, leads to the conclusion that levels of connections do not average out in the aggregate traffic, but, on the contrary, have a strong influence on it. Capturing this effect will be the main goal of this section; but first, let us propose a more quantitative level detecting method in individual user sessions, which establishes the presence of multiscale levels more firmly than the anecdotal evidence of Fig. 17 and 18.

---

<sup>3</sup>Similar diagrams exist in [1].

## 6.5 Detecting levels quantitatively in user sessions: the Interval Detection Algorithm (IDA)

The purpose of this experiment is to provide quantitative information on the levels present in a session. The tool developed herein bears many similarities to Tools 1 and 2 of section 8, providing similar results, but by following a different (and much simpler) method, based on the idea of detecting the lengths of periods of activity and inactivity.

We start by describing the Interval Detection Algorithm; we will come back to its motivation below.

Take a user session and bin it using an initial time bin, but in a special way: omitting packet sizes, assign a value of 1 to every bin in which a packet emission took place, and 0 otherwise. Subsequently, choose a base  $b$ , and run on the session the *Interval Detection Algorithm*:

### 1. Part 1:

- (a) Record the lengths of all intervals of value 0 (*gaps*) in the data set.
- (b) For every  $i \geq 0$ , find the sum  $s(i)$  of the lengths of gaps  $G$  that satisfy  $\lceil \log_b(|G|) \rceil = i$ .

### 2. Part 2:

For all  $i \geq 0$  such that  $i \leq \lfloor \log_b(\text{Session Length}) \rfloor + 1$

- (a) Invert the session bin values logically.
- (b) Run Part 1.
- (c) Store the result as the  $i$ th column of the array  $a(j, i)$  (we will call these results the  $i$ th stage of the detection of 1-intervals of levels or simply the  $i$ th stage of the IDA).
- (d) Invert the session bin values logically.
- (e) Assign value 1 to all bins of the gaps  $G$  that satisfy  $\lceil \log_b(|G|) \rceil \leq i$ .
- (f) Set  $w(i)$  to be the session values sum.

### 3. Part 3: Choose $0 < \gamma < 1$ . Then, for all $j \geq 0$

- (a) Compute  $M = \max_i(a(j, i))$ .
- (b) Set  $i$  equal to the maximum possible value, and start decreasing it, until  $a(j, i) < \gamma M$ , but  $a(j, i - 1) \geq \gamma M$ . Set  $I = i$ .
- (c) For all  $i$ , set  $a(j, i) \leftarrow a(j, i)/w(I)$ .
- (d) Set  $s(i) \leftarrow s(i)/w(I)$ .

### 4. Part 4 (Representation of the results):

- (a) Let  $im$  be an array. Choose numbers  $c_1 > c_2$ . Then, for all  $i \geq 0$ :
  - i. Find the maximum of the  $i$ th column of  $a$ ,  $m_1$ .
  - ii. Find the second maximum of the  $i$ th column of  $a$ ,  $m_2$ .
  - iii. If  $m_1 > c_1 m_2$  and  $m_2 > c_2 m_1$  then  $\forall j : a(j, i) \leftarrow a(j, i)/m_2$  else  $\forall j : a(j, i) \leftarrow \min(a(j, i)/m_2, 1)$ .
- (b) Repeat the three steps above for  $s$  (*optional*).
- (c)  $\forall i, j$ , let  $im(j, i) = a(j, i)$ .
- (d) Append to  $im$  a column of 0s (*optional*).
- (e) Append  $s$  to  $im$  as a column.
- (f) Mesh  $im^T$  in greyscale: the higher a value of  $im$  is, the darker the point representing it (this will be the *greyscale representation*).
- (g) Set  $v_1$  to be a vector, whose  $i$ th element is the sum of the elements of the  $i$ th row of  $im$ , excepting its last column (the 0-interval stage).
- (h) Set  $v_0$  to be the last column of  $im$ .

- (i) Normalize  $v_1$  and  $v_0$  so that they both have maximum value equal to 1 and plot them (this will be the *sum representation*).

Within the framework of the greyscale representation, the IDA will indicate that a level for the 0-intervals exists where  $s(\cdot)$  has a high value, whereas a level for the 1-intervals will exist where local maxima of  $a(\cdot, i)$  align for many different  $i$ . On the other hand, within the framework of the sum representation, levels for the 1- and the 0-intervals will be assumed to exist at the local maxima of  $v_1$  and  $v_0$  respectively.

Notice that the two representations are not equivalent, since the sum representation does not show the individual stages of the 1-interval detection. However, as far as level detection is concerned, they can be considered equivalent: if many stage maxima cluster at a particular time scale, then the sum of the stage values at this particular time scale will tend to be rather large, and vice versa. Therefore, the two representations can be used interchangeably for our purposes.

To explain how the IDA gives us this information, we first describe our way to simulate multi-scale sessions similar to the real sessions appearing in Fig. 17 and 18, and see how the IDA allows us to observe their structure. The following is our simulation strategy:

1. Generate a vector of isolated 1s separated by intervals of 0s; these intervals represent the RTTs and should be independent and identically distributed.
2. Generate a vector of alternating intervals of value 1 and 0. These intervals should also be identically and independently distributed, but also cross-independent. The two generating distributions, though (for intervals of value 1 and 0), need not be the same.
3. Repeat the previous step as many times as necessary, by choosing distributions with progressively smaller mean. Simulated traffic with  $n$  levels will result, if the step is repeated  $n$  times.
4. Multiply the vectors obtained above.

This strategy contains the main idea behind levels, that coarse 1-intervals get recursively subdivided into finer and finer 1- and 0-intervals.

In order then to detect the structure of a user session (whether simulated or real), it will suffice to parse this user session only once in order to find the (unnormalized) histogram of the 0-interval lengths, which is exactly what Part 1 of the IDA does. The detection of 1-interval lengths will be trickier, however, since such intervals are not immediately present in the session: the 0-intervals of finer levels fragment them into small pieces, and their continuity has to be restored before they can be detected. Part 2 takes care of this by computing sequentially the histogram of the 1-interval lengths, after “filling in” larger and larger 0-intervals.

Finally, the IDA deals with the normalization of the histograms it produces. Making a traditional histogram by counting how many interval lengths can be logarithmically rounded to a certain time scale, and turning the histogram into a probability density by dividing with the total number of intervals that contributed to it will not do in this case, since the coarser the intervals, the more rare they are, but this does not mean they become less important, as this normalisation would suggest. The normalization must reveal the strength of the presence of a level within the session. One way to do this is to add the lengths of all intervals that contribute to a certain entry of the histogram and divide by the session length, which is equivalent to finishing the IDA in Part 2. But this will bias in favor of the coarse levels a lot, since a level does not really live on the whole session, but on the immediately coarser level only. Thus, the best normalization will be obtained by dividing not by the session length, but by the sum of 1-interval lengths of the immediately coarser level, on which the level in question resides. An easy way to determine this normalization factor is to observe when the values of the unnormalized histograms corresponding to the time scale in question become negligible: if, after filling the gaps with length approximately equal to  $b^j$ , the histogram values corresponding to time scale  $b^j$  become negligible, the proper normalization is  $\forall k, a(i, k) \leftarrow a(i, k)/w(j)$  and  $s(i) \leftarrow s(i)/w(j)$ , as Part 3 explains. This method is approximate, of course: its main drawback is that the normalization depends entirely on the 1-intervals. However, it seems to work in practice, as we are about to see.

The normalization issue discussed above suggests that the location of the maxima may be misleading, if one attempts to detect the 1-intervals of the levels based on them: indeed, despite the improved normalization discussed above, our simulations show that the maxima of the different stages of the detection of 1-intervals still span a wide

numerical range. This is why we decided to suppress this information in the final presentation of the results of the IDA, and use other information instead, as suggested in Part 4 of the IDA algorithm.

As the algorithm evolves and gaps of the data set get filled, the maxima of the stages will be moving towards larger scales. In the case of simulations with clearly separated and defined levels, this motion will be discontinuous: if the 1-intervals of a level have approximate lengths of  $b^i$  and the ones of the immediately coarser level  $b^j$ , then for stages immediately before  $i$  the maximum will be at  $i$ , but for stages  $i$  up to  $j$  it will be at  $j$ : indeed, filling gaps of lengths between  $b^i$  and  $b^j$  will be of no effect, because the number of these gaps, by assumption, is not significant. The IDA then produces results such as in Fig. 19(a), (b), where the sudden jumps and the long immobility periods of the maxima are very eloquently depicted (more information about Fig. 19 will follow shortly).

In the case of simulations with diffused levels or of real data sets, though, the maximum will be moving more or less smoothly. When depicting the results of the IDA in the greyscale representation, this motion will appear as a diagonal line of maxima in the figure (see e.g. Fig. 20(a), (c), and 20(a)). However, there will still be time scales where maximum (or nearly maximum) values will seem to persist for more than one stages (such as time scales 12 and 18 in Fig. 20(a), (b)), just as in the case of non-diffused levels, indicating the existence of a level there. Thus, the algorithm will not rely upon the maximal values of the stages for the detection of 1-intervals, but will instead pick the time scales where large values of the stages tend to “cluster”, as Part 4 of the IDA description states.

In order to test the performance of the IDA, we applied it on six simulated sessions, generated by the session simulation algorithm presented above; the results are shown in Fig. 19 and 20. Each one of the six simulations, which have a behavior very similar to Fig. 17 and 18, features 3 levels, whose 1-intervals have mean size  $2^6$ ,  $2^{11}$ , and  $2^{16}$ , and whose 0-intervals have mean size  $2^2$ ,  $2^7$ , and  $2^{12}$ , i.e. they are 16 times smaller. The interval lengths are uniformly distributed around their mean in Fig. 19 and Fig. 20(a), (b), and the ratio of the allowed variation over the mean is 0 in Fig. 19(a), (b), 0.3 in Fig. 19(c), (d), 0.6 in Fig. 19(e), (f), and 0.9 in Fig. 20(a), (b). The levels in Fig. 20(c), (d) are exponentially distributed around their mean, and levels in Fig. 20(e), (f) follow a Gaussian distribution, whose mean in each case coincides with the level mean, and whose variance is proportional to the mean:  $\sigma^2 = 4\mu$ . The IDA picks out the positions of the 0- and 1-intervals reasonably accurately, even when the variance becomes large: for scales (horizontal axis) at which 1-intervals of levels exist, the greyscale column is much “taller” than at other scales; the scales at which 0-intervals of levels exist are picked out by the top greyscale line. In particular, it is always clear, except in the exponential case in Fig. 20(c), (d), that there are 3 distinct levels.

The Averaging functions corresponding to two of the above simulations (19(b) and 20(a)) are shown in Fig. 21. At this point, we would like to jumb ahead a bit, and ask the reader to notice the clear correspondence between the way the Averaging function curves, and the position of the levels, as captured by the IDA. Indeed, the following sections will demonstrate the relation between these two phenomena.

Having thus assured ourselves of the efficiency of the IDA on simulated sessions, we use it in Fig. 22 and 23 on two individual sessions taken from the data sets. In each case, the IDA identifies time scales that stand out. In particular, regarding the longest session of trace 94 (Fig. 22), the IDA predicts that the 1-intervals of levels have lengths between  $2^{10}ms$  and  $2^{20}ms$ , whereas the 0-interval lengths lie between  $2^4ms - 2^{14}ms$  and  $2^{17}ms - 2^{19}ms$ , which means that this session appears to have levels all over the place. Jumbling ahead once more, let us note that the Averaging function seems to suggest the same thing (see the discussion in sections 6.7 and 6.9 for the connection between Averaging function curving and levels), as the position of the “bumps” of the Averaging function (Fig. 22(c)) corresponds exactly to the position of the levels predicted by the IDA.

In two occasions above, a simulated and a real session, the IDA and the Averaging function were found to yield compatible results about where the 1- and 0-intervals of the session levels lie. Is then this always the case? Unfortunately, another real session, the one that was also used in Fig. 17, answers the question in the negative.

For this session, the IDA detects 0-intervals of levels in two areas (see Fig. 23(a), (b)): at  $2^{18}ms - 2^{19}ms \approx 250s - 500s$ , and at  $2^8ms - 2^{14}ms \approx 0.25s - 16s$ . In Fig. 17, we had identified by mere observation levels at 400, 15, 10, and 4s which fits very well. On the other hand, the IDA detects 1-intervals at  $2^{15}ms \approx 30s$  and at  $2^{18}ms - 2^{21}ms \approx 250s - 2000s$ , whereas in Fig. 17 we observe 1-intervals with lengths of 1000s – 2000s, 500s, and 40s. Hence, visual inspection and the IDA yield almost identical results. But how does the IDA compare to the Averaging function (Fig. 23(c))? Although the IDA detects a very prominent level with 0-intervals around  $2^{13}ms$ , the Averaging function seems to ignore it completely. Although this appears to be a potential failure for our model at first sight, it is not. We will come back to that issue in section 6.8, where we will discuss explicitly levels with unequal 1- and 0-intervals.

As a general remark, compared to the simulations of Fig. 19, the behavior of real traces seems to be more

complex: actually, the percentage is almost nowhere equal to 0, which should mean that levels, even weak ones, exist in almost all time scales.

Having established the effectiveness of the IDA on individual sessions, simulated or observed, let us now turn our attention to aggregate information: we apply the algorithm to *each* session in trace 94, and superpose the individual results. The result is shown in Fig. 24 (note here that bin sizes increase geometrically by  $\sqrt{2}$  rather than by 2), which shows clearly that some levels persist in the whole trace: their 1-interval lengths lie between  $2^9ms$  and  $2^{13}ms$ , and also between  $2^{15}ms$  and  $2^{18}ms$ , whereas their 0-interval lengths lie between  $2^7ms$  and  $2^{15}ms$ . Comparison with the Averaging function of trace 94 (see Fig. 24(c)), which shows an extended period of activity between  $2^7ms$  and  $2^{16}ms$ , and also a little “bump” at  $2^{18}ms$ , demonstrates that the two methods are compatible, yielding similar results.

The fact that the IDA detects levels in Fig. 24 suggests that the majority of the connections of trace 94 share some levels, which appear then in the aggregate results, and that, consequently, it is possible to attribute levels to an entire data set, thus extending the notion of levels. The excellent agreement of the two methods (IDA and Averaging function — see also section 6.9) corroborates strongly the legitimacy of the extension of the notion of levels to entire traces, and also implies that the much simpler Averaging function can be used for their detection, instead of the IDA. Indeed, on the same computer, the IDA needed two days to process trace 94 entirely, whereas the Averaging function only takes a few seconds.

## 6.6 Theorem D: statement and proof

Theorem D below implies that the covariance structure of total traffic is strongly dependent on its levels.

**Theorem D.** Let  $A^\Delta(W) = \Delta^{-1} \left( \mathbf{Var} \left( \int_0^\Delta W(t)dt \right) - \mathbf{Cov} \left( \int_0^\Delta W(t)dt, \int_\Delta^{2\Delta} W(t)dt \right) \right)^{1/2}$  and let  $\widetilde{W}_i^d(t)$  be the same as  $W_i^b(t)$  but with  $O_f^b(i) = 0$  a.s. and  $O_n^b(i) = \infty$  a.s. Also, take  $\widehat{W}_i^d(t)$  to be the same as  $W_i^a(t)$  (notice that  $\widehat{W}^d$  represents a continuous traffic (no spikes traffic), while  $\widetilde{W}^d$  represents a discrete traffic, where  $RTT$  is present (spikes traffic)).

$$a) A^\Delta \left( \widetilde{W}_1^d \right) \approx \Delta^{-1/2} \rightarrow 0 \text{ as } \Delta \rightarrow \infty$$

$$b) A^\Delta \left( \widehat{W}_1^d \right) \rightarrow 0 \text{ as } \Delta \rightarrow 0 \text{ or } \Delta \rightarrow \infty \text{ and there exists a constant } K > 0 \text{ such that}$$

$$A^\Delta \left( \widehat{W}_1^d \right) \geq K \text{ for } \Delta = \mathbf{E}(O_n^b + O_f^b)/2$$

*Proof.* For a). Assume that the  $R_{i,j}^b$  are exponentially distributed with  $\mathbf{E}(R) = \gamma > 0$ . Let  $Q_{k,\Delta} = \int_{(k-1)\Delta}^{k\Delta} W_1(t)dt$ , then clearly  $\{Q_{k,\Delta}\}_{k=1}^\infty$  are i.i.d. Poisson with parameter  $\lambda = \Delta/\gamma$ . Thus

$$A^\Delta = \Delta^{-1} \sqrt{\mathbf{Var}(Q_{1,\Delta}) - \mathbf{Cov}(Q_{1,\Delta}, Q_{2,\Delta})} = \gamma^{-1/2} \Delta^{-1/2} \rightarrow 0, \text{ as } \Delta \rightarrow \infty.$$

The “exponentiality” assumption on  $R^b$  makes the proof easier, since it implies  $\mathbf{Cov}(Q_{1,\Delta}, Q_{2,\Delta}) = 0$  and it simplifies the computation of  $\mathbf{Var}(Q_{1,\Delta})$ . However, it can be shown that under much more general assumptions on the  $R$ , it is still true that  $|\mathbf{Cov}(Q_{1,\Delta}, Q_{2,\Delta})| \leq \lambda_1 \mathbf{Var}(Q_{1,\Delta})$  for some  $\lambda_1 < 1$  and  $\mathbf{Var}(Q_{1,\Delta}) = \lambda_2 \Delta$  for some  $\lambda_2 > 0$ .

For b). The first step is to establish that  $A^\Delta \rightarrow 0$  as  $\Delta \rightarrow \infty$ . [24] showed that

$$\mathbf{Var}(Q_{1,\Delta}) \underset{\text{large } \Delta}{\approx} \Delta^{2/p} \text{ and } \mathbf{Cov}(Q_{1,\Delta}, Q_{2,\Delta}) \geq 0$$

and these two results imply that  $A^\Delta \underset{\text{large } \Delta}{\approx} \Delta^{1/p-1} \rightarrow 0, \text{ as } \Delta \rightarrow \infty.$

For the case  $A^\Delta \rightarrow 0$ , as  $\Delta \rightarrow 0$ , we observe that, for  $\Delta$  small enough,  $Q_{k,\Delta} = \int_{(k-1)\Delta}^{k\Delta} W_1(t)dt$  has the following structure

$$Q_{k,\Delta} = \begin{cases} 0 & \text{with probability } p_1(\Delta) \\ u & \text{with probability } c\Delta \\ \Delta & \text{with probability } p_2(\Delta) \end{cases} \quad (18)$$

where  $u$  is a r.v. uniformly distributed on the interval  $[0, \Delta]$ ,  $c = 2/(\mathbf{E}(O_n) + \mathbf{E}(O_f))$ ,  $p_1(\Delta) = (\mathbf{E}(O_f) - \Delta)/(\mathbf{E}(O_n) + \mathbf{E}(O_f))$ , and  $p_2(\Delta) = (\mathbf{E}(O_n) - \Delta)/(\mathbf{E}(O_n) + \mathbf{E}(O_f))$ . In order to simplify the computation, assume that  $\mathbf{E}(O_n) = \mathbf{E}(O_f) = 1$ . Then,

$$\mathbf{E}(Q_{1,\Delta}) = \Delta/2, \quad \mathbf{E}((Q_{1,\Delta})^2) = \Delta^2/2 - \Delta^3/3.$$

It is clear, using the very same argument as in (18), that, for small  $\Delta$  and  $u$  a uniform r.v. on interval  $[0, \Delta]$ ,

$$Q_{1,\Delta}Q_{2,\Delta} = \begin{cases} 0 & \text{with probability } 1/2 \\ \Delta & \text{with probability } 1/2 - 2\Delta \\ u\Delta & \text{with probability } 2\Delta \end{cases}$$

Thus

$$\mathbf{E}(Q_{1,\Delta}Q_{2,\Delta}) = \Delta^2/2 - 2\Delta^3 + 2\Delta^5/3$$

Putting this together

$$\begin{aligned} A^\Delta &= \Delta^{-1} \sqrt{\mathbf{E}(Q_{1,\Delta})^2 - \mathbf{E}(Q_{1,\Delta}, Q_{2,\Delta})} \\ &\underset{\text{small } \Delta}{\approx} \Delta^{-1} \sqrt{5\Delta^3/3 - 2\Delta^5/3} \underset{\text{small } \Delta}{\approx} \Delta^{1/2} \rightarrow 0 \text{ as } \Delta \rightarrow 0. \end{aligned}$$

Finally, the last statement of part b) has to be established. Here, the assumptions will be simplified considerably. Let  $O_n, O_f$  be uniformly distributed on the interval  $[1, 2]$  and let  $\Delta = 1$ . Then, trivially

$$Q_{1,\Delta} = \begin{cases} 0 & \text{with probability } 1/8 \\ u & \text{with probability } 3/4 \\ 1 & \text{with probability } 1/8 \end{cases}$$

where  $u$  is a uniformly distributed r.v. on the interval  $[0, 1]$ . Also, since  $O_n \leq 2$  a.s.,  $Q_{1,\Delta}Q_{2,\Delta} = 0$  a.s. Therefore:

$$A^\Delta = \Delta^{-1} \sqrt{\mathbf{E}(Q_{1,\Delta})^2 - \mathbf{E}(Q_{1,\Delta}, Q_{2,\Delta})} = 3/8$$

Clearly,  $O_n$  and  $O_f$  have been chosen in order to simplify the computation. The extension to more general distributions for  $O_n$  and  $O_f$  is much more involved, but nevertheless straightforward. Namely, one can show that under much more general assumptions it is still true  $|\mathbf{Cov}(Q_{1,\Delta}, Q_{2,\Delta})| \leq \lambda_1 \mathbf{Var}(Q_{1,\Delta})$  for some  $\lambda_1 < 1$  and that  $\mathbf{Var}(Q_{1,\Delta}) = \lambda_2 \Delta^2$  for some  $\lambda_2 > 0$  (provided that  $\Delta \approx \mathbf{E}(O_n)$ ). □

## 6.7 Explanation of the curvature of the Averaging/Energy function

The following argument explains the link between Theorem D and the curving of the Averaging/Energy function. Namely, assume there is a level at time scale  $j_0$ , and no other levels nearby. It will be assumed that  $2^{j_0} \gg RTT$ . Then:

- For  $j < j_0$  and  $2^j \gg RTT$ , the ON-periods appear continuous, and can be modeled by no spikes traffic  $\widehat{W}^d$ . Consequently, part b) suggests that the Averaging function increases.
- For  $j > j_0$ , the ON-periods again appear continuous, so part b) suggests that the Averaging function decreases, as  $j \rightarrow \infty$ .

Because the Averaging function is strictly positive, the points above suggest that it must have a maximum around the level  $j_0$ . This has indeed been confirmed by simulations (Fig. 25(b)).

However, the Averaging function of real traces initially decays, unlike the simulations in Fig. 25(b). Part a) of Theorem D explains this behavior as well:

- For  $j_0 < j$  and  $2^j \approx RTT$ , the ON-periods appear discrete and can be modeled by spikes traffic  $\widetilde{W}^d$ . Part a) takes over and ensures White noise-like behavior, i.e.  $\log_2 A_j \approx -j/2$ .

In case more than one levels are present, the argument above can be repeated, the role of RTT being now played by the size of the previous (finer) level. Therefore, the Averaging function should initially decrease, then change slope around the level, and have a “bump” around every level after the first. Simulations indeed verify this statement (Fig. 25(a)). The exact form of these “bumps” has to do with the “sharpness” of the level, i.e. with the variance of the durations of ON and OFF intervals. Very sharp levels, i.e. with small variance, seem to lead, at the time scale of the level, to the phenomenon of *superconvergence*<sup>4</sup>, i.e. convergence to the mean value faster than what the CLT predicts, which manifests itself through a slope less than  $-0.5$  (Fig. 25).

We would like to emphasize that we have introduced levels in our model consistent with our wish for “local” models (in the sense that the sessions are constructed by putting together appropriate building blocks, rather than the “global” approach of e.g. Random Cascades.) Our inspiration for the model was taken from direct inspection of observed traces; it does however differ from our earlier step in that we cannot point to a particular feature in user behavior or network protocol that could cause them. The scales of the levels, their sharpness, and their possible evolution in time may well be of interest to network engineers. For this reason we propose tools, in section 8, that are faster than the level-detector introduced above. Note also that heavy-tailed distributions were *not* needed in this construction: long range dependence and levels thus appear to be completely separate characteristics.

Now that we have understood the role played by levels, we are in position to explain the shape of the Energy and Averaging functions in the case of Slow Start simulations (Fig. 13), where the two functions are actually piecewise linear, not linear. The change of slope occurs between scales 7 and 9. But the mean value of the connection size was 5, and the mean RTT was 100, which implies that the mean total duration of the session was  $500 \approx 2^9$ , and this is exactly the level of the traffic.

One could argue that if the simulations of Fig. 16 and 7 were repeated with different parameters, some sort of curving might be achieved. This is true, to some extent (Fig. 26), but the curvature achieved is slight and does not resemble the one of real traces.

Finally, let us reexamine Fig. 16, armed with this qualitative understanding of levels. Trace 94 seems to have several levels between the time scales 8 and 15, and maybe around 20. A comparison with our discussion of Fig. 24 shows a good correspondence, although Fig. 24 gives a more detailed picture. Trace 97 has probably just one strong level at 13; trace L4 has one level at 8 and one at 15; trace L5 seems to have levels all over the place, but mainly one at some small scale (between 0 and 4), one at 8 and one at 15; traces M6, M7, and U8 appear to have levels at 12, 16, and 19, and M6 maybe has one more at 21; finally, trace 89 has levels at 2, 13, 16 and 19. In the next session, tools will be developed to quantify such guesswork.

## 6.8 Levels with unequal 0- and 1-intervals

Although Theorem D does not require the 0- and 1-intervals to follow the same distributions, the discussion in section 6.7 considered exclusively equally distributed 0- and 1-intervals, in order to enhance clarity. Unfortunately, as we have seen so far (for example, see Fig. 17 and 18, or Fig. 22 and 23), different distributions seem to be the rule rather than the exception, with the 1-intervals being typically much larger than the 0-intervals, so we need to determine how the Averaging function will respond to such a situation. Fig. 27(a) shows the Averaging function of a simulated session containing just one level whose 1-intervals have lengths around  $2^{15}$ , but whose 0-intervals have average lengths that are 1, 2, 4, ... times smaller. Observe that the Averaging function appears to “lock” on the 0-intervals, the existence of the larger 1-intervals being only alluded to by the size of the “bumps”, which are more prolonged than usual. Observe also (in Fig. 27(b)) that, if the lengths of the 0-intervals are much smaller than the lengths of the 1-intervals, and their distributions sufficiently diffused, it is possible for the bump to become negligible, and thus for the Averaging function to give the impression, by visual inspection, that no level exists.

<sup>4</sup>In real traces, we observed this behavior in the fine and middle scales of traces M6, M7, U8, and 89. See also 8S in Fig. 25.

An excellent example of a real session where the above observations apply is the session of Fig. 23 in section 6.5 (remember the last remarks made therein): it appears there is a quite pronounced level with 0-intervals around  $2^{13}ms$ , but comparison with Fig. 23(b) shows that the Averaging function does not seem to “feel” it. Does this suggest a potential failure of the model? Hardly so, in view of the discussion of the previous paragraph. Indeed, according to Fig. 17, the 0-intervals of the session levels are much smaller than the corresponding 1-intervals, and therefore it is highly probable that the Averaging function responds to their presence very “moderately”, just as is the case in Fig. 27(b). But even such a moderate response can still be detected by means of suitably designed tools, if not by eye alone, such as the ones presented in section 8.

## 6.9 Averaging function vs. IDA

Up to this point, two completely independent methods have been developed for the detection of levels: the Averaging function and the IDA. Naturally, two questions need to be answered now:

1. Are the results they give compatible?
2. Which one is more efficient to use?

The discussion in sections 6.5 and 6.7 implies that in principle the two methods yield equivalent results. In turn, Fig. 20 corroborates this statement: the session on the left seems to have very diffused levels that only slightly influence the curving of the Averaging function. However, the level at 19 has a strong impact on the Averaging function. The session on the right, on the contrary, seems to have sharp levels, as the correspondence of the two methods is almost 1-1. Indeed, the extended region of activity between the scales 5 and 14 corresponds to a region of intensive curving of the Averaging function. The fact that the latter extends in higher scales also can be attributed to the different distributions of 0- and 1-intervals, as explained in section 6.8. Notice that the coarse levels above scale 17 impact the Averaging function strongly, as was the case for the previous session, too.

Regarding efficiency, the Averaging function is far easier and faster to compute than to run the IDA on all of the trace sessions: the Averaging function can be computed in seconds, whereas the IDA typically requires days. The advantage of the IDA, however, is that it gives more detail, as it can distinguish the distributions of 0- and 1-intervals. Because of its computational speed, only the Averaging function will be used in the sequel.

## 7 The complete model

It was mentioned earlier that spikiness and levels are two phenomena highly uncorrelated, and that, as such, they can be studied independently. Following this principle, spikiness was studied in section 5 and levels in section 6, each ignoring the existence of the other. A successful simulation, though, should contain both, so our model would not be complete without an algorithm that combines spikiness and levels in a simulated trace.

The independence of the two features suggests that this combination can be done trivially; just use the algorithm of page 35, but interject the following step between the original Step 1 and Step 2:

- 1-2. Set the Slow Start maximum at  $M$ , and consider two indices,  $i$  and  $j$ . Set  $j \leftarrow 1$ . Then:
  - (a) Generate a heavy tailed integer random variable  $N$ .
  - (b) Move  $i$  to the next 1 value of the vector (generated by Step 1 at page 35). If end of vector found, then stop.
  - (c) Set the vector value at  $i$  equal to  $j$ , set  $N \leftarrow N - j$ , set  $j \leftarrow \min(2 * j, M)$ . If  $N \leq 0$ , go to Step (a) and set  $j \leftarrow 1$ .
  - (d) Go to Step (b).

All this step does is to supply the level algorithm with a Slow Start background. The shortcoming of this construction, though, is that the simulated Slow Start sessions in the final simulated trace do not necessarily correspond to sessions that could have possibly been generated in practice; indeed, the later steps of the algorithm may “chop” the beginning or the middle of a Slow Start session, and obviously such behavior cannot exist in practice. So, at this point, our construction deviates slightly from the actual network mechanisms, but this does not affect the results at all.

It is possible, however, to change the algorithm slightly and remove these artifacts. Just go back to the algorithm of page 35, and add the following step at the end this time:

5. Set the Slow Start maximum at  $M$ , and consider two indices,  $i$  and  $j$ . Set  $j \leftarrow 1$ . Choose a number of consecutive levels, starting with the finest one, and label them as “RTT levels”. Then:
  - (a) Generate a heavy tailed integer random variable  $N$ .
  - (b) Move  $i$  to the next 1 value of the vector (produced at the end of the algorithm of page 35). If end of vector found, then stop.
  - (c) If the gap between the previous and the current value of  $i$  is an RTT or belongs to an RTT level, generate a new heavy tailed integer random variable  $N$  and set  $j \leftarrow 1$ .
  - (d) Set the vector value at  $i$  equal to  $j$ , set  $N \leftarrow N - j$ , set  $j \leftarrow \min(2 * j, M)$ . If  $N \leq 0$ , go to Step (a) and set  $j \leftarrow 1$ .
  - (e) Go to Step (b).

Here, the “RTT level” 0-intervals play the role of additional RTTs that a session may encounter. This additional step in the algorithm, then, essentially identifies whether a gap should be considered a RTT or a 0-interval: in the former case, the Slow Start session continues over it normally; in the latter, the current Slow Start session ends, and a new one starts.

## 8 Discussion and Applications

**Correlation of user activity.** It has been systematically assumed in the previous models that the user streams  $W_i(t)$  are independent. By adopting this assumption, one neglects effect of network topology on the traffic. Congestion is taken into account only to the extent that it randomizes the RTT and maybe decreases the maximum  $M$  of Slow Start, but this clearly does not introduce cross-correlation among the users. Let us look a little closer at this seemingly drastic limitation.

The possible causes for interdependence between users are *path sharing* and *server sharing*. The former means that the data belonging to different users flow along network paths that share some links, or that exhibit correlation otherwise (ISP policies etc.). The latter means that two or more users access the same server, and perhaps the same information, i.e. that the end of the two paths is the same.

As regards to path sharing, the size of the Internet makes it very improbable today that, in a WAN setting, a major number of users will share a significant number of links; traffic typically goes through many hops (8 to 15), so that, if correlation builds up somewhere, it will vanish later, as user streams split again, assuming that delays on different links are independent. Of course, this will not be the case if the majority of users share the first link, but this will mean that the users belong to the same LAN (perhaps Ethernet, FDDI ring etc. [25]), which violates the WAN setting assumption.

As regards to server sharing, the variety of interests of Internet users suggests that this will hardly ever be a problem. Extreme scenarios, such as users massively accessing news sites in order to get news about an emergency, are clearly rare, and no attempt was made here to model them.

As a final comment, the combination of models C and D produces traffic statistically indistinguishable from the real one, from the point of view of the statistical tools hitherto presented: the Averaging function, the marginal distributions, and the autocorrelations yield identical results for simulations and real traffic. The fact that this was achieved without modeling any user dependence suggests that its effect is, in reality, less important than it is believed to be, or at least not detectable by these measurements.

**Burstiness and levels:** In our analysis, spikiness of the traffic and curvature of the Energy/Averaging function are two separate issues, due to different and independent mechanisms (geometric increase in transmission rate versus fragmentation of ON-intervals). Heavy-tailed distributions have no effect on the latter, but influence directly the former.

Tools that could detect spikiness and levels could prove useful. Some tools, based on the theorems proved earlier, are given below:

**Level-detecting tools:** Since levels leave a trace on the Averaging function, the Averaging function can be used to detect the level structure in a particular data set. This would allow for monitoring of user behavior without resorting to a connection-wise study of the trace, which is a very inefficient technique: for trace 94, the Averaging function was about 20000 times faster than computing the function in Fig. 24, on the same computer. We propose the following two algorithms:

Given the binary logarithms of the Averaging function:  $\log_2(A(0)), \dots, \log_2(A(n-1))$ , we compute slopes  $S_i = \log_2(A(i)) - \log_2(A(i-1))$ ,  $i = 1, \dots, n-1$  and slope changes  $|S_{i+1} - S_i|$ ,  $i = 1, \dots, n-2$ . These last quantities are equivalent to second derivatives, which, as is well known, measure the local curvature: as we argued in our discussion of Theorem D, the Averaging function has “bumps” around its levels, thus any curvature indicates the presence of levels. There is, though, one more point: it is not really important how much adjacent slopes differ, but how much they differ with respect to their absolute magnitudes. It seems then more appropriate to consider:

$$Sc_i = \frac{|S_{i+1} - S_i|}{\max(\min(|S_i|, |S_{i+1}|), \varepsilon)}, \quad i = 1, \dots, n-2$$

where  $\varepsilon$  is a small positive number, which will safeguard against division by 0, or an extremely small number (we used  $\varepsilon = 0.01$ ).

**Tool 1: (*Levels detector*)**

$$L(i) = Sc_i, \quad i = 1, \dots, n-2$$

The local maxima are considered to be levels.

Since White Noise leads to an Averaging function whose binary logarithm is just a straight line of slope  $-0.5$  (see corollary B), a much simpler idea would be to declare that a level exists where the slope becomes too large, as a signed quantity (ideally, it should become positive). How large it should be exactly is, in view of the lack of an accurate method to determine this, a matter of taste. We think that, due to the “noise” induced by the finite number of measurements available, it is very hard to distinguish a decay of type  $(\cdot)^{-0.1}$  from no decay at all, thus we set a threshold at  $-0.1$ .

**Tool 2: (*Detecting flat regions*)**

$$F(i) = 1_{S_i > -0.1}, \quad i = 1, \dots, n-1$$

Levels are considered to exist within flat (or concave) regions where  $F(i) = 1$ .

The results of Tools 1 and 2 are shown in Fig. 28, 29 and 30 for the real traces and some of the simulations, respectively.

**Spikiness calibration tools:** Spikiness varies widely, as was explained before, according to the protocol specifications, the amount of the transported data etc. For example, trace 94 seems much “wilder” than trace 97 (Fig. 1). Since spikiness is intimately related to the marginal distribution, the Kolmogorov distance between the trace distribution and the Gaussian curve seems to be a good measure of it. But a knowledge of the degree of persistence of spikes through different time scales is also desirable, therefore the Kolmogorov distance should be computed for each of them.

A possible extension would be to add information about how much the degree of spikiness varies within a particular time scale; this may be of particular importance in view of the oscillation of the process between Gaussianity and p-Stability (recall the discussion of model C). Thus, “windowed” marginals can be taken: the total trace, in a certain time scale, will be divided into adjacent parts (sub-traces) of consecutive points, the marginal of each and the corresponding Kolmogorov distances will be computed, and finally their mean value will be taken, in order to combine all this information into a single number-index.

In order to combine into a single number the results from every time scale, we compute a (weighted) average. There is considerable liberty here regarding the choice of the weights: Tool 3 below utilizes an equiweighted sum, whereas Tool 4 uses weighted averages, inspired by the discussion in section 5.

**Tool 3: (*Calibrating Deviation from Gaussian Process*)**

Given data  $X_i$ : for  $i = 1, \dots, N = 2^n$  and their coarser versions  $X_i^j = X_{(i-1)2^{j+1}} + \dots + X_{i2^j}$ , for  $i = 1, \dots, N_j = N2^{-j}$  and  $j = 0, \dots, k-1$ , compute the empirical cumulative distribution  $F_j(t) = N_j^{-1} \sum_{i=1}^{N_j} 1_{\widehat{X}_i^j \leq t}$ , where  $\widehat{X}_i^j$  stands for the centered and normalized version of  $X_i^j$  (i.e.  $\widehat{X}_i^j = (X_i^j - \overline{X_i^j}) / \text{Std}(X_i^j)$ ), and then  $D_j = \sup_{t \in \mathbb{R}} |F_j(t) - \Phi(t)|$ , where  $\Phi(t)$  is the standard normal cumulative distribution. The index of burstiness is:

$$D = k^{-1} \sum_{j=0}^{k-1} D_j$$

For Gaussian traffic,  $D = 0$ ; the larger  $D$  is, the more the traffic deviates from Gaussianity.

Different  $k$  can be considered, but we suggest  $k \leq n - 10$ , since for larger  $k$  sample size would not be sufficient, and thus the deviation of the empirical distribution from the true one would be no more negligible.

**Tool 4: (*Calibration of Burstiness of the Traffic*)**

Given data  $X_i$  and  $X_i^j$  as before and constants  $k$  and  $s$  (we suggest  $s \geq 9$  and  $k \leq n - s - 7$ ) let  $N_{j,s} = N2^{-j-s}$ .

Compute  $F_{j,l}(t) = 2^{-s} \sum_{i=(l-1)2^s+1}^{l2^s} 1_{\widehat{X}_i^j \leq t}$  for  $j = 0, \dots, k-1$  and  $l = 1, \dots, N_{j,s}$  (where  $\widehat{X}_i^j$  stands for centered and studentized version of  $X_i^j$ ). In other words,  $F_{j,l}(t)$  is the empirical cumulative distribution of the  $l$ 'th window of the  $j$ 'th time scale. Next, compute  $D_{j,l} = \sup_{t \in \mathbb{R}} |F_{j,l}(t) - \Phi(t)|$ ,  $T_{j,l} = \sum_{i=(l-1)2^s+1}^{l2^s} \widehat{X}_i^j$ , and  $\overline{D}_j = N_{j,s}^{-1} \sum_{l=1}^{N_{j,s}} D_{j,l}$ , which represent the Kolmogorov distance of each window, the total traffic of each window and the mean Kolmogorov distance for the time scale  $j$ , respectively. Next, for a fixed  $j$ , compute the cross-correlation between the sequences  $\{D_{j,l}\}_{l=1}^{N_{j,s}}$  and  $\{T_{j,l}\}_{l=1}^{N_{j,s}}$ :

$$C_j = \text{Corr}(\{D_{j,l}\}_{l=1}^{N_{j,s}} \text{ and } \{T_{j,l}\}_{l=1}^{N_{j,s}})$$

The result is computed as:

$$O = \frac{\sum_{j=0}^{k-1} C_j \overline{D}_j}{\sum_{j=0}^{k-1} \overline{D}_j}$$

The larger  $O$  is, the burstier is the traffic.

Note here that the main quantity considered is the correlation and that Kolmogorov distances are used as weights. The results will in general be negative (see discussion in section 5).

Tools 1 and 2 seem to reveal more or less the same information, as to where the levels are, but Tool 1 is a bit more detailed than Tool 2, in showing how “prominent” levels are (Fig. 28 and 29). The accuracy of the tools was tested by their results on simulated data (Fig. 30): they nicely match the curvature of the Averaging function for real traces, and they perform reasonably well with the simulations, where levels were artificially induced. As for tools 3 and 4, they reveal that trace 97 is the least spiky trace. This is in agreement with visual inspection (Fig. 1 and 2).

Before closing this section, let us submit Tool 2 to a final (and hard) test: can it detect correctly the levels of the trace 94 session presented in Fig. 17 and 23? We saw earlier in Fig. 23 in section 6.5 that there seems to be a very prominent level with 0-intervals around  $2^{13}ms$  (actually extending from  $2^{10}ms$  to  $2^{16}ms$ ), which nonetheless does not seem to affect the Averaging function much. Later, in section 27, we explained why this is the case. But is it then still possible for Tool 2 to detect the “traces” of this level on the Averaging function, however weak these may be? Actually it can, as Fig. 31 demonstrates. Tool 2 detects levels near  $2^7ms$ ,  $2^{11}ms$ , and  $2^{16}ms - 2^{19}ms$ , which are very close to the ones detected by the IDA in Fig. 23: in particular, the one detected at  $2^{11}ms$  corresponds to the IDA-detected level in question.

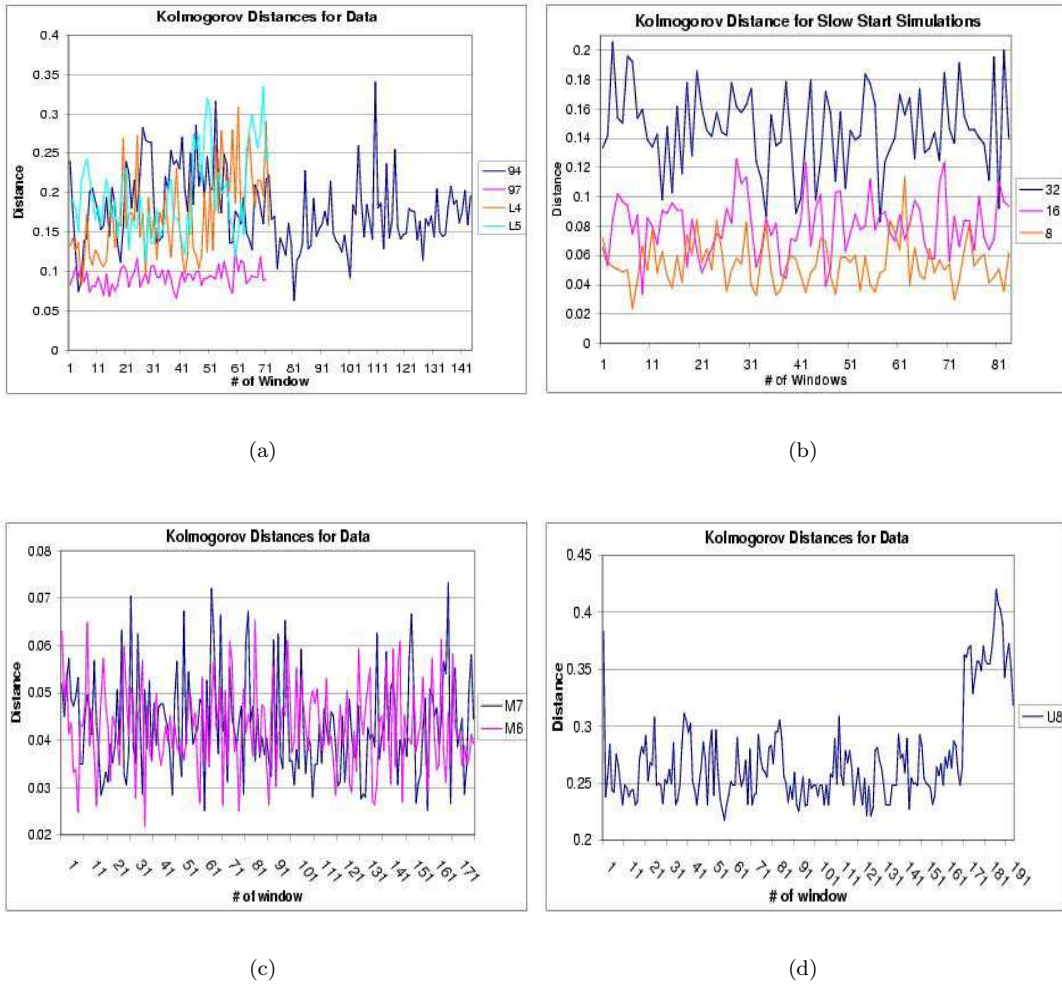
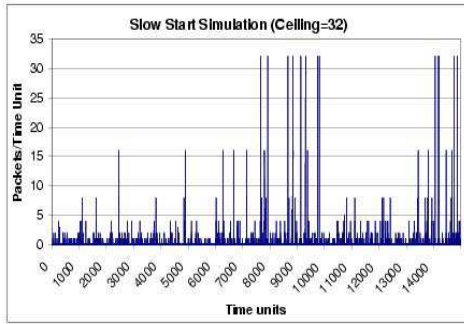
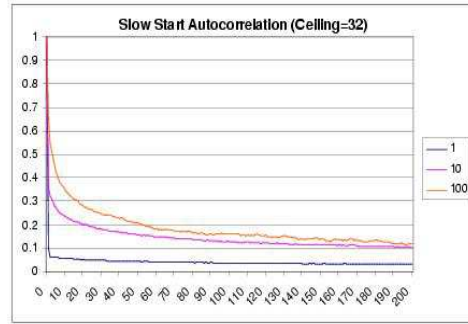


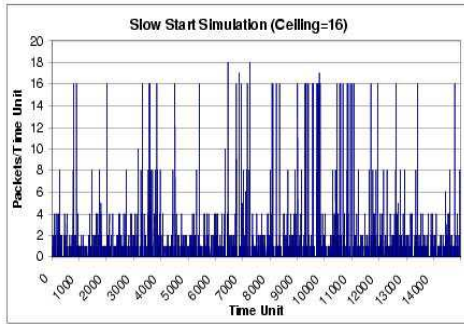
Figure 12: Kolmogorov Distances of trace marginals -(a), (c), (d)- and Slow Start simulation marginals -(b)- from the  $N(0,1)$  distribution. The numbers in (b)'s index denote  $M$ , the Slow Start maximum. Marginals have been computed using non-overlapping consecutive windows of  $2^9 = 512$  bins: the oscillations, and the distances themselves, are too large to be attributed to the finite number of observations used for the computation of the empirical marginals. A time bin of 100ms was used in (a) and of 1ms in (c) and (d). Note the different vertical scales in the different figures.



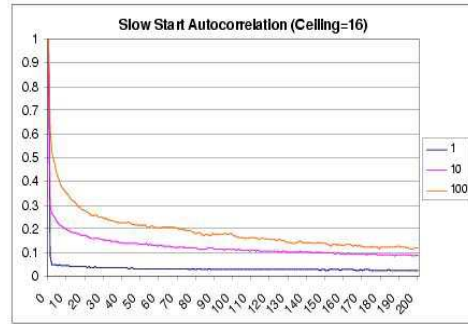
(a)



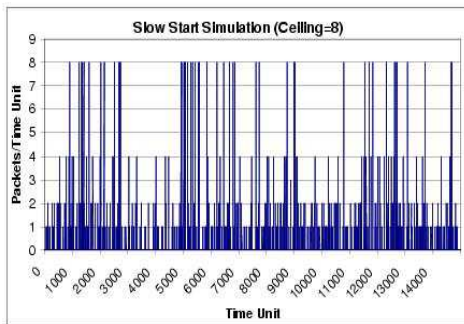
(b)



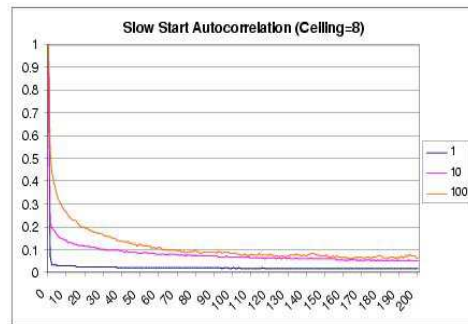
(c)



(d)

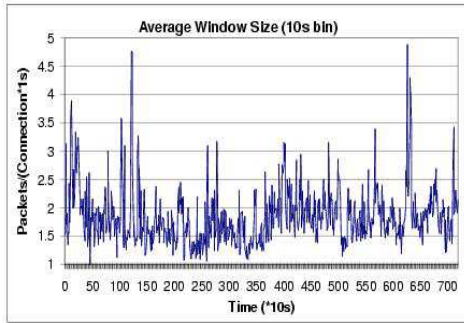


(e)

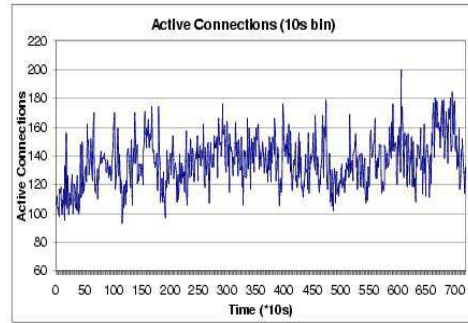


(f)

Figure 13: Excerpts of Slow Start simulation traces with (a)  $M = 32$ , (c)  $M = 16$ , (e)  $M = 8$ , and their corresponding (b),(d),(f)- autocorrelations.

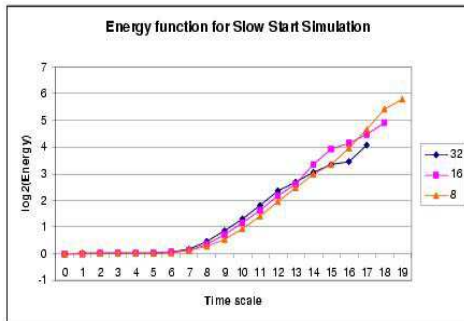


(a)

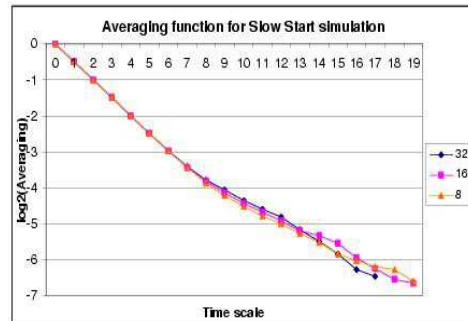


(b)

Figure 14: Average window size (a) and number of active connections (b) for 94 trace, using a time bin of 10s.

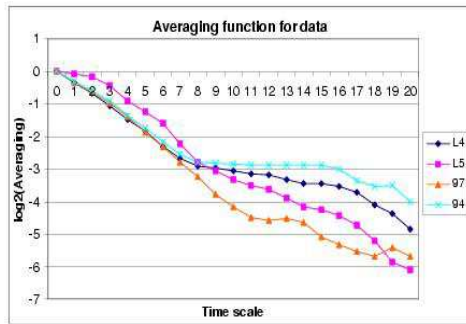


(a)

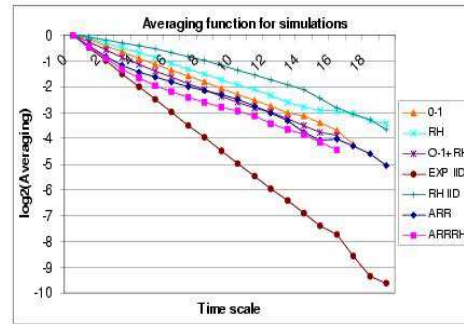


(b)

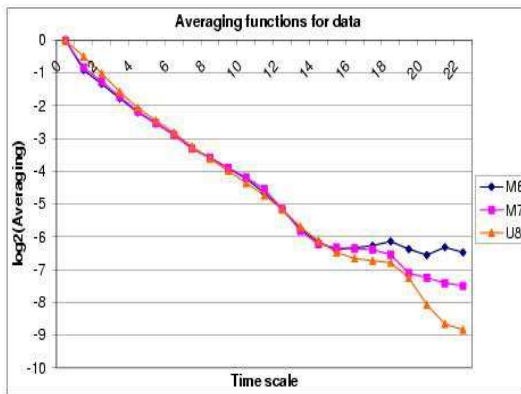
Figure 15: Energy (a) and Averaging (b) functions for the Slow Start Simulations: although some slight curving is present in these simulations, it is much more modest than what is observed in real traffic (see Fig. 7).



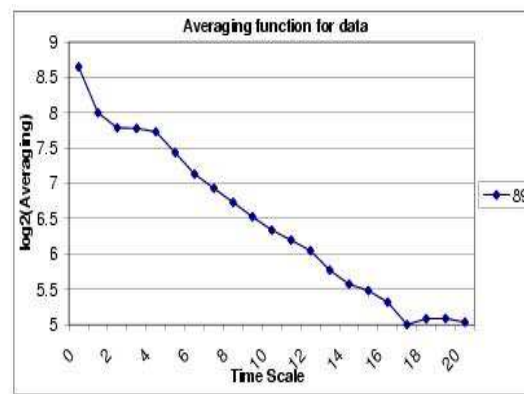
(a)



(b)

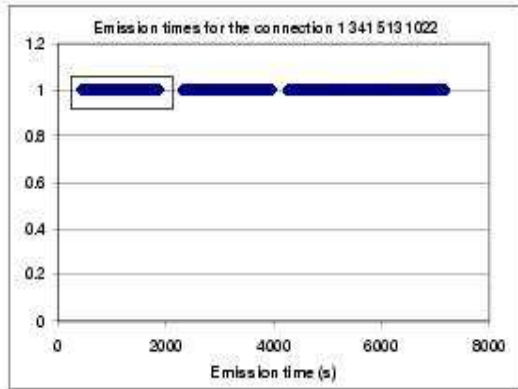


(c)

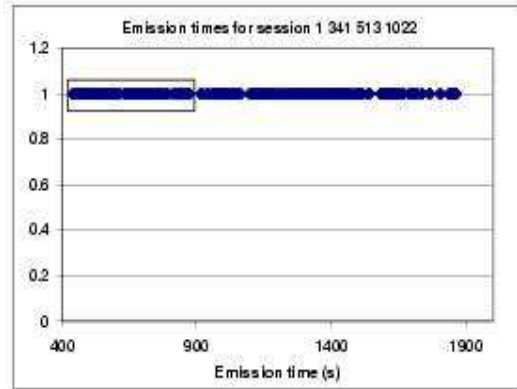


(d)

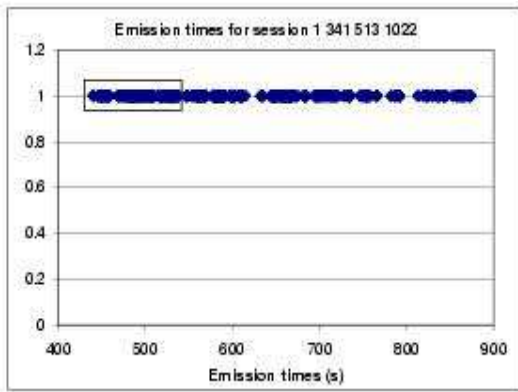
Figure 16: Averaging functions for data -(a), (c), (d)- and simulation (b) traces.



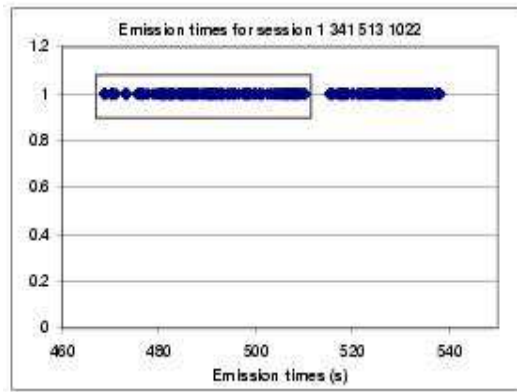
(a)



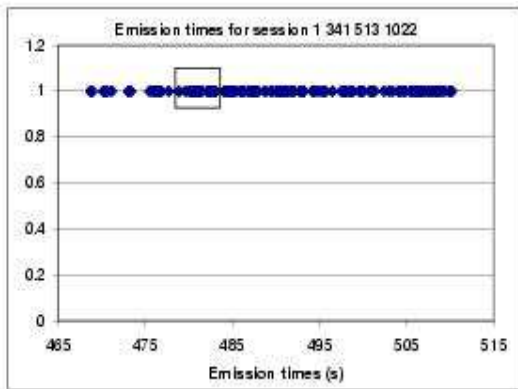
(b)



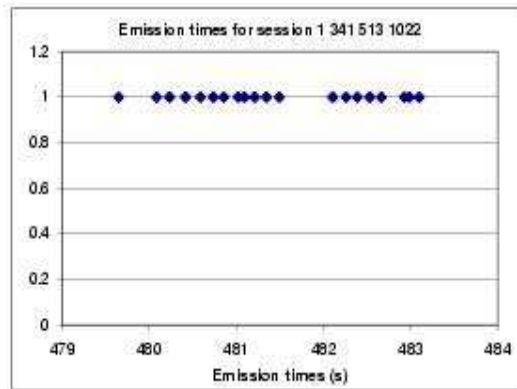
(c)



(d)

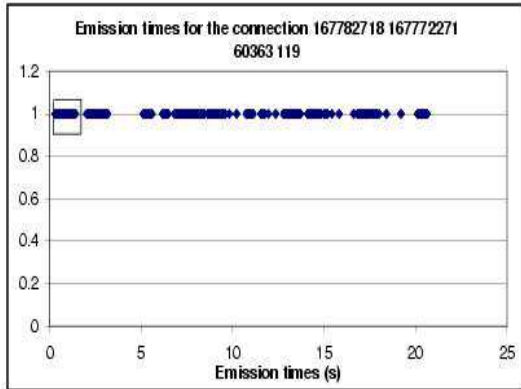


(e)

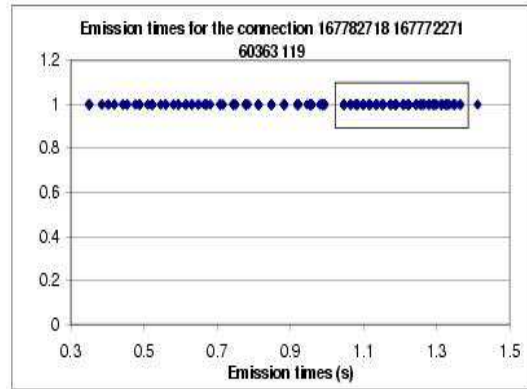


(f)

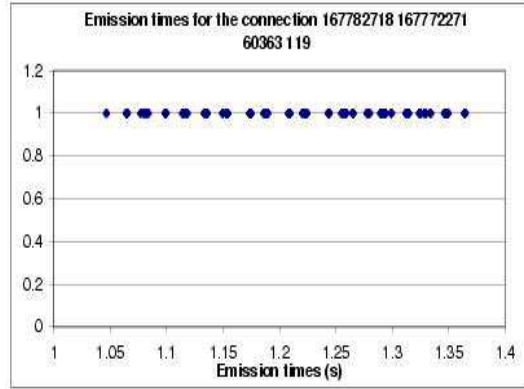
Figure 17: The characteristic function of connection 1 341 513 1022 from trace 94, in 6 detail levels. Each figure presents a “zoom-in” in the boxed segment of the previous one, illustrating a fractal-like behavior. Here, 6 levels can be detected: the (approximate) lengths of their 1-intervals are 2000, 500, 100, 40, 5, and 0.1s, whereas the lengths of their 0-intervals are much smaller in each case: 400, 15, 10, and 4s. Note that 0s are not plotted.



(a)



(b)



(c)

Figure 18: The characteristic function of connection 167782718 167772271 60363 119 from trace M6, in 3 detail levels. Here, 3 levels can be detected: the “approximate” length of their 1-intervals is 2, 0.44, and 0.01, whereas the corresponding 0-intervals are much smaller. Notice that coarser levels are not present in the data set, due to its short duration. Notice also that 0s are not plotted.

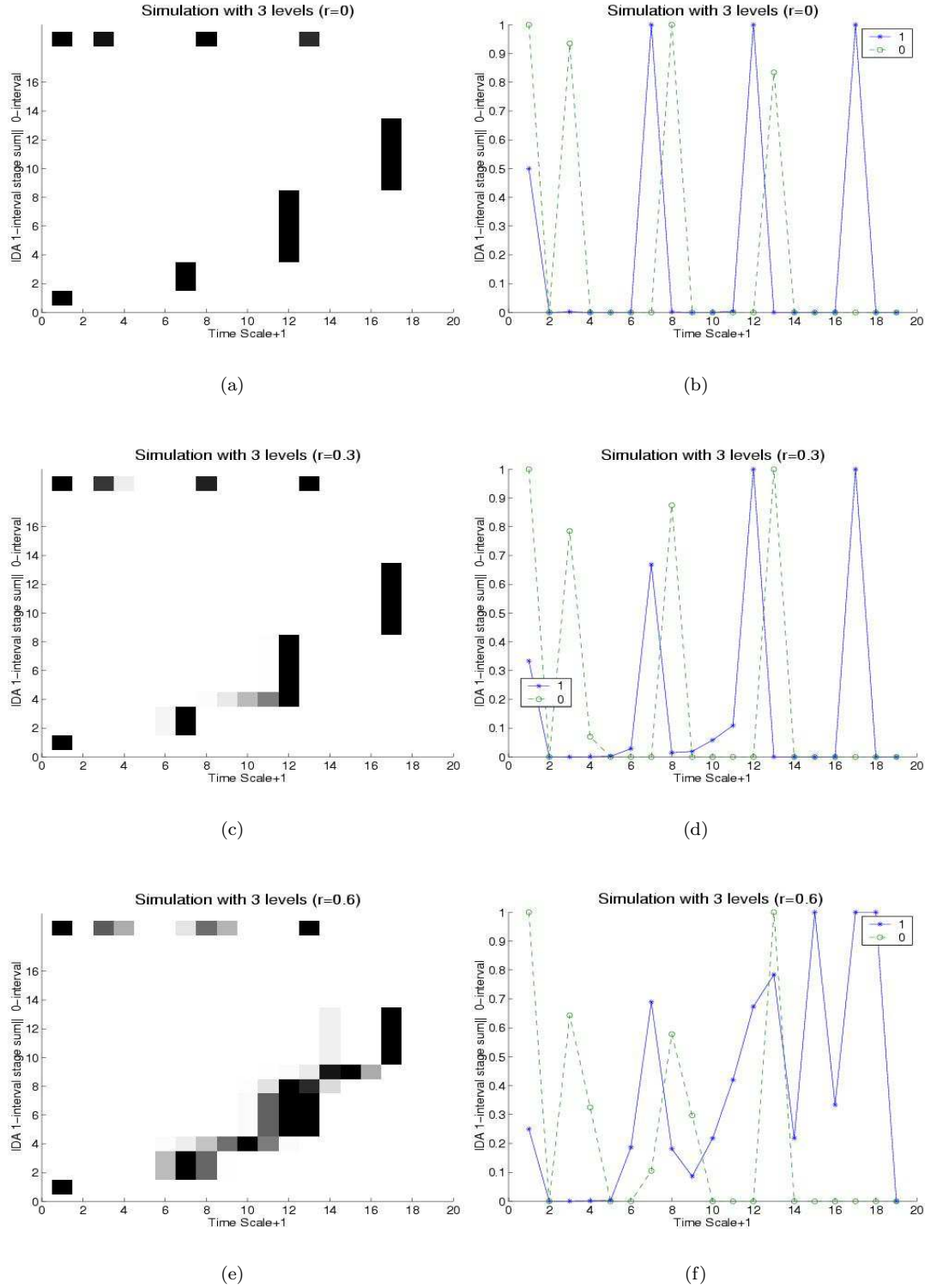


Figure 19: Detection of 0- and 1-intervals of levels in simulated sessions (part I): the 1-interval mean sizes are at  $2^6$ ,  $2^{11}$ , and  $2^{16}$ , and the 0-interval mean sizes are at  $2^2$ ,  $2^7$ , and  $2^{12}$ . The intervals are uniformly distributed around their mean, and the width of variation over the mean is 0 in (a), (b), 0.3 in (c), (d), and 0.6 in (e), (f) . Notice that after filling the gaps of the coarsest level, the IDA considers the whole data set as an 1-interval, hence there should be an indication of a level at time scale 18; this artifact has been removed from all pictures, except (f), where it was left for demonstration purposes.

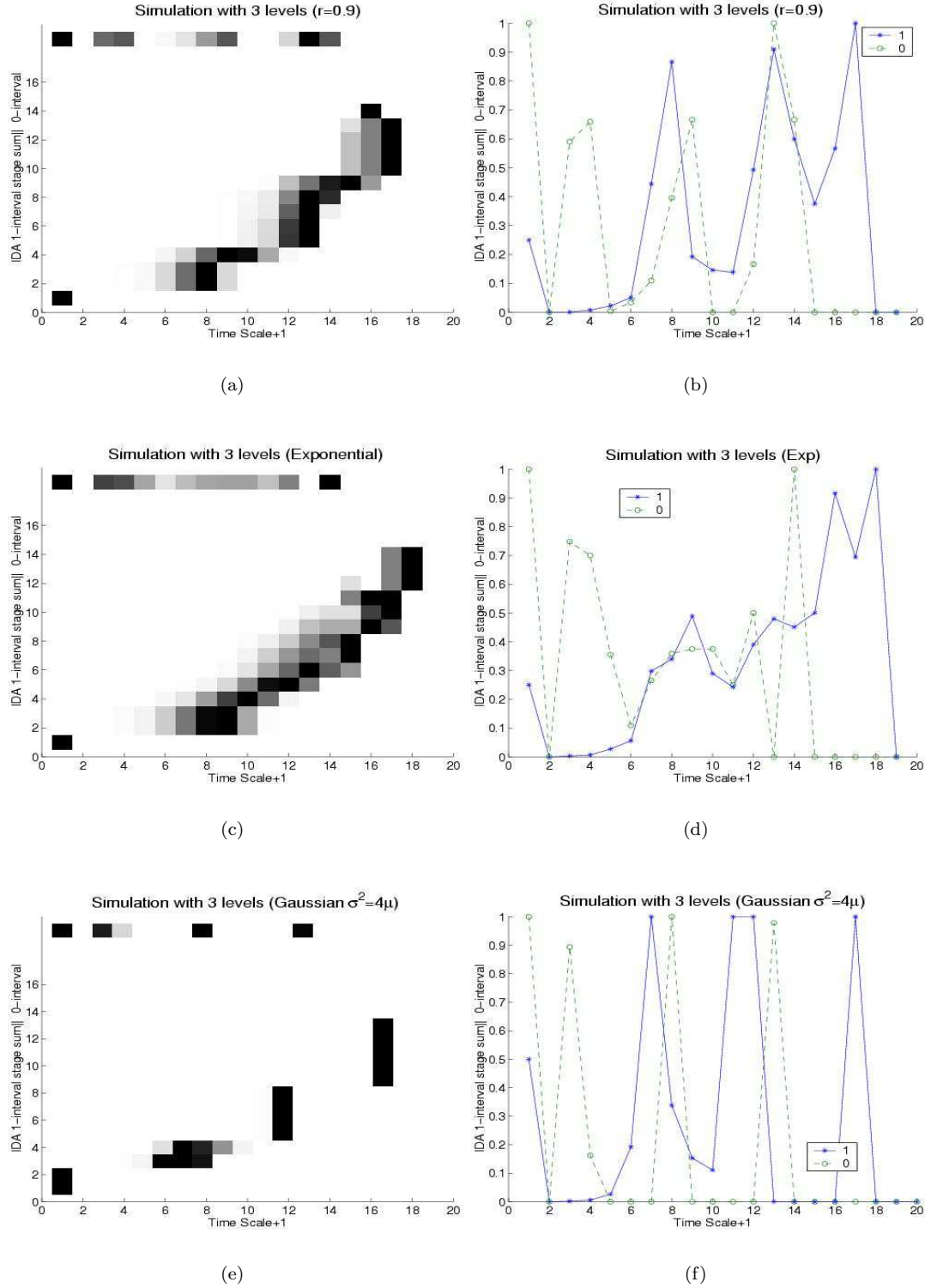


Figure 20: Detection of 0- and 1-intervals of levels in simulated sessions, part II: the 1-interval mean sizes are at  $2^6$ ,  $2^{11}$ , and  $2^{16}$ , and the 0-interval mean sizes are at  $2^2$ ,  $2^7$ , and  $2^{12}$ . In figures (a) and (b) the intervals are uniformly distributed around their mean, and the width of variation over the mean is 0.9. In (c) and (d) the intervals are exponentially distributed, whereas in (e) and (f) they are gaussianly distributed, the variance for each level being proportional to the mean:  $\sigma^2 = 4\mu$ . Notice that after filling the gaps of the coarsest level, the IDA considers the whole data set as an 1-interval, hence there should be an indication of a level at time scale 18; this artifact has been removed from all pictures, except (c) and (d), where it was left for demonstration purposes.

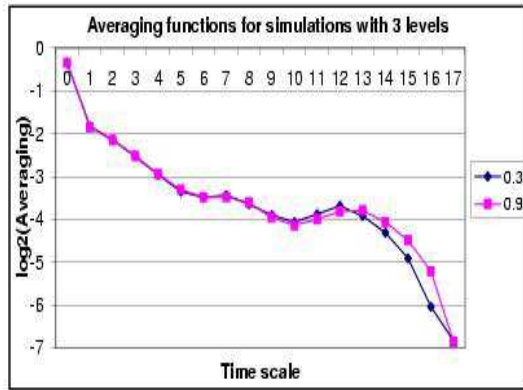


Figure 21: Averaging functions corresponding to the simulations of Fig. 19(b) and 20(a).

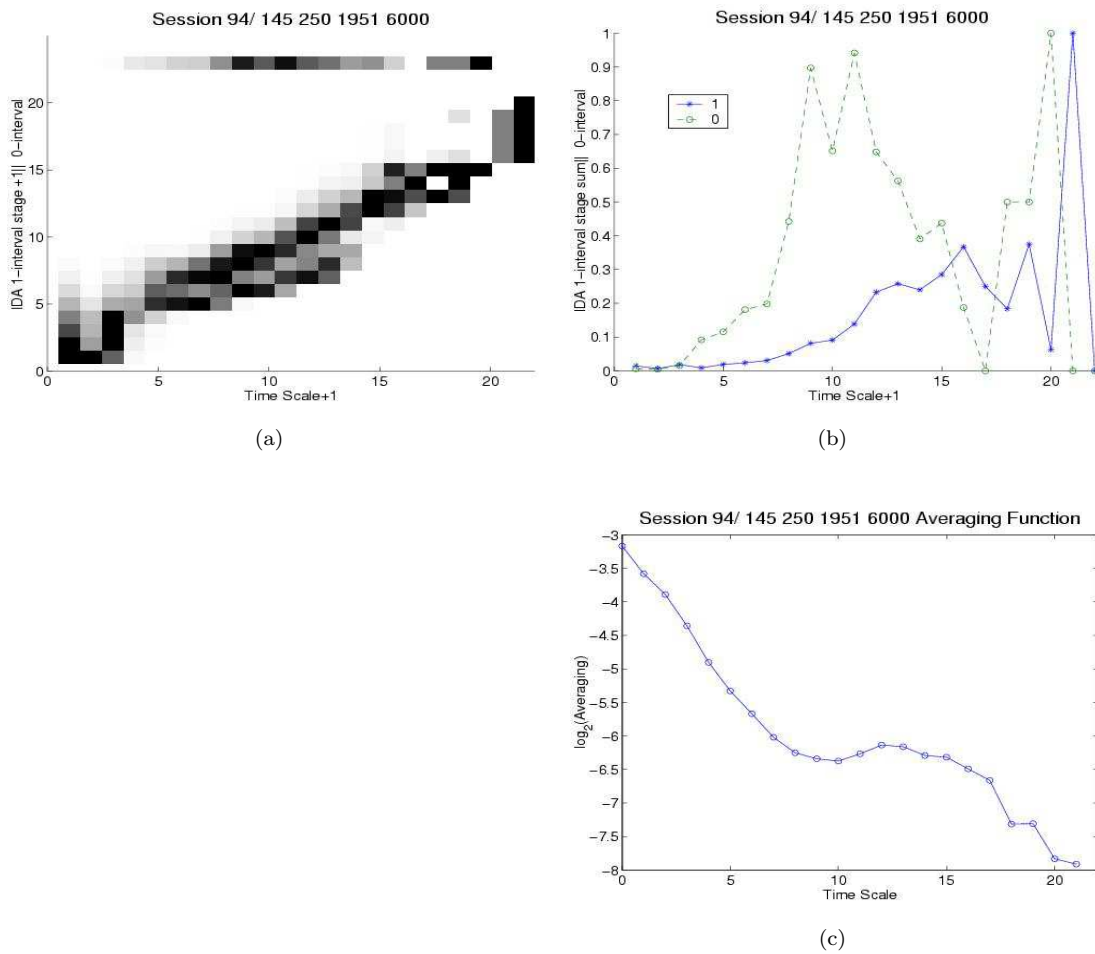


Figure 22: Detection of 0- and 1-intervals of levels in the longest session of trace 94: (a) and (b) are the greyscale and sum representation of the IDA results, respectively; (c) shows the Averaging function, which is included here in order to facilitate comparison (see section 6.7).

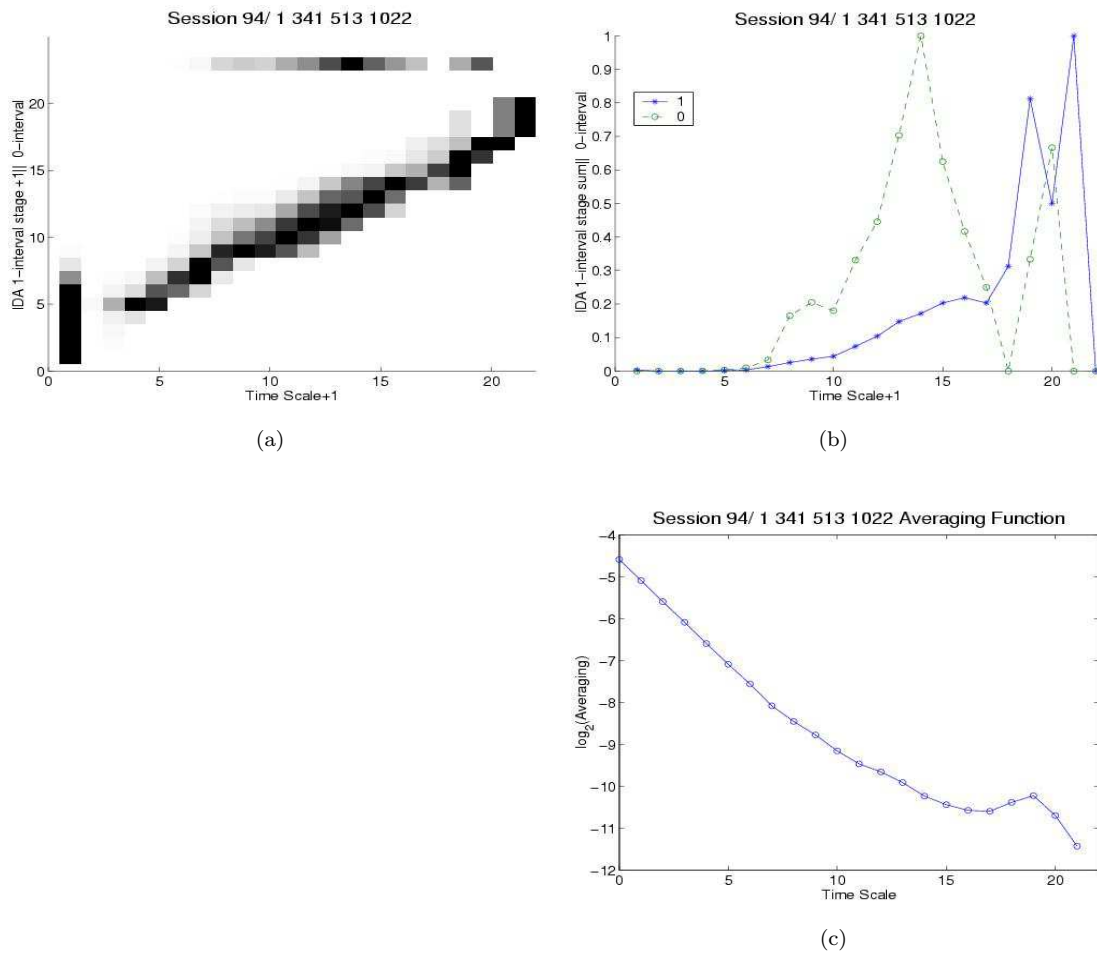
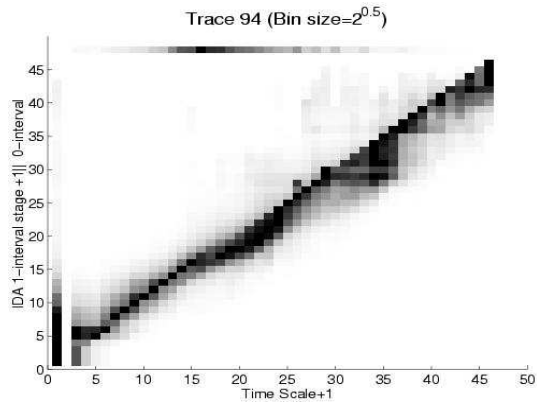
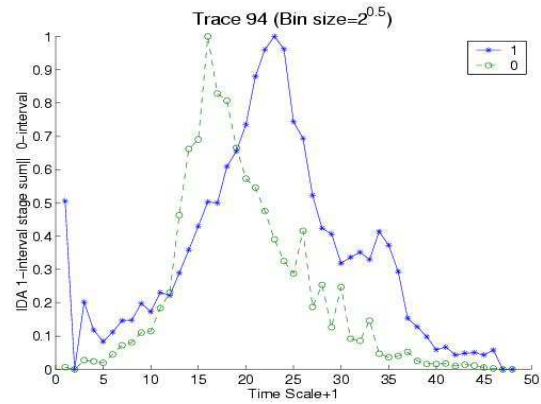


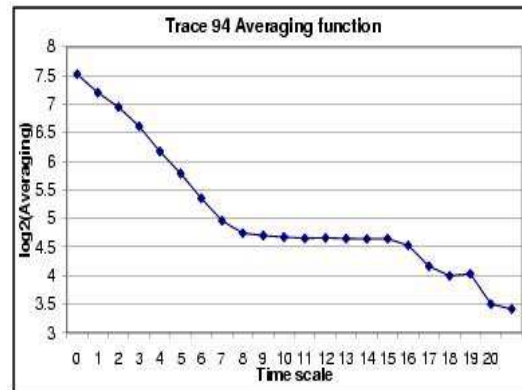
Figure 23: Detection of 0- and 1-intervals of levels in the session of trace 94 used in Fig. 17: (a) and (b) are the greyscale and sum representation of the IDA results, respectively; (c) shows the Averaging function, which is included here in order to facilitate comparison. According to the results of section 6.7, one might think that here the IDA and the Averaging function disagree; we will come back to that in sections 6.8 and 8.



(a)

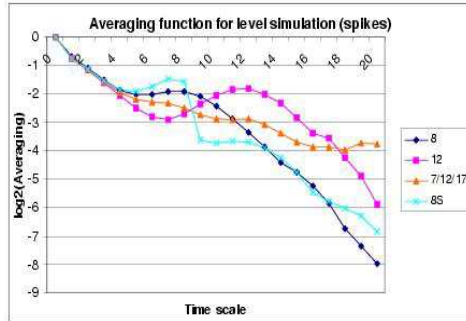


(b)

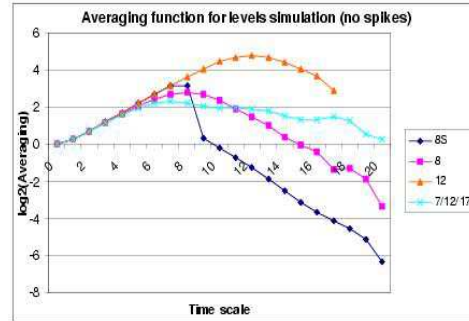


(c)

Figure 24: Aggregate results of the detection of 1- and 0-intervals of levels in all trace 94 sessions are shown in (a) and (b): the fact that the algorithm detects levels in this figure suggests that individual sessions have levels in common, which combine in a constructive, not destructive, way. Therefore, it is legitimate to assign levels to entire traces. Note here that the bins increase geometrically, as usual, but with a step of  $\sqrt{2}$  instead of 2. The Averaging function of trace 94 is shown in (c).

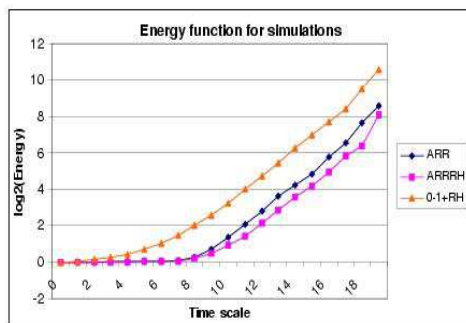


(a)

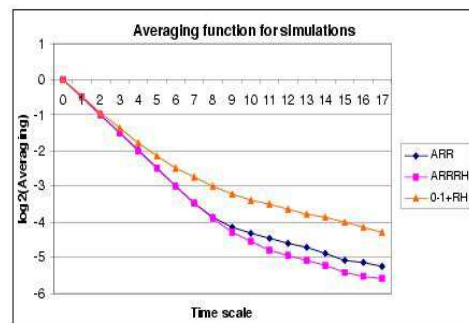


(b)

Figure 25: Average functions of some model D simulations: 8 has a level at  $2^8$ , 12 at  $2^{12}$  and 7/12/17 three levels at  $2^7, 2^{12}, 2^{17}$ . ON and OFF intervals of the levels are exponentially distributed, the mean being the level. In 8S, ON/OFF intervals are uniformly distributed within  $\pm 10\%$  around the mean. In (a), RTT is present: the ON intervals of the finest level consist of spikes of height 1, separated by exponentially distributed intervals with mean 4. In (b), RTT is not present, and the ON intervals of the finest level are continuous.



(a)



(b)

Figure 26: Some more simulations: curvature is present, since there is one single change of slope, the smoothness of which varies. Hence, there is one level in these traces.

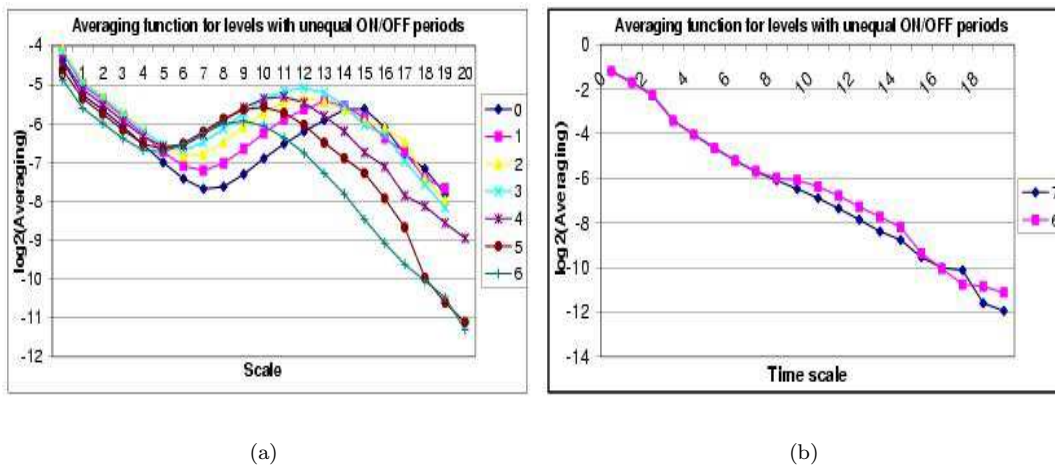
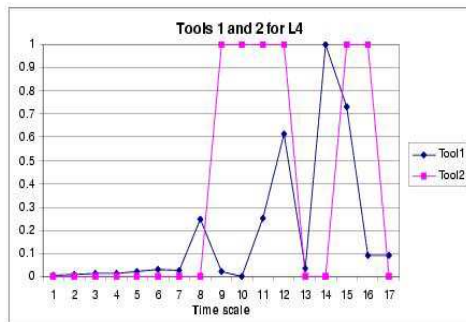
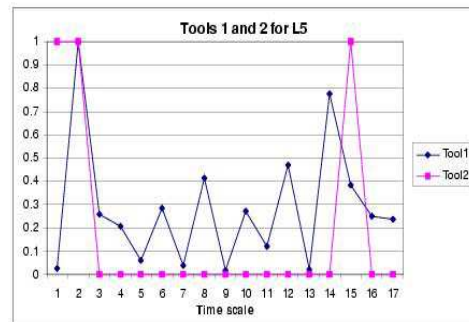


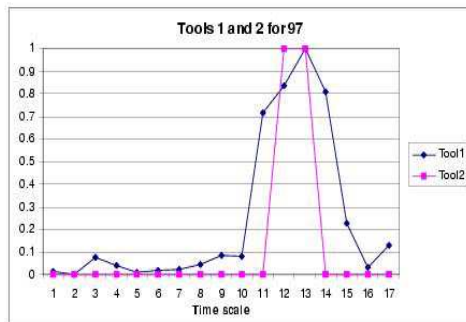
Figure 27: Averaging function of a simulated session with only one level whose 1-intervals live in time scale 15, but whose 0-intervals live in time scale  $15 - i$ , where, for each curve,  $i$  can be read from the legend. In (a), as a rule, the local maximum of the bump “locks” on  $15 - i$ , the scale of the 0-intervals. In (b), using a more diffused interval length distribution, the bump is negligible.



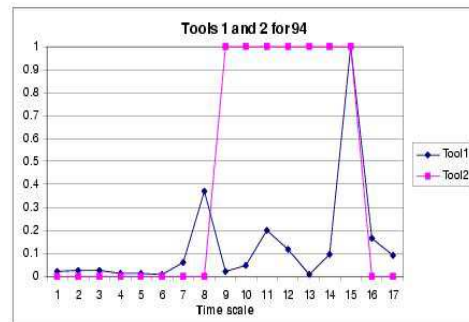
(a)



(b)

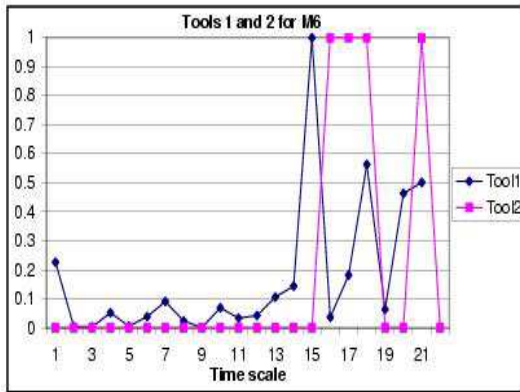


(c)

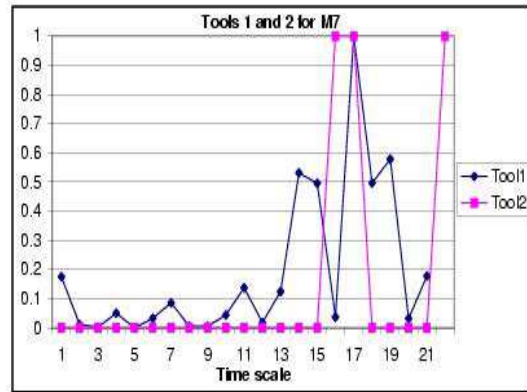


(d)

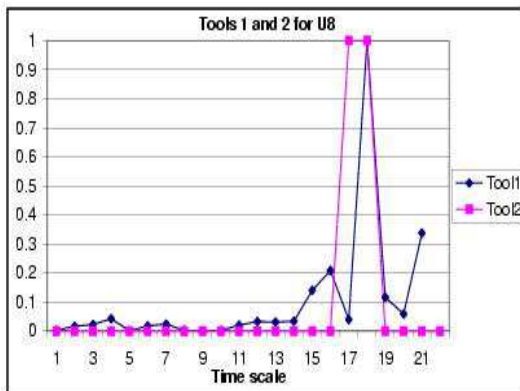
Figure 28: Tools 1 and 2 applied to real traces.  $\epsilon = 0.01$  was used.



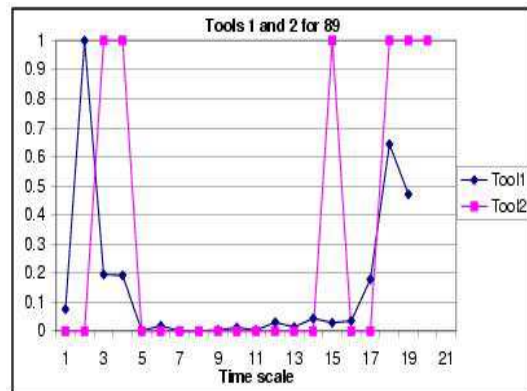
(a)



(b)

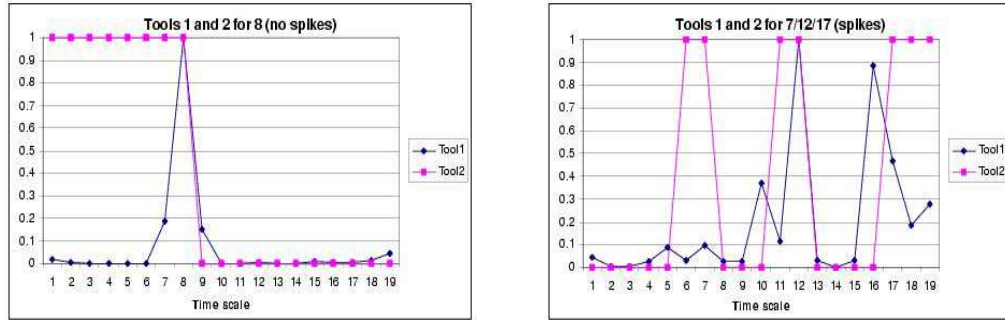


(c)



(d)

Figure 29: Tools 1 and 2 applied to real traces.  $\epsilon = 0.01$  was used.



(a)

(b)

Figure 30: Tools 1 and 2 applied to two model D simulations: 8 (No spikes) and 7/12/17 (Spikes)

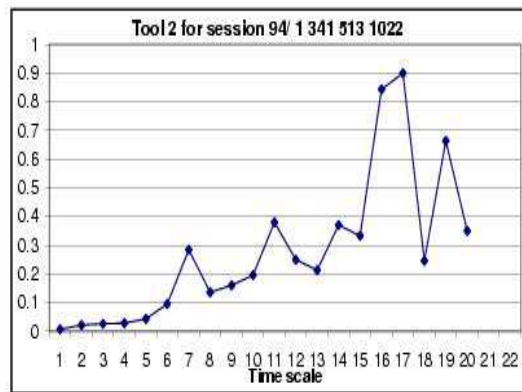


Figure 31: Tool 2 applied on session 94/ 1 341 514 1022: it clearly identifies levels near  $2^7ms$ ,  $2^{11}ms$ , and  $2^{16}ms - 2^{19}ms$

## 9 Acknowledgements

The authors would like to thank Dr. Walter Willinger and Dr. Andy Ogielski of AT&T for their comments, ideas, and support, Anja Feldmann of the Computer Science Department, University of Saarbrücken, for the procurement of the data set 97, and Prof. Ingrid Daubechies of the Department of Mathematics, Princeton University, for contributing to the shaping of the key ideas, and improving decisively this treatise both aesthetically and scientifically, working as hard as the authors themselves did. K. Drakakis would also like to thank the Lilian Boudouris Foundation for the scholarship it granted him. Finally, the authors would like to thank NSF, AFOSR, ONR, DARPA, and AT&T for their financial support.

## References

- [1] V. Paxson, S. Floyd. *Wide-Area Traffic: The Failure of Poisson Modelling* IEEE/ACM Transactions on Networking, Vol. 3 No. 3, pp. 226-244, June 1995

Results of Tools 3 and 4 for real traces:

<i>Trace</i>	94	97	L4	L5	M6	M7	U8	89
<i>Tool 3</i>	0.274	0.084	0.272	0.289	0.016	0.017	0.145	0.125
<i>Tool 4</i>	-0.479	0.101	-0.541	-0.425	-0.084	-0.123	-0.340	-0.797

Table 2: The results of Tools 3 and 4 when applied to the real traces: notice that both of them indicate that trace 97 is very close to Gaussianity.

- [2] A. Erramilli, O. Narayan, W. Willinger. *Experimental Queueing Analysis with Long-Range Dependent Packet Traffic* IEEE 1996
- [3] V. Ribeiro, R. Riedi, M. Crouse, R. Baraniuk. *Simulation of non-Gaussian Long-Range-Dependent Traffic using Wavelets* ACM 1999
- [4] W. Willinger, M. Taqqu, R. Sherman, D. Wilson. *Self-Similarity Through High-Variability: Statistical Analysis of Ethernet LAN Traffic at the Source Level* IEEE/ACM Transactions on Networking, Vol. 5, No.1, February 1997
- [5] M. Taqqu, V. Teverovsky, W. Willinger. *Is network traffic self-similar or multifractal?* Fractals. **5** (1997) 63-73
- [6] Y. Zhang, V. Paxson, S. Shenker. *The Stationarity of Internet Path Properties: Routing, Loss, and Throughput* ACIRI Technical Report, May 2000
- [7] B. Ryu, A. Elwalid. *The importance of Long-Range Dependence of VBR Video Traffic in ATM Traffic Engineering: Myths and Realities* Proc. ACM SIGCOMM '96, Stanford University, CA, Aug. 1996
- [8] C. Nuzman, I. Saniee, W. Sweldens, A. Weiss. *A compound Model for TCP Connection Arrivals* February 2000 (work in progress)
- [9] J. Cao, W. Cleveland, D. Lin, D. Sun. *On the nonstationarity of Internet Traffic* Performance Evaluation Review: Proc. ACM Sigmetrics 2001, 29:102-112
- [10] J. Levy, M. Taqqu. *Renewal-reward processes with heavy-tailed interrenewal times and heavy-tailed rewards* Bernoulli. **6** (2000) 23-44
- [11] V. Pipiras, M. Taqqu. *The limit of a renewal-reward process with heavy-tailed rewards is not a linear fractional stable motion* Bernoulli. **6** (2000) 607-614
- [12] A. Veres, M. Boda. *The Chaotic Nature of TCP Congestion Control* Proc. IEEE INFOCOM 2000, Tel Aviv, March 2000
- [13] M. Crovella, C. Lindermann. *Internet Performance Modeling: The State of the Art at the Turn of the Century* Performance Evaluation, March 2000
- [14] V. Paxson, S. Floyd. *Why We Don't Know How To Simulate The Internet* Proceedings of the 1997 Winter Simulation Conference, December 1997
- [15] A. Feldmann, A. Gilbert, W. Willinger. *Investigating the multifractal nature of Internet WAN traffic* Computer Communication Review, Vol. 28. No. 4, Proceedings of the ACM/SIGCOMM'98, September 1998, Vancouver, Canada pp. 12–55, 1998
- [16] A. Feldmann, A. Gilbert, P. Huang, W. Willinger. *Dynamics of IP traffic: A study of the role of variability and the impact of control* Proceedings of the ACM/SIGCOMM'99, August 29–September 1, 1999, Cambridge, MA
- [17] K. Park, G. Kim, M. Crovella. *On the relationship between file sizes, transport protocols, and self-similar network traffic* ICNP '96

- [18] A. Feldmann, A. Gilbert, W. Willinger, T. Kurz. *The changing nature of network traffic: Scaling phenomena* Computer Communication Review, April 1998
- [19] W. Leland, M.S. Taqqu, W. Willinger, D. Wilson. *On the self-similar nature of Ethernet traffic (extended version)* ACM/SIGCOMM'93. Computer Communication Review, **23** (1993), 183-193
- [20] R. Riedi, J. Lévy-Véhel. *Multifractal Properties of TCP Traffic: a Numerical Study* INRIA research report 3129, February 1997
- [21] R. Riedi. *Introduction to Multifractals* Long range dependence: theory and applications, eds. Doukhan, Oppenheim and Taqqu (to appear 2001)
- [22] R. Riedi. *Multifractal Processes* Long range dependence: theory and applications, eds. Doukhan, Oppenheim and Taqqu (2000)
- [23] S. Sarvotham, R. Riedi, R. Baraniuk. *Network Traffic Analysis and Modeling at the Connection Level* Technical Report, ECE Dept., Rice University, June 30, 2001
- [24] M. Taqqu, W. Willinger, R. Sherman. *Proof of a Fundamental Result in Self-Similar Traffic Modelling* Computer Communication Review, **27** (1997) 5-23
- [25] L. Peterson, B. Davie. *Computer Networks: A System Approach (Second Edition)* Morgan-Kaufmann, 2000
- [26] A. Araujo, E. Giné. *The central Limit theorem for Real and Banach Valued Random Variables* Wiley, New York (1980)
- [27] D. Pollard *Convergence of Stochastic Processes* Springer, New York (1984)
- [28] M. Ledoux, M. Talagrand. *Probability in Banach Spaces* Springer-Verlag (1991)
- [29] T. Mikosch, S.I. Resnick, H. Rootzén, A. Stegeman. (2001) *Is network traffic approximated by stable Levy motion or fractional Brownian motion?* Ann. Appl. Probab. (2001), to appear.